5-2017

A Comparison of Force and Pressure Coefficients on Dome, Cube and Prism Shaped Buildings due to Straight and Tornadic Wind Using Three Dimensional Computational Fluids Dynamics

Majdi A. A. Yousef
University of Arkansas, Fayetteville

A Comparison of Force and Pressure Coefficients on Dome, Cube and Prism Shaped Buildings due to Straight and Tornadic Wind Using Three Dimensional Computational Fluids Dynamics

A dissertation submitted in partial fulfillment
of the requirements for the degree of
Doctor of Philosophy in Engineering

by

Majdi Yousef
University of Omar Al-Mukhtar
Bachelor of Science in Civil Engineering, 2000
Universiti Putra Malaysia
Master of Science in Civil Engineering, 2005

May 2017
University of Arkansas

This dissertation is approved for recommendation to the Graduate Council.

_____

Dr. R. Panneer Selvam
Dissertation Director

_____ _____

Dr. Micah Hale
Committee Member

Dr. Rick J. Couvillion
Committee Member

_____

Dr. Ernie Heymsfield
Committee Member

ABSTRACT

Tornadoes induce very different wind forces than a straight-line (SL) wind. A suitably designed building for a SL wind may fail when exposed to a tornado-wind of the same wind speed. It is necessary to design buildings that are more resistant to tornadoes. Most studies have been conducted to investigate tornado forces on cubic, gable-roof and cylinder buildings. However, little attention has been paid to investigate tornado force on dome buildings; hence, further research is conducted in this study. The forces on a dome, cube and prisms were analyzed and compared using Computational Fluid Dynamics (CFD) for tornadic and SL winds. One typical tornado parameter was considered for comparison. The conclusions drawn from this study were illustrated in visualizations. The tornado force coefficients on the cube and prisms were larger than those on the dome by at least 90% in the x-y directions, and 140% in the z direction. The tornado pressure coefficients on cube and prisms were greater at least 200%. The force coefficients on cube and prisms due to SL wind were higher than those on the dome due to tornado wind by about 100% in the z-direction.

The ratio of tangential (V_θ) to translational (V_t) velocity reported in recent studies is 10 or greater, which is larger than the field observation ratios. The influence of V_θ/V_t ratios on the tornado force coefficient for a cubic, prism and dome buildings were compared using a systematic study. The V_θ/V_t ratios were considered to be 1, 3, 6, and 8 for comparison. These ratios were very much in agreement with field observation ratios. The magnitudes of the forces were found to be larger for slower translation speed or higher V_θ/V_t ratios. For faster translation speeds or, lower V_θ/V_t ratio, the maximum force coefficients shifted to the left of the time history.

ACKNOWLEDGMENTS

Firstly, I would like to express my sincere gratitude to my advisor Prof. R. Panneer Selvam for the continuous support of my Ph.D. study and related research, for his patience, motivation, and immense knowledge. His guidance helped me during the entirety of the research and writing of this thesis. I could not have imagined having a better advisor and mentor for my Ph.D. studies.

Besides my advisor, I would like to thank the rest of my dissertation committee: Prof. Micah Hale, Prof. Ernie Heymsfield and Prof. Rick J. Couvillion, for their insightful comments and encouragement, but also for the hard questions, which incented me to widen my research in various directions.

My sincere thanks also go to my research group, Dr. Piotr Gorecki, Dr. Nawfal Ahmed, and Dr. Matthew Strasser, and Scott Ragan, Blandine Kemayou, Alhussin Aliwan, Damoso Dominguez and Mohamad Kashefizadeh for their support and friendship during my study. Without their support, it would not have been possible to conduct this research.

I acknowledge and appreciate the computer support provided by the College of Engineering, University of Arkansas, for their help with this work. I also acknowledge the financial support scholarship provided by the Libyan Government.

I would also like to thank my father, mother, brothers and sisters. They were always supporting me and encouraging me with their best wishes.

Finally, I would like to thank my wife, Salma Ibrahim. She was always there cheering me on and standing by me through the good times and bad. Thanks to my children, Jana, Saba and Ahmad who provided me with hope to finish my degree.

TABLE OF CONTENTS

LIST OF FIGURES

LIST OF TABLES

NOMENNCLATURE

English

A	Aspect ratio
Ax	Area x (Height times length) (m^2)
Ay	Area y (Length times length) (m^2)
Az	Projected Area (floor plan Area) (m^2)
C_D	Drag force coefficient
C_L	Lift force coefficient
Cp	Pressure coefficient
C_s, C_k	Empirical constants
Cx, Cy, Cz	Force coefficients in *x, y, z*
D	Dome diameter ,or prism width (m)
Fx, Fy, Fz	Forces in *x, y, z* directions
G	Gust effect factor for rigid buildings and structures
GCp	External pressure coefficient
H	Building Height (m)
h_1, h_2,h_3	Control volume spacing in the *x, y,* and *z* directions
H_D	Domain height
h_D	The height of the dome from the lower point to the spring line (figure 4..3)
IM, JM,KM	Number of grid points in the *x*-, *y*- and *z*- directions
K_{zt}	Topography factor
K_d	Wind directionality factor
K_z	Velocity pressure exposure coefficient
L	Building Length (m)

L*, U*	Non dimensional length, velocity respectively
L_D	Domain Length
P	pressure over density
qh	Velocity pressures for leeward, side walls and roofs evaluated at height h.
Qi	Positive and negative internal pressure
q=qz	Velocity pressures for windward walls evaluated at height *z* above ground
R	distance from tornado center
Re	Reynolds number
r_{max}	tornado radius where the maximum tangential velocity occurs
St	Strouhal number
T	Time
t*	Non-dimensional time unit
U, V, W	velocities in *x*, *y* and *z* directions
Ui	Non-dimensional velocity components in (*x*, *y* and *z*)
V	Volume (m^3)
V_θ	Tangential velocity
V_t	Translational velocity
v_t	Turbulent eddy viscosity
V_i	Velocity of grid
V_{max}	Maximum velocity
Vs	Wind speed
W_D	Domain width
z_0	known height

Z_f	Boundary layer profile

Greek

A	Rotational constant
Δ	Fine grid
P	Density of the fluid (kg / m^3)
V	Reference velocity
N	Kinematic viscosity of the fluid (m^2 / s)
Θ	Degrees on dome (Figure aaa)
K	Kurbulent kinetic energy
K	Surface roughness length
Δt	Time step
Δ_p	Pressure difference

Acronyms

BRV	Burgers-Rott Vortex
CFD	Computational Fluid Dynamics
CM	Cubic Model
DM	Dome Model
CWE	Computational wind engineering
EF	Enhanced Fujita
FDM	Finite Difference Method
FEM	Finite Element Method
ISU	Iowa State University
LES	Large Eddy Simulation

ND	Non-Dimensional
NHS	Natural Hazard Statistics
NS	Navier-Stokes
NWS	American National Weather Service
PM	Prism Model
RCVM	Rankine Combined Vortex Model
SL	Straight-Line
SV	Sullivan Vortex
UA	University of Arkansas

CHAPTER 1: INTRODUCTION AND OBJECTIVE

1.1 Introduction

Every year in the United States, approximately 1,200 tornadoes cause 60-65 fatalities, 1,500 injuries and at least 400 million dollars in economic damage, as reported by the American National Weather Service (NWS, 2010). The U.S. Natural Hazard Statistics (NHS, 2014) considers tornado losses as the second largest loss next to floods as shown in Figure 1.1. In order to mitigate this damage, it is necessary to design buildings that are more resistant to tornadoes. Tornadoes produce different types of wind forces than a Straight-Line (SL) wind. The first requirement for accomplishing this goal is a better understanding of tornado-structure interaction and tornado-induced loads on buildings. Development in tornado wind modeling can lead to a better prediction of tornado maximum forces. Then, the outcome can be implemented for improving building design standards.

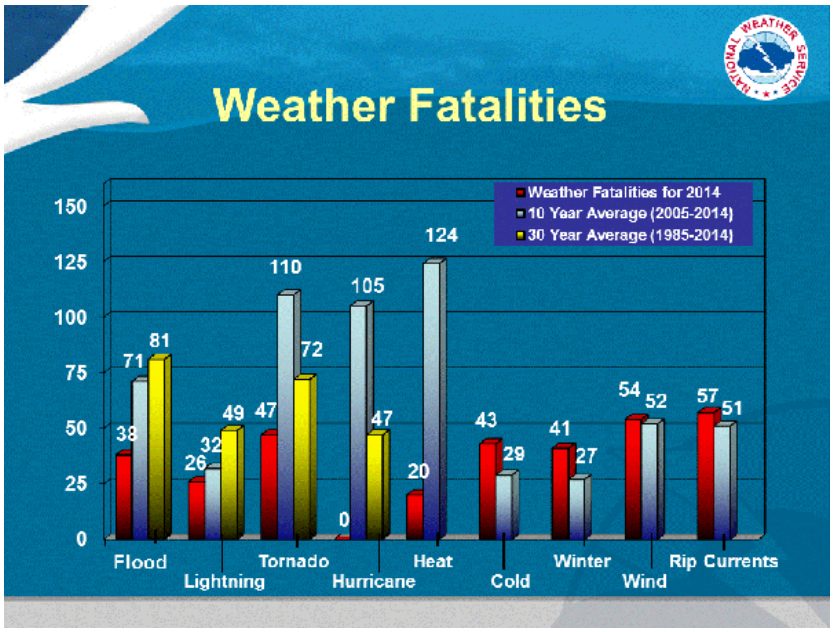

Figure1.1: Average losses due to severe events taken from U.S. NWS (2014)

1.2 Field observation of tornado interacting with dome type structures

In the tornado-damaged areas, dome buildings seem to have less damage. In one instance, 1,700 homes were demolished by an EF4 or EF5 tornado at Moore, OK (2013), only one simple concrete dome structure survived in the middle of all the destruction as illustrated in Figure 1.2a (Praker, 2013). In another instance, a wood dome house survived after it was hit by the EF5 tornado in West Jefferson County, NC as shown in Figure 1.2b (Age Dome, 2013). From these observations, one can say that the dome shape may have reduced the wind forces.

(a) (b)

Figure 1.2: Dome survived with partial failure in (a) Moore, OK (Parker, 2011) and (b) West Jefferson County, NC (AGE dome, 2015)

1.3 The tornado force on structures using laboratory and computer model

The challenges to understanding the tornado-structure interaction date back to 1970. In-site measurements of tornadic winds around a structure were costly to assess the actual wind effects (Mehta et al. 1976). Wurman et al. (2013) found it difficult to acquire in-site measurements. Thus, researchers have started studying the tornadic wind fields on structures in laboratory tornado simulators or using CFD. Several studies utilized laboratory and computer tornado simulators to study tornado force and pressure on buildings as summarized in Table 1.1.

Table 1.1 Summary of studies on the influence of the tornadic wind fields on structures.

Reference	*Vθ/Vt*	Building Shape	Model	*Cx*	*Cy*	*Cz*
Sarkar et al. (2006)	35	Tall Cube	Exp.	2.01	2.01	1.77
	18			1.78	1.78	1.66
Case et al. (2011)	78	Gable-roof	Exp.	0.75	1.20	2.4
	26			0.70	1.00	2.0
Sengupta et al. (2008)	40	Cube	Exp.	1.97	1.97	1.24
	20			1.82	1.82	1.22
Sengupta et al. (2008)	40	Tall Cube	Exp.	2.17	2.17	1.54
	20			1.75	1.75	1.78
Sengupta et al. (2008)	40	Tall Cube	Num.	2.01	2.01	1.77
	20			1.78	1.78	1.66
Sengupta et al. (2008)	40	Cube	Num.	1.57	1.57	1.09
	20			1.4	1.4	0.98
Hana et al. (2010)	80	Gable roof	Exp.	1.1	1.2	3
Hu et al. (2011)	18	Gable roof	Exp.	0.9	0.7	2.8
Yang et al. (2011)	24	Tall Cube	Exp.	2.0	0.4	0.7
Selvam et al. (2005)	2	Cube	Num.	0.82	1.36	1.81
Zhao et al. (2016)	10	Dome	Num.	0.69	0.13	0.52

The most recent research to investigate the tornado force on non-dome buildings are listed in Table 1.1. Here *Cx, Cy* and *Cz* are force coefficients in the *x, y* and *z* directions, respectively. Zhao et al. (2016) studied the tornado force on dome buildings, but they did not have proper grid resolution. In addition, all the reported work had larger *Vθ/Vt* ratio than field observation; hence, further detailed work is conducted in this study.

1.4 Dissertation motivation and objectives

Despite the research reported in recent studies, the wind effects of tornadoes on dome buildings has not been sufficiently explored, which justifies the necessity of the research in this study. Most of the work has been on one or two tornado translation speeds of tornado's effects on building forces. In addition, the V_θ/V_t ratio reported in recent studies have measured the wind loads on low-rise buildings in simulated tornadoes as 10 or greater, which is larger than the field

observation ratios. In this work, the effect of V_θ/V_t ratio on tornado force coefficients over buildings will be systematically investigated.

A UA computer model is used to compare in detail the interaction of a tornado with a dome, cube and prisms. Then, the numerical results are compared with those resulting from SL wind. In this model, the Navier-Stokes equations are solved using the control volume method or finite element method. The large eddy simulation is used to model the turbulence. The effect of grid resolution in the domain is considered. Since it is difficult to have a dome and cubic or prism models with the same surface area, height and volume, it is necessary to create six models so that these issues can be considered in the analysis. The classifications for the dome, cube and prism dimensions are presented in Figure 1.3. The dome model (DM1) is assumed to be the reference model with constant dimensions (Table 1.2). Five models with different dimensions represent the cube and prisms (CM2, PM3, PM4, PM5, and PM6), in order to have the dome, cube or prism with the same surface and height, the same volume and height, the same width and height, and a prism fitting inside a dome (Figure 1.4). The six models described below:

1. Model 1 (DM1): The hemispherical dome is assumed to be the reference model with constant dimensions 20mx20mx10m. A common dome home size is 66 feet (20 m) in diameter with a 32-foot (10) diameter center section (Monolithic, 2009). However, it can be much larger.

2. Model 2 (CM2): Cube with dimensions 10.0mx10.0mx10m; this model is created so that the height (H) of the cube are same as the dome in DM1.

3. Model 3 (PM3): Rectangular prism with dimensions 17.7mx17.7mx10m; this model is created so that the projected area (A_z) and the height (H) of the prism are same as the dome in DM1.

4. Model 4 (PM4): Rectangular prism with dimensions 14.47mx14.47mx10m; this model is

created so that the volume (*V*) and the height (*H*) of the prism are the same in DM1.

5. Model 5 (PM5): Rectangular prism with dimensions 20 mx20mx10m; this model is created so that the width (*D*) and height (*H*) of the prism and the dome in DM1 are the same.

6. Model 6 (PM6): Rectangular prism with dimensions 13.40mx13.40mx7.5m; this model is created so that it can fit inside the dome in DM1.

In this work, the effect of V_θ/V_t ratio on tornado force coefficients over buildings will also be systematically investigated. The V_θ/V_t ratios are considered to be 1, 3, 6 and 8 for comparison. These ratios are very much in agreement with field observation ratios. The UA computer model based on Rankine Combined Vortex Model will be used also to calculate the effect V_θ/V_t ratio on tornado force coefficient for dome (DM1), cubic (CM1) and prism (PM1) building.

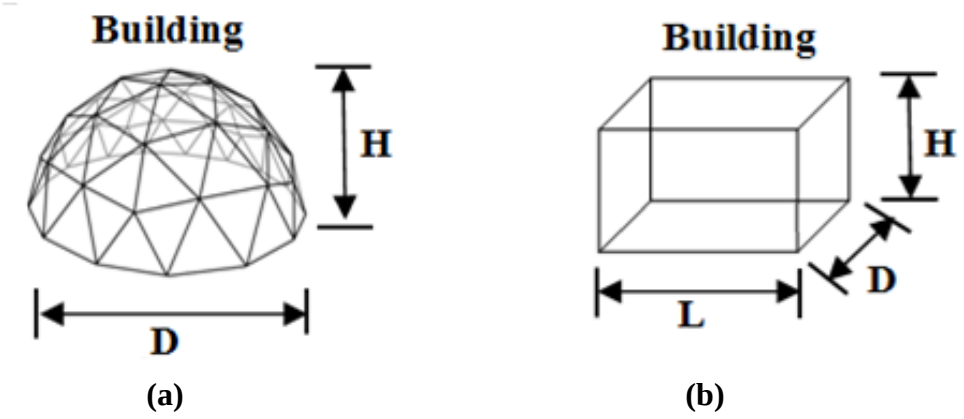

Figure 1.3: Nomenclature Dimensions **(a)** Dome Model, and **(b)** Cubic, Prism Model

Table 1.2 The parameters of the five models

Name	Shape	Units	Length=Width *(L=D)*	Height *(H)*	Area *(Ax=Ay)*	Area *(Az)*	Volume *(V)*
DM1	Dome	M	20.0	10.0	157	314	2,094
		Ft	65.62	32.81	1690	3380	73,934
CM2	Cube	M	10.0	10.0	100	100	1,000
		Ft	32.81	32.81	1076.5	1076.5	35,320
PM3	Prism	M	17.72	10.0	177.2	314	3140
		Ft	58.14	32.81	1970	3380	110,888
PM4	Prism	M	14.47	10.0	144.2	209.4	2,094
		Ft	47.47	32.81	1557	2253.4	73,934
PM5	Prism	M	20.0	10.0	200	400	4,000
		Ft	65.62	32.81	2153	4306	141,270
PM6	Prism	M	13.40	7.5	100	180	1,347
		Ft	43.96	24.61	1082	1932	47,558

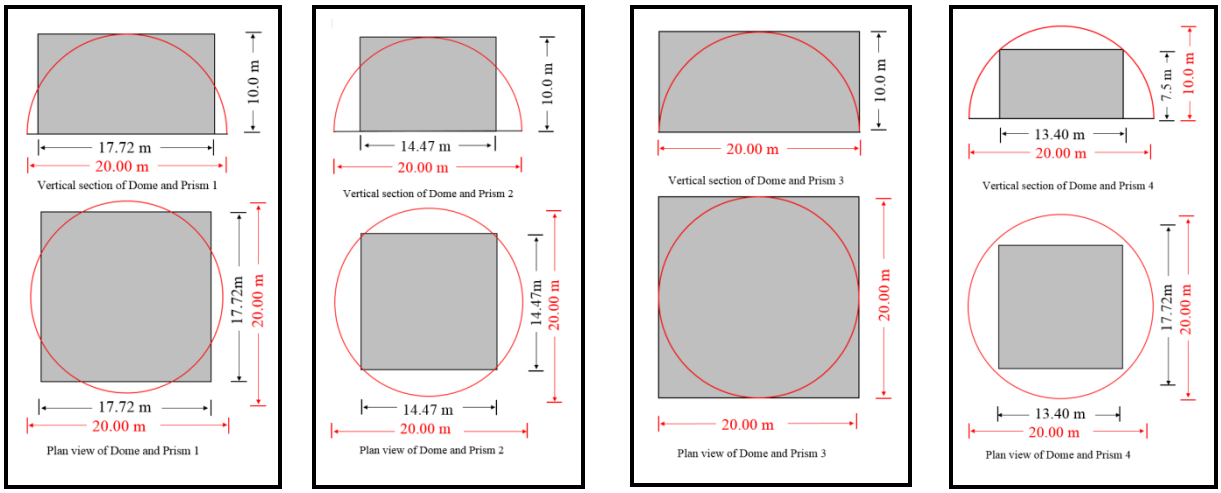

(a) **(b)** **(c)** **(d)**

Figure 1.4: Plan view of dome and prism with same: (a) Projected area and height (b) Volume and height (c) Width and height (d) Prism fit inside the dome

The objectives of this dissertation are to fill the literature gaps and to provide standards for better building design, especially in tornado regions. The three objectives in this dissertation are listed below.

1.4.1 Objective 1: Investigate the effect of SL wind on a dome, cube and prisms, using ASCE 7-10 provision and a CFD Model

The SL wind effect on a dome, cube and prisms are calculated, primarily based on the ASCE 7-10 provisions. Then, the computed force and pressure coefficients for SL wind is compared with the ASCE 7-10 to determine if the computer model values are relevant to the ASCE 7-10 provisions.

- Wind force coefficients on a dome, cube and prisms are compared due to SL wind; with respect to the height, surface area or volume (eg. the height, surface area or volume is assumed to be same for both models), primarily based on the ASCE 7-10 provisions. The model's details are presented in section 1.4.
- The presented models are investigated due to SL wind, using a CFD model.
- The wind force coefficients that are calculated from ASCE 7-10 provisions and the CFD model are compared, to validate the model.

1.4.2 Objective 2: Compare the effect of tornado on a dome, cube and prisms, using a CFD model

The objective of this chapter is to investigate and compare the force and pressure coefficients on dome and prisms due to SL and tornado wind using a CFD model. The six models (DM1, CM2, PM3, PM4, PM5 and PM6) shown in Figure 1.4 are considered in this objective.

- Some flow visualizations are included to understand the flow behavior around the dome, cube and prism buildings.
- The tornado force and pressure on dome, cube and prisms are compared.

- The force and pressure coefficients on dome, cube and prisms resulting from SL and tornado wind are compared.

1.4.3 Objective 3: Investigate the influence of tangential to translational velocity ratio on tornado coefficients on structures, using a CFD model

The effect of V_θ/V_t ratio on tornado force coefficients over buildings will be investigated with systematic study. The V_θ/V_t ratios are considered to be 1, 3, 6 and 8 for comparison. These ratios are very much in agreement with field observation ratios. Three models (DM1, CM2, and PM3) listed in Table 1.2 are compared in this objective.

- Some flow visualizations are reported to understand the flow behavior due to the different $V\theta/Vt$ ratios.
- The tornado force on dome, cube and prism are compared due to the different V_θ/V_t ratios.

CHAPTER 2: LITERATURE REVIEW

2.1 Introduction

A tornado is a storm of short duration lasting from 5 to 10 minutes produced by winds rotating at very high speeds, usually in a counter-clockwise direction. This creates a wind vortex structure rotating around a hollow cavity in which centrifugal forces generate a partial vacuum. As intensification takes place around the vortex, a light cloud illuminates the familiar and frightening tornado funnel that usually appears as an extension of the dark, heavy cumulonimbus clouds of thunderstorms, descending to the ground. Some funnels touch the earth's surface and rise again, and others never touch down. Air surrounding the funnel is part of the tornado whirlpool. As the whirlwinds tear a path along the earth, this external circle of rotational winds becomes dark with dust and debris, which may finally darken the whole funnel. These storms form several thousand feet above ground, usually during warm, humid, unstable weather, and usually in conjunction with a severe thunderstorm. Sometimes, groups of two or more tornadoes accompany their thunderstorm of origin. When the winds of the thunderstorms collide with lower wind speeds closer to the ground, tornadoes may form at interval along its path, move for some miles, and then dissipate. The vortex winds of a tornado may reach 300 mph, the path of tornado damage may be an excess of 50 miles long and one mile wide, and the speed of movement along the ground has been observed to range from almost no movement to 70 mph. Every single state is at danger from this hazard.

Tornadoes are one of the strongest winds on earth and more likely to cause significant damage if they pass through a heavily populated area. Although tornadoes occur across the world, the U.S. experiences more tornadoes than any other country, they are an annual phenomenon. Every year, an average of 1,200 tornadoes kill at least 60 people, injure 1,500

more and cause over $400 million in damage (NOAA, 2011). This means that tornadoes are the most significant severe weather hazard in the U.S. in two aspects, loss of life and insured losses. Due to the large losses, high frequency, and severity of tornadoes, many scientists and researcher's intend to develop a better understanding of tornadoes. The main objective of this chapter is to discuss the available tornado knowledge in general and provide the state of the art information for tornado-terrain interaction. Tornado phenomenon has been investigated with three main approaches: numerical simulation, experimental simulation and field investigation. In this review, all these approaches are reviewed, but more focus is placed on numerical simulation and post damage investigation.

Figure 2.1: The winds of some tornadoes have been estimated to exceed 300 mph. (Photo courtesy of NOAA Photo Library, NOAA Central Library; OAR/ERL/National Severe Storms Laboratory (NSSL))

2.2 How a tornado is formed

Tornado forming requires the existence of layers of air with contrasting features of temperature, wind flow, moisture and density. The tornado vortex is created by complicated energy transformations. Many theories have been presented as the style of energy transformation needed to generate a tornado vortex, and none has won general approval. The two most

encountered theories visualize tornado generation as the effect either of thermally induced rotational flow, or as the effect of converging rotational winds. Presently, scientists appear to agree that neither process generates tornadoes independently. It is more possible that the combined effects of mechanical forces and temperature, with one or the other force being the stronger generating agent, produce tornadoes.

Considerable observation of lightning strokes and a variety of luminous features in and around tornado funnels have led scientists to guess about the relationship between tornado formation and thunderstorm electrification. This theory explores the alternative potential that atmospheric electricity accelerates rotating winds to tornado speed, or that those high-speed rotational winds produce large electrical charges. Here, as in most efforts to understand complex atmospheric relationships, the reach of theory exceeds the understanding of the evidence. The tornado structures are shown in Figure 2.2.

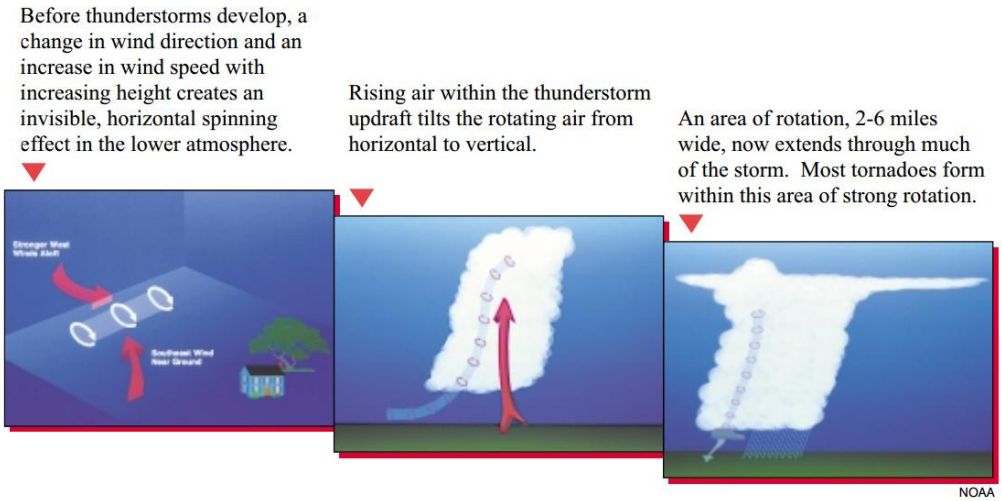

Figure 2.2: Tornado structures (NWS, 2010)

2.3 Size, speed and duration of tornado

Tornadoes vary greatly in size, intensity, and appearance. Most of the tornadoes, about 88%, that happen every year fall in the weak category. The wind speeds of those weak tornadoes are in the range of 110 mph or less. Weak tornadoes account for less than 5% of all tornado deaths. Approximately one out of every three tornadoes, about 11% of all tornadoes, are categorized as strong. The strong tornadoes have wind speeds reaching to 205 mph, with an average path length of 9 mi, and a path width of 200 yd. About 30% of all tornado deaths every year occur from this type of storm, and almost 70% of all tornado fatalities result from violent tornadoes. Although very rare, about only 1% are violent, these powerful tornadoes can stay for hours. Average tornado widths and path lengths are 425 yd and 26 mi, respectively. The largest of these tornadoes may exceed a mile or more in width, with wind speeds reaching 300 mph. Figure 2.3 shows the size, speed and duration of tornadoes.

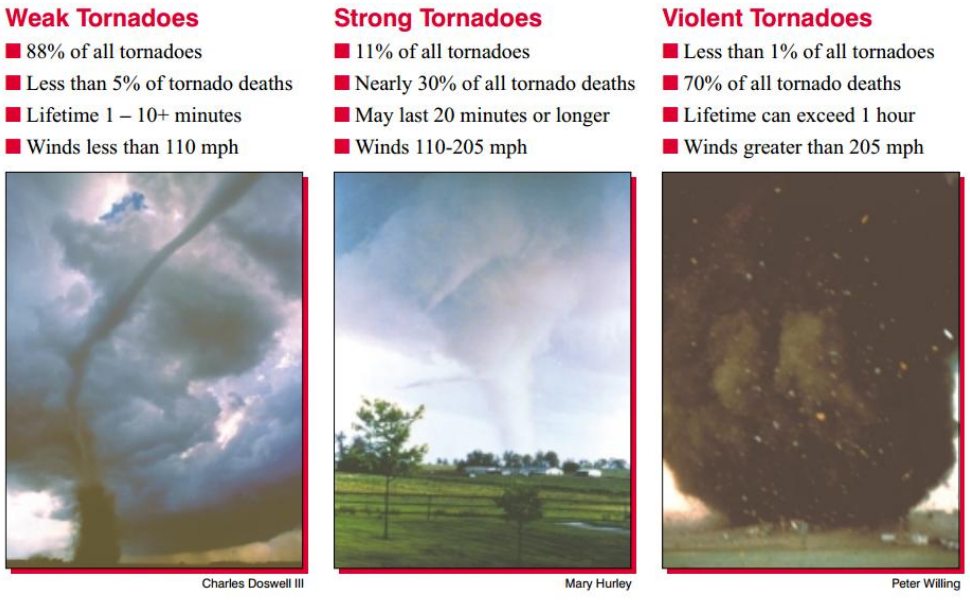

Figure 2.3: Tornado shape and size (NWS, 2010)

2.4 Tornado facts (NOAA, 2012)

- Tornadoes have been documented to travel in every direction, but the common tornados travel from southwest to northeast.
- The average speed of tornadoes is 30 mph but may fluctuate from almost stationary to 70 mph.
- The strongest tornadoes have rotating winds of more than 250 mph.
- Tornadoes can escort tropical storms and hurricanes when they travel on land.
- Waterspouts are tornadoes, which are formed by warm water. They can travel on seashore and damage coastal areas.

2.5 Place and time occurrence of tornadoes (NOAA, 2012)

- Tornadoes can take place at any time of the year.
- Tornadoes have happened in every state, but most of them occur east of the Rocky Mountains during the spring and summer months.
- The peak tornadoes season occurs in the southern states from March through May and in the northern states during the late spring and summer.
- Time occurrence of tornadoes is between 3 and 9 p.m. but can take place at any time.

2.6 The tornado vortex

Tornadoes are one of the most difficult subjects in the field of atmosphere science because, being violent and obscure, they do not lend themselves to intimate study. The simple concepts of a tornado flow are illustrated in Figure 2.4, taken from Whipple (1982).

The most important characteristics of the tornado vortex are described in Figure 2.4. Both the ground and the wall cloud are in contact with a rotating funnel cloud. Circulation rate decreases far away from the tornado. Characteristic air suction is observed inside the vortex.

Wurman et al. (1996) provided very accurate tornado structure theory. A real tornado was analyzed using data retrieved from a Doppler radar. Figure 2.5 shows the five different flow regions that were distinguished as a result. Region I is a rising outer-flow region, where the tornado is embedded. Region II represents the tornado core. This region connects pressure drop and wind velocities. Region III can be defined as a tip of Region II. There, friction interaction with the surface makes the tornadic flow intensified and disrupted. Region IV is the surface boundary layer region around Region III. The angular momentum of the vortex in Region V is concentrated and transported downward.

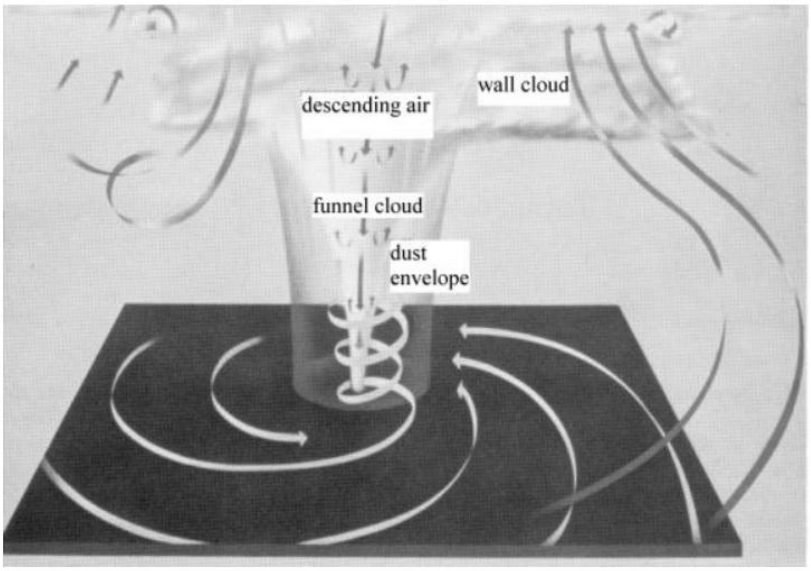

Figure 2.4: Organization of tornado vortex (Whipple, 1982)

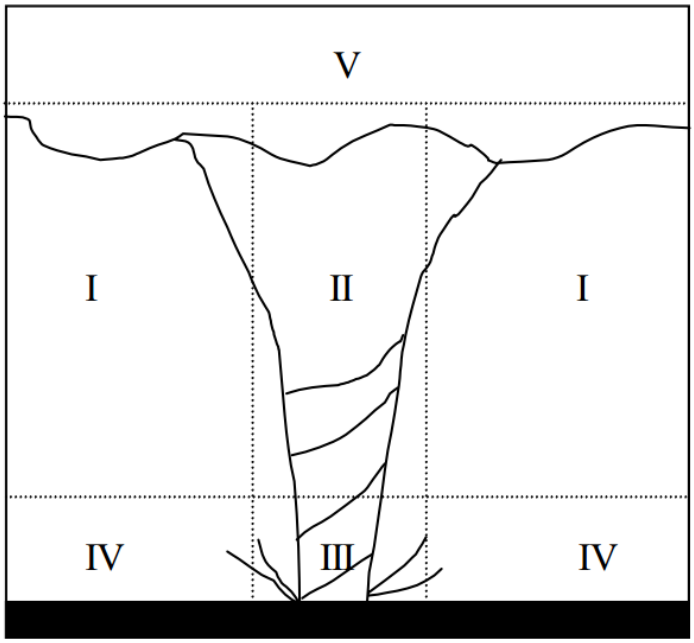

Figure 2.5: Conceptual model of the flow regimes associated with a tornado (from Wurman et al. 1996)

2.7 Tornado-wind speed and path characteristics

2.7.1 Wind speed of a tornado based on post-damage research

Tornado- wind speed is the most significant parameter. The wind speed of a tornado is in a straight line relation to the damage intensity of the damage. Fujita, (1971) developed a scale for evaluation the tornado intensity. The maximum tornado wind velocity is provided based on intensity of experiential damage. The intensity of tornadoes is defined according to the Fujita Scale (or F scale), which ranges from F_0 to F_6 as outlined below. The Fujita scale categorizes tornadoes according to the tornadoes' damage. Approximately half of all tornadoes are the F_1category that cause moderate damage. These tornadoes arrive at speeds of 73-112 mph and can turn over mobile homes and automobiles, uproot trees, and rip off the roofs of houses. About one percent of tornadoes are the F_5 category that causing incredible damage. With wind speeds in excess of 261 mph, they are capable of lifting houses off their foundations and hurling them considerable distances. The Fujita part of the scale is shown in Table 2.1. These wind speed

numbers are guesses and have never been scientifically verified. Different wind speeds may cause similar-looking damage from place to place even from building to building. Without a methodical engineering analysis of tornado damage, the actual wind speeds of the tornado damage are unknown.

Table 2.1 Fujita Tornado Damage Scale

Scale	Wind Estimate (MPH)	Typical Damage
F_0	< 73	Light damage: Some damage to chimneys; branches broken off trees; shallow-rooted trees pushed over; signboards damaged.
F_1	73-112	Moderate damage: Peels surface off roofs; Mobile homes pushed off foundations or overturned; moving autos blown off roads.
F_2	113-157	Considerable damage: Roofs torn off frame houses; mobile homes demolished; boxcars overturned; large trees snapped or uprooted; light-object missiles generated; cars lifted off ground.
F_3	158-206	Severe damage: Roofs and some walls torn off well-constructed houses; trains overturned; most trees in forest uprooted; heavy cars lifted off the ground and thrown
F_4	207-260	Devastating damage: Well-constructed houses leveled; structures with weak foundations blown away some distance; cars thrown and large missiles generated
F_5	261-318	Incredible damage: Strong frame houses leveled off foundations and swept away; automobile-sized missiles fly through the air in excess of 100 meters (109 yds); trees debarked; incredible phenomena will occur.

A team of meteorologists and wind engineers (2007) made an update to the the original F-scale, to be implemented. The Enhanced Fujita Scale was accepted in 2007, which provides an improved association between the tornado damage and its maximum wind speed (NOAA, 2012). The comparison of the two scales is included in Table 2.2. The Enhanced F-scale still is a set of wind estimates (not measurements) based on damage.

Table 2.2 Comparison of wind speeds between tornado EF-scale and F-scale (NOAA, 2012)

FUJITA Scale			Derived EF Scale		Operational EF Scale	
F Number	Fastest 1/4-mile (mph)	3 Second Gust (mph)	EF Number	3 Second Gust (mph)	EF Number	3 Second Gust (mph)
0	40-72	45-78	0	65-85	0	65-85
1	73-112	79-117	1	86-109	1	86-110
2	113-157	118-161	2	110-137	2	111-135
3	158-207	162-209	3	138-167	3	136-165
4	208-260	210-261	4	168-199	4	166-200
5	261-318	262-317	5	200-234	5	Over 200

2.7.2 Tornadoes and tornado-related deaths

Fujita Scale Class presents the following pie charts of all tornadoes and tornado-related deaths from 1950 to 2012. The majority of tornadoes, which are either weak without damage or weak with damage, are illustrated in Figure 2.6. Fortunately, only a small percentage of tornadoes are recorded as violent. Figure 2.7 illustrates that although aggressive tornadoes are a small percentage of tornadoes, they cause an extremely high percentage of tornado-related deaths.

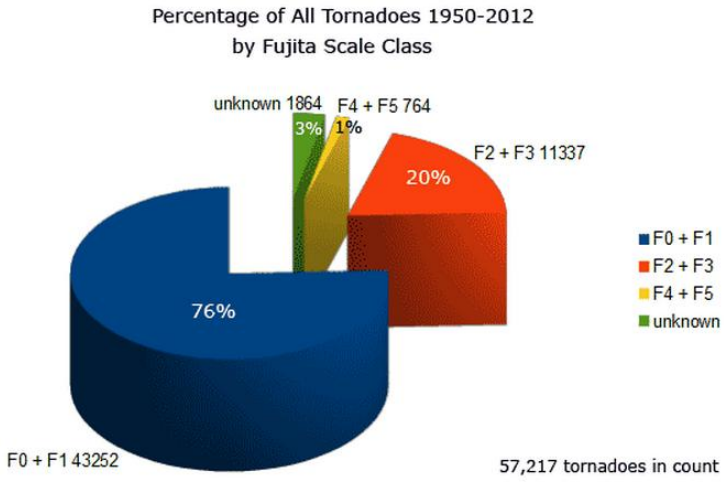

Figure 2.6: The percentage of all tornadoes 1950-2011

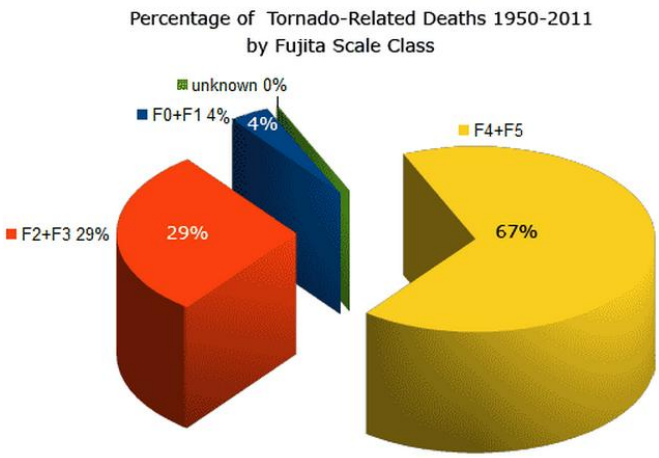

Figure 2.7: The percentage of tornado-related deaths 1950-2011

2.8 Field observation of tornado interacting with dome type of structures

Monolithic Dome Construction (2013) reported that several dome houses survived after they were hit by tornadoes. In one instance, in Moore, OK (2013) a tornado destroyed more than 1700 homes. In the middle of this destruction, a concrete dome building survived as shown in Figure 1.2a. In another instance, a concrete dome house was hit by an EF4 or EF5 tornado in the Blanchard, OK (2011). That dome shell survived although it was badly damaged by heavy, flying debris as shown in Figure 2.8. The same tornado hit another dome house shown in Figure 2.9, which was built in 1981 by an independent builder who did not follow monolithic specifications. This dome house suffered light damage, losing some windows and a skylight. Whereas, the conventional homes hit by this tornado were destroyed. Furthermore, a satellite image shows the dome house one year before and after the tornado. The tornado destroyed all the trees around and to the east of the dome house while the dome house was left standing as shown in Figure 2.10.

Figure 2.8: A dome hit by a tornado on May 24, 2011 in Blanchard, OK (Josh South)

Figure 2.9: A dome hit by a tornado in Blanchard, OK (Josh South)

(a) (b)

Figure 2.10: A dome was hit by tornado on May 24, 2011 in Blanchard, OK (a) before the tornado and (b) after the tornado (Google earth).

The New Age Dome Construction (NADC, 2015) reported that a wood dome house shown in Figure 2.11 survived after it received a direct hit from an EF5 tornado. They also reported that another dome house, shown in Figure 2.12, survived after it was hit by an EF5 tornado in West Jefferson County, NC (1998). Furthermore, a dome and box homes were hit by an EF4 tornado in Jacksonville, Texas. The dome house survived, and the box homes were destroyed by the tornado even though the tornado hit the dome home house first before passing onto the box homes. This damage is shown in Figure 2.13. From these observations, one can say that shape may reduce the forces on a structure.

Figure 2.11: A dome built by New Age Construction hit by an EF5 tornado (NEW AGE dome)

Figure 2.12: A dome house hit by an EF5 tornado in West Jefferson County 1998 (AGE dome)

Figure 2.13: A dome hit by a tornado in Jacksonville Texas (AGE Dome)

2.9 Straight Line wind on structures

2.9.1 SL wind on conventional structures using wind tunnel testing and a CFD model

Wind tunnel testing of common building models dates back to the end of the nineteenth century. Jensen and Frank (1965) established the boundary layer wind tunnel to set up building standards. In addition to Jensen and Frank, a number of researcher, such as Stathopoulos and Mohammadian (1986), Holmes (1986), Krishna (1995), and Meecham et al. (1991) studied the wind loads for low-rise buildings.

Ahmad and Kumar (2002) studied the effect of structures' geometry on wind pressures for hip-roofed building models with a roof pitch of 30º and different overhang ratios. They found that the windward edges, corners and the hip ridge near this corner have a very high pressure. Endo et al., (2006) investigated a Texas Tech University building model at a geometric scale of 1:50 under simulated atmospheric boundary layer conditions. In that study, the external point pressures at the mid-plane and roof corner pressures were investigated for a wider range of the wind. For the mid-plane locations, they found a correspondence between full-scale pressures and the model. Ho et al. (2005) stated that the sharper roof slope leads to a significant drop in force.

Their results indicated similar aerodynamic behavior for roof slopes less than 10º ±. However, significant changes were recorded for roof slopes between 10º and 20º.

Cope et al. (2005) studied the effects of pressure fields on the roof panels of low-rise gable-roof buildings. They found that the mean pressure coefficient on the windward roof portion was higher for lower pitched roof models. Ginger and Letchford (1999) conducted similar observations on low-rise gable-roof buildings. Wagaman et al. (2002), Gao and Chow (2005), and Richards and Hoxey (2006) investigated the flow separation over cubes. Prasad et al. (2009) studied the wind loads on low-rise building models with different roof configurations. They found that the wind load produces higher pressure on a flat roof than the 45º gable and hip-roofed building models, about 85% and 91 % more, respectively. Furthermore, the pressure on hip-roofed models was less than on gabled models by about 42%.

Gloria et al. (2005) presented the results of wind tunnel model tests for pressure distributions for irregular-plan shapes (L- and U-shaped models). The results for both shapes showed different wall pressure distributions that those for single rectangular blocks. They also used a CFD model to provide a better understanding of the flow around these irregular-plan models and of the pressure distributions induced on models faces.

2.9.2 SL wind on dome structure using wind tunnel testing and CFD model

Many wind tunnel studies have been undertaken to determine wind loads on domes and hemispheres in boundary layer flows. Maher (1965) investigated a dome structure for a straight-line wind without much inflow turbulence. Then, Taniguchi & Sakamato (1981), Toy et al. (1983), Newman et al. (1983), and Savoy & Toy (1986) included a turbulent shear flow over a range of Reynolds numbers. Only, Ogawa et al. (1991), Taylor (1991) and Letchford & Sarkar (2000) presented measurements of fluctuating pressures on a dome model. Furthermore,

Letchford & Sarkar (2000) reported the dual dome mean, rms and peak pressure contours and loads.

The CFD model has been widely used to predict wind flow around bluff bodies in wind engineering. Few studies focus on the CFD simulation of the wind load on dome buildings. Meroney et al. (2000) compared the numerical and wind tunnel simulation of mean pressure distributions over single and paired dome sets. Chang and Meroney (2001) also examined the effect of surroundings with different separation distances on surface pressures on low-rise dome buildings in wind tunnel and CFD models. Horr, et al. (2003) used the CFD analysis to create a computational wind tunnel to compute the pressure load on large domes. Sevalia et al. (2012) studied the effects of wind on tall structures under different geometric plan configurations having the same plan area. These buildings were modeled using CFD and then a comparative study was done. A common finding is that wind pressure coefficient is the maximum in the case of a square plan shape, and pressure coefficient is the minimum in the case of a circular plan shape. Numerical simulation produces higher overall forces on square plan shape than circular plan shape, about 180% more in z-direction.

Thus, a lot of work has been done with significant improvements in experimental techniques. With the help of better instrumentation, accurate measurements can be performed that enhance understanding of the flow structure and help design buildings with better configurations that can withstand strong winds. However, the relationship between a dome and a cubic or prism model, considering height, surface area or volume, has never been clearly stated.

2.10 Tornado wind field models

Early research on the effects of tornadic winds on structures can date back to 1970 (Mehta et al., 1976). In-site measurements of tornadic winds around the structure (near the

ground) are valuable to obtain the actual wind effects. However, it is very challenging to obtain the in-site measurements (Wurman et al., 2013). Therefore, researchers started to study the tornadic wind fields and wind effects on structures in laboratory tornado simulators or using CFD.

2.10.1 Tornado experimental (Wind Tunnel) models

In this section, wind tunnel work is discussed to demonstrate the current state of knowledge to study tornado-structure interaction. Several tornado simulators have been created in the last four decades. Ying and Chang (1970) made the first tornado simulator that is shown in Figure 2.14. Then, Ward (1972) created another tornado simulator similar to Ying's model. However, the inward flow height, exhaust fan speed and the diameter of the rising air column in the Ward model are changeable. In addition, at the top opening of the chamber, Ward introduced a new technique to represent the atmosphere condition. The Ward model is illustrated in Figure 2.15. This model becomes the standard referable model by almost all the other new models. Davis-Jones (1973) re-analyzed the Ward's output and concluded that it is not important to have huge radial inflow momentum to produce the vortex; however, it is necessary to have high volume flow rate for certain swirl ratio. Church et al (1977) at Purdue University used the Ward model with modifications, which are depth of the inflow, the radius of updraft opening, updraft flow rate and the tangential velocity. This is model is shown in Figure 2.16.

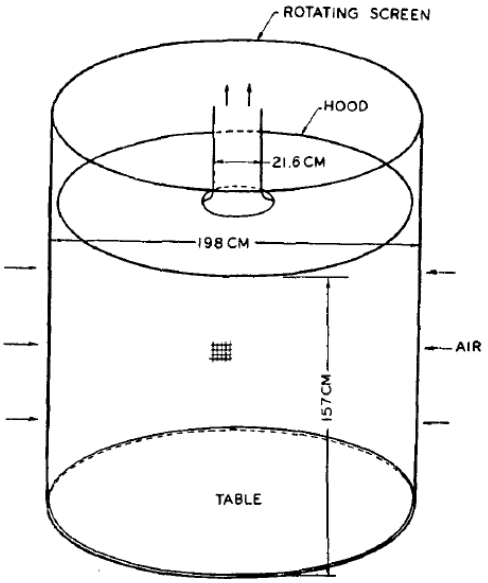

Figure 2.14: Schematic illustrations for Ying and Chang's apparatus (Ying and Chang, 1970)

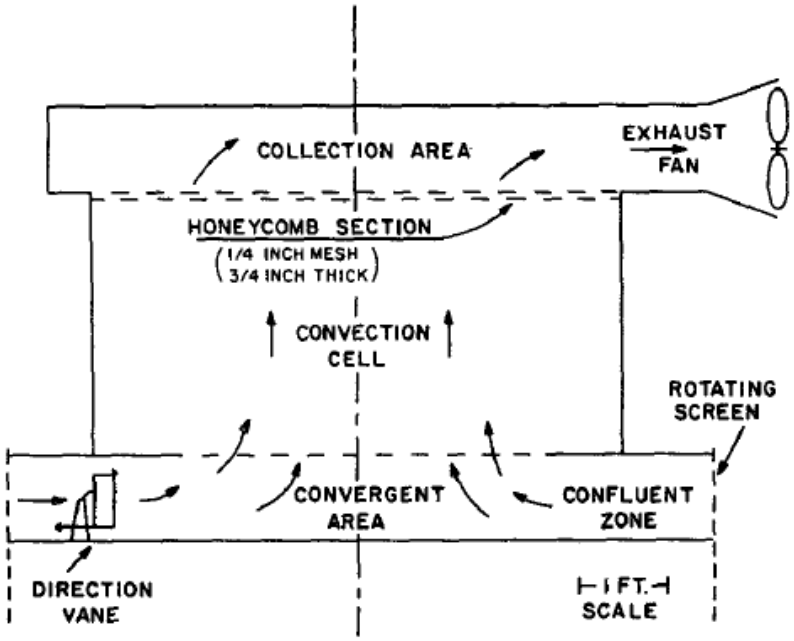

Figure 2.15: Schematic of Ward's (1972) apparatus (Davis-Jones, 1973)

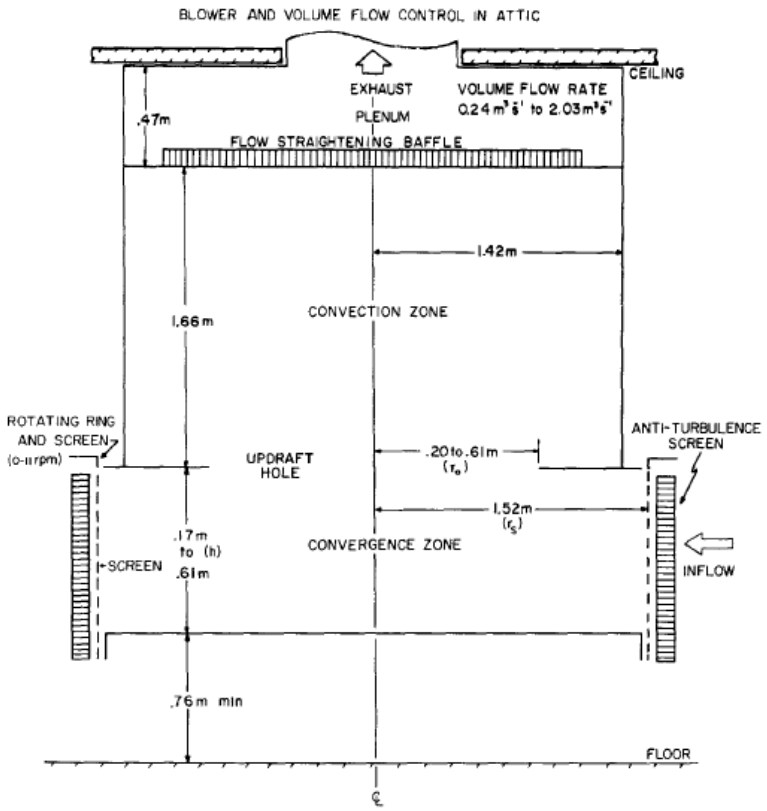

Figure: 2.16: Purdue University simulators schematic section (Church et al., 1977)

Besides the previous Ward-type tornado simulator and its updated versions the recently developed simulations in North America are located at Iowa State University (ISU), Texas Tech University (TTU) and Western University (WU). The ISU and TTU simulators are shown in Figure 2.17 and 2.18, respectively. Using the tornado simulator at ISU, the wind flow around a one-story, gable-roofed building in tornado-like winds (Hu, 2011) and the wind effects on this structure (Haan et al., 2010) have been studied. That showed the tornado-induced lateral forces were about 50% larger than those by ASCE 7-05 and the tornado-induced vertical force (uplift) were two or three times as large as those by the provision. The tornado forces on buildings reported in previous studies are summarized in Table 2.3. Other similar research can be found in (Chang, 1971; Bienkiewicz et al., 1993; Fouts et al., 2003; Mishra et al., 2008). Using a Ward type tornado simulator at Tokyo Polytechnic U (a Ward type), an experimental investigation was

conducted to gain a better understanding of the effect of building location with respect to the tornado center (Rajasekharan et al., 2013), and the effect of ground surface roughness on the internal pressures developed inside a building model (Sabareesh et al., 2013).

Using the capability of generating translating tornado-like winds in the tornado simulator at ISU, the influence of the translating speed on wind effects was investigated through a gable-roof, cubic and tall building. It showed that a lower translating speed induces greater wind loading on the structure than a higher one (Sarkar et al., 2006, Sengupta et al., 2008, and Case et al., 2011). They reported that a lower translating speed induces greater wind loading on the structure as shown in Table 2.3. Haan et al. (2010) also found that the translation speed of a tornado plays an important role in the nature and magnitude of the aerodynamic forces acting on low-rise buildings in tornadoes. The magnitudes of the forces were found to be larger for slower translation speeds. It was also found that for faster translation speeds, the entire time history shifted with respect to the x axis that measured the distance of the center of the vortex to the center of the building model and was normalized with the diameter of the core of the vortex (x/D) (Haan et al., 2010). The V_θ/V_t ratio reported in recent studies that have measured the wind loads on low-rise buildings in simulated tornadoes is about 10 or greater, which is larger than the field observation ratios. The V_θ/V_t ratio average from real tornadoes has been reported to be from 1.0 to 8.0 (Ahmed and Selvam (2016). Therefore, the influence of V_θ/V_t ratios on the tornado force coefficient for a cubic, prism and dome buildings were compared with systematic study. The V_θ/V_t ratios were considered to be 1, 3, 6 and 8 for comparison. These ratios were very much in agreement with field observation ratios.

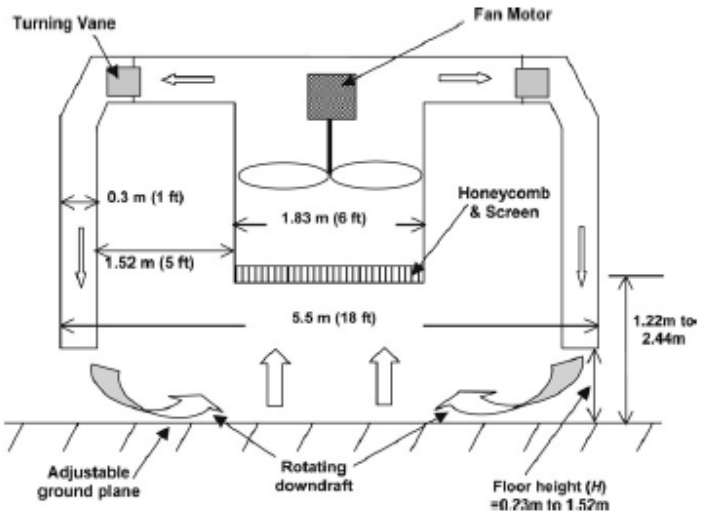

Figure 2.17: Iowa State University tornado simulator (Sarkar et al., 2006)

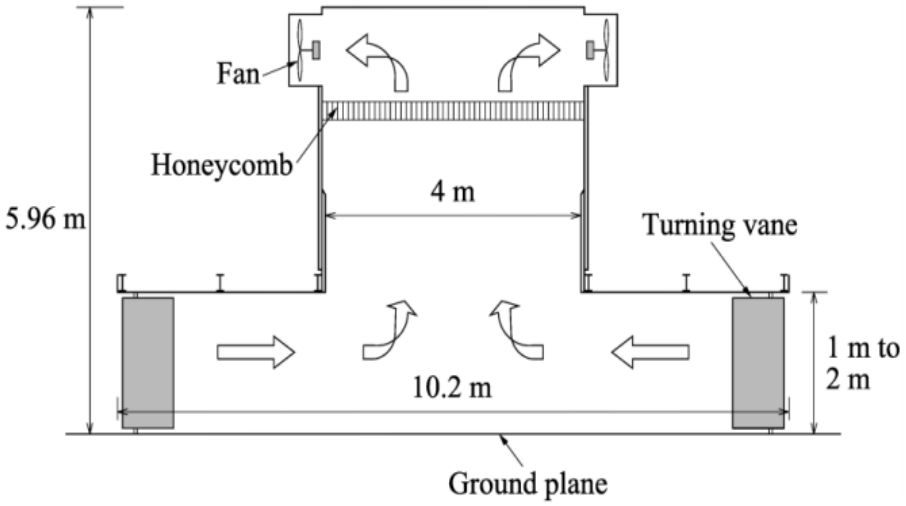

Figure 2.18: Texas Tech University Simulator (Tang et al., 2016)

2.10.2 Tornado-structure interaction using computer model

CFD simulation has also been employed to simulate the tornadic wind field and determine the wind effects on structures. The CFD modeling of tornado flow over structures has developed in the last four decades due to great advancement in computer software and hardware. Tornado computer models are utilized for different interests (e.g. meteorological and civil engineering studies). A tornado has been modeled as a stationary vortex, as well as translating

vortex without any interaction with structures for studying tornado outbreaks and tornado characteristics. In this section, the interaction of a tornado with structures is reported.

CFD simulation has been employed to simulate the tornadic wind field and determine the wind effects on structures. Selvam (1985) established potential flow simulation around 2D sections. The mathematical model was Rankine Combined Vortex Model (RCVM). The time dependent boundary conditions are reported in detail in Selvam (1985). Then, Selvam (1993) applied the RCVM model to study flow around the Texas Tech building using k-ε model. In this model, the boundary layer effect is included by varying the wind field with a logarithmic profile. There were some difficulties in applying proper boundary conditions using k-ε model. To alleviate this problem, Selvam and Millett (2003 and 2005) employed a large eddy simulation as turbulence model and obtained reasonable results for flow around a cube. They concluded that the translating tornado produced about 100 % force on the roof and about 45 % more on the walls compared to wind loads. Ishihara et al. (2011) investigated how the swirl ratio affects the shapes of the generated tornado with a large eddy simulation (LES) to model turbulence. Alrasheedi and Selvam (2011) investigated the tornado impact on buildings with different plan area sizes using the CFD model, presented by Selvam and Millet (2003). They reported that tornado force coefficients on buildings, which have a much wider plan area than the tornado radius, are similar to the straight boundary layer wind force coefficients. Ragan et al (2012) and Selvam and Gorecki (2012) studied an influence of the different ratios for tornado size to circular cylinder size on the tornado forces. They found that tornado forces depend on the size of the building. When the building size decreases, comparing to the tornado size, the forces increase. The study was conducted up to ratio of a 30:1. They concluded that the tornado forces tend to be constant when tornado to cylinder ratio is more than 18:1. Although the aforementioned studies

are about vortex-structure interaction in 2D, they reveal the effect of structure size on tornado forces. Strasser and Selvam (2015) studied the influence of relative vortex-to- circular cylinder size on structural loading. They used 2D simulation to study the force coefficients around circular cylinder for vortices having radii of 1·D to 100·D. They concluded that the vortex no longer influences maximum force coefficients on cylinder when $r_{max} \geq 20D$; however, force coefficients do not reach their asymptotic value until $r_{max} \geq 50D$. Where r_{max} and D are critical radius for the vortex and diameter of the cylinder, respectively.

Selvam and Gorecki (2013) and Ahmad (2015) also used the modified version of a CFD model, reported by Selvam and Millet (2003), to study the interaction between a tornado and a longitudinal hill. They found that the hill creates a sheltering region on the hill leeward side. Ishihara et al. (2011) investigated how the swirl ratio affects the shapes of the generated tornado with large eddy simulation (LES) to model turbulence

Zhao et al. (2016) studied the flow and pressure around a dome due to SL and tornado wind by moving the dome. They moved the dome with the dynamic mesh method and at each time step they deformed the mesh and generated or eliminated elements. In this simulation, the building can be moved only in the allowed region of vortex chamber. They concluded absolute maximum pressure and vertical force coefficients induced by tornadic winds are found to be 2.4 and 2.7 times as large as that induced by SL winds, respectively. However, the lateral force coefficient (in the x-direction) induced by the tornadic winds is 6 times as large as that induced by the SL winds. Only one V_θ/V_t ratio has been considered for the studies and is reported in this subsection as shown in Table 2.3.

Table 2.3: Summary of studies on the influence of the tornadic wind fields on structures

Reference	*Vθ/Vt*	Building Shape	Model	*Cx*	*Cy*	*Cz*
Sarkar et al. (2006)	35	Tall Cube	Exp.	2.01	2.01	1.77
	18			1.78	1.78	1.66
Case et al. (2011)	78	Gable roof	Exp.	0.75	1.20	2.4
	26			0.70	1.00	2.0
Sengupta et al. (2008)	40	Cube	Exp.	1.97	1.97	1.24
	20			1.82	1.82	1.22
Sengupta et al. (2008)	40	Tall Cube	Exp.	2.17	2.17	1.54
	20			1.75	1.75	1.78
Sengupta et al. (2008)	40	Tall Cube	Num.	2.01	2.01	1.77
	20			1.78	1.78	1.66
Sengupta et al. (2008)	40	Cube	Num.	1.57	1.57	1.09
	20			1.4	1.4	0.98
Hana et al. (2010)	80	Gable roof	Exp.	1.1	1.2	3
Hu et al. (2011)	18	Gable roof	Exp.	0.9	0.7	2.8
Yang et al. (2011)	24	Tall cube	Exp.	2.0	0.4	0.7
Selvam et al. (2005)	2	Cube	Num.	0.82	1.36	1.81
Zhao et al. (2016)	10	Dome	Num.	0.69	0.13	0.52

2.11 Summary of the reviewed works

From field observation, one can say that the dome shape may reduce tornado forces, and substantial work has been done on the aerodynamics of buildings. For a regular straight wind, wind tunnel and CFD simulation are used to calculate wind force and pressure on various building shapes. For a tornado wind, the interaction between a traveling tornado and various buildings is not yet thoroughly understood. Numerical and experimental tornado simulators are employed to compute tornado force coefficients on a building (e.g. circular cylinder, gable-roofed, cubic building). However, little attention has been paid to study the tornado force on a dome structure even though it was reported that dome buildings survived after tornadoes. Despite the research reported in recent studies, the wind effects of tornadoes on a dome building has not been sufficiently explored, which justifies the necessity of the research in this study.

CHAPTER 3: COMPUTER MODELING

3.1 Introduction

Since tornado-structure interaction is a complex phenomenon, CFD in recent years has been studied to clarify and understand this phenomenon. Therefore, The Computational Mechanics Laboratory at the University of Arkansas has been involved in the computer modeling of tornado forces on buildings for more than 30 years. The University of Arkansas (UA) numerical simulator is able to study flow around a building and pressure on the building in detail. The input of UA numerical simulator can be changed for having different tornadoes, structure and strength (intensity), so that it provides chances to study an extensive variety of cases economically. The effect of tornadoes on structures is not well-understood. In these research findings, the building is assumed to be rigid and a model tornado vortex interacts with buildings and structures.

3.2 Development of the UA numerical simulator

The analytical tornado vortex model is used for translating tornadoes. The tornado is described using mathematical equations. Selvam (1985) established potential flow simulation around 2D sections. The mathematical model used was Rankine Combined Vortex Model (RCVM). The time dependent boundary conditions are reported in detail in Selvam (1985). Then, Selvam (1993) applied the RCVM model to study flow around the Texas Tech building using the k-ε model. In this model, the boundary layer effect is included by varying the wind field with a logarithmic profile. There were some difficulties in applying proper boundary conditions using the k-ε model. To alleviate this problem, Selvam and Millett (2003) used a large eddy simulation as turbulence model and obtained reasonable results for flow over a cube. Selvam and Millet (2005) related more a refined grid close to the structure. They applied 1.6

million nodes and the results were still not converging. The grid resolution in the boundary layer of the previous model was unreachable because of the large number of grid points, which resulted limited computing capabilities. Selvam (2010 b) reported the advance study of the appropriate grid refinement, but the work was limited due to the lack of computing and storage systems. Recently, Alrasheedi & Selvam (2011), Gorecki & Selvam (2015), and Ahmad & Selvam (2015) used more than 6 million nodes for a tornado-structure interaction model. For more particulars relating to the evolution of a tornado-structure interaction simulation, readers should refer to Selvam (2008) and Selvam (2010).

3.3 Fluid-structure interaction modeling

The flow around the structure is computed by solving the Navier-Stokes (NS) equations. The turbulence is modeled using LES. Either Finite Element Method (FEM) or Finite Difference Method (FDM) approximates the flow equations. Selvam and Millett (2003 and 2005) have used the FDM code previously to study flow over cubic buildings. This is based on an orthogonal grid system, and it is computationally very efficient. The same code is used to compute the forces around the rectangular prism (Gorecki and Selvam 2015, Alrasheedi and Selvam 2011). The FDM code based on a body-fitted grid system was developed to study flow around a dome, but it had more error in transporting the tornado like vortex. Hence, the FEM code based on a body-fitted grid was developed to study flow around a dome. Ahmad and Selvam (2015) used this numerical model to study the tornado-terrain interaction. They validated this numerical model by comparing the results with experiments. The detail of the equations and methods are documented in the above references. The superiority of FEM to FDM in transporting vortices is reported in Selvam (1998). The FEM code takes more computer time and hence parallel computing is utilized by Ahmad and Selvam (2015). They used single- and multi-processors to find the

optimum number of processors which provide the minimum run time. They concluded that 24 processors provide the minimum run time which is 72 hours for problems with 7.569 million points.

3.4 Vortex flow modeling

The tornado wind field model is a numerical simulation that governs the wind velocities in the geometric domain to represent real life tornadoes, and this simulator also needs to satisfy the Navier-Stokes equations. There are reasonably a quite good number of numerical simulations which represent tornadoes. However, there is a small number of these models satisfying the Navier-Stokes equations (e.g the Rankine Combined Vortex Model (RCVM), Burgers- Rott Vortex (BRV), and Sullivan Vortex (SV)). Millet (2003), Alrashidi (2012) and Strasser (2015) present a detailed comparison of these models.

The wind field model is studied by applying the Rankine Combined Vortex Model (RCVM), which is the simplest computer model that can satisfy the Navier Stokes (NS) equations, as reported in Lewellen (1996). This model consists of two different flow fields, which are the force vortex region and free regions vortex region as illustrated, in Figure 3.1. In the force vortex region where $r \leq r_{max}$, the tangential velocity of tornado V_θ, increases linearly up to radius r_{max}, i.e. $V_\theta = \alpha\, r$ where r is the radius from the center of tornado and α is a constant. In the free vortex region where $r > r_{max}$, the tangential velocity is decreasing inversely to the radius in the region V_θ, varies as $\alpha\, r_{max}^2/r$. In this model, a translational velocity V_t, and the building overlap onto the RCVM wind field in addition to the vertical logarithmic profile to calculate the boundary layer as stated by Selvam (1993). The RCVM model satisfies the conservation equations, so which is why the vortex superposition does not create any anomalies. The vortex is held only in the forced vortex region. Outside the vortex core in the free vortex

region, the RCVM only assigns the horizontal velocities. While the vortex is transported downstream, vertical velocities are developed due to the boundary layer wind profile as reported in Filipone and Afgan (2008) and Gorecki and Selvam (2015).

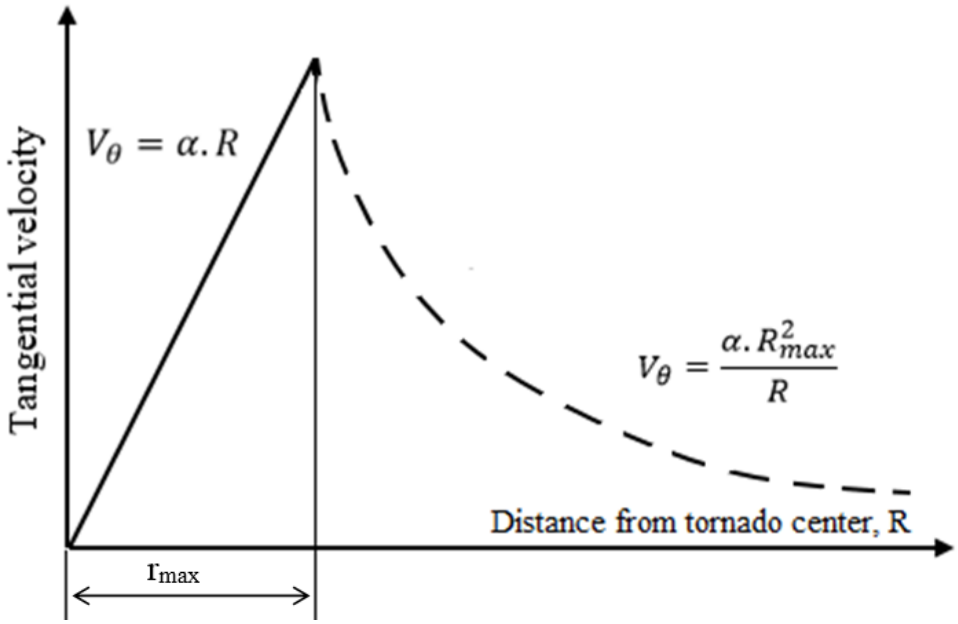

Figure 3.1: Rankine combined vortex model

Large Eddy Simulation (LES) is used to model the turbulence. To simulate tornado travel over a dome building, the computer model solves the NS equations by using the Finite Elements Method (FEM). Even though FEM takes more computer time, the transport accuracy of the vortices is very high, as reported in Selvam (1998), which is needed in this study. The model is parallelized due to the large computing time. More details for FEM can be found in Ahmed (2015). To simulate tornado travel on a prism building, the computer model approximates the NS equations by using the Finite Different Method (FDM) as reported in Selvam and Millet (2003 and 2005). The approximate (NS) equations are resolved using a semi- implicit method as presented in the next section.

3.5 Navier-Stokes equations

3.5.1 For a dome building

To simulate tornado travel over a dome building, the computer model approximates the Navier-Stokes (NS) equations by using the Finite Elements Method (FEM). The NS equations for the incompressible flow used to simulate the vortex flow:

Continuity Equation:

$$U_{i,i} = 0.0 \tag{3.1}$$

Momentum Equation:

$$U_{i,t} + U_j U_{i,j} = -(\frac{p}{\rho} + \frac{2k}{3})_{,i} + \left[(\nu + \nu_t)(U_{i,j} + U_{j,i})\right]_{,j} \tag{3.2}$$

Where:

$$\bar{S}_{ij} = U_{i,j} + U_{j,i} \tag{3.3}$$

$$\nu_t = (C_s h)^2 \left[2(S_{i,j})^2\right]^{\frac{1}{2}} \tag{3.4}$$

$$h = (h_1 h_2 h_3)^{\frac{1}{3}} \tag{3.5}$$

$$k = \frac{\nu_t^{\,2}}{(C_k h)^2} \tag{3.6}$$

Where: U_i, is the mean velocity, p is the mean pressure, V_t is the turbulent eddy viscosity, V_i is the velocity of grid, k is the turbulent kinetic energy, and ρ is the fluid density. The variables h_1, h_2 and h_3 control volume spacing in the x, y, and z directions, respectively. The area or volume of the element is used for the computation of h. A comma represents differentiation, t represents time, and i=1, 2 and 3 refers to variables in the x, y and z directions. The C_s and C_k empirical constants are taken to be, respectively, 0.1 and 0.094, as proposed by Murakami and Mochida (1995). Selvam (1997) found an excellent agreement between flow field over a structure and the LES simulation for the C_s and C_k values proposed by Murakami and Mochida in 1995. In this

work, a procedure is used to solve the unsteady NS equations in which the momentum equation is used to solve velocities; then, the new velocities are used to solve the pressure. The final form of pressure equation is:

$$\Delta p = \frac{\left(\frac{\partial U}{\partial x}+\frac{\partial V}{\partial y}+\frac{\partial W}{\partial z}\right)}{\Delta t} - \left[\frac{\partial\left(U\frac{\partial U}{\partial x}+V\frac{\partial U}{\partial y}+W\frac{\partial U}{\partial z}\right)}{\partial x}+\frac{\partial\left(U\frac{\partial V}{\partial x}+V\frac{\partial V}{\partial y}+W\frac{\partial V}{\partial z}\right)}{\partial z}+\frac{\partial\left(U\frac{\partial W}{\partial x}+V\frac{\partial W}{\partial y}+W\frac{\partial W}{\partial z}\right)}{\partial z}\right] \quad (3.7)$$

Where: *U, V,* and *W* are the velocities in *x, y* and *z* directions, *P* and *Δt* are the pressure over density and the time step, respectively. Here *U, V* and *W* are the velocities in the *x, y* and *z* direction, *P* is the pressure over density and *Δt* is the time step. The velocity equations are solved by line iterations in *x*-, *y*- and *z*- directions. In each time step, the velocities are calculated successively using the implicit method. The iterations are repeated to the convergence value. That value is defined to be IM × JM × KM × 10-5, where IM, JM and KM are number of grid points in the *x*-, *y*- and *z*- directions. The sub-iteration is to check that a converged solution is acquired. The velocities are assumed as undisturbed values in the beginning of the computation. Which is why the sub-iteration is extremely high to decrease the error. The number of sub-iteration could be around 5. The general version of the above procedure is employed by de Sampio et al. (1993) using the least square FEM. The FEM is used to solve the above equations. The FEM is preferred in this study because the transport accuracy of the vortices is very high (Selvam, 1998). Because the FEM takes more computer time, the model was parallelized by making a subdomain in the vertical direction (Ahmad, 2016). The data is transferred from one processor to another using MPI. Sarkar and Selvam (2009) reported the parallel computing in detail. Preconditioned conjugate gradient (PCG) is used to solve the equations. The time step is computed according to the Courant-Frederick-Lewis (CFL) number. The CFL number is kept to less than one. The time step used is about 0.01 time units (0.01 sec). The total of the computer

model is 60 time units which takes 720 hrs. (30days) serial computing (one processor). However, when the distributed parallel computing (24 processor, MPI) is used, the time is reduced ten times to 72 hrs. (3 days). The detail of the parallel computing is reported in Ahmed (2016).

3.5.2 For a cubic or prism building

To simulate tornado travel over a cubic or prism building, the computer model approximates the Navier-Stokes (NS) equations by using the control volume procedure. The equations are solved in time using a semi-implicit method, as suggested by Selvam (1997b). For an approximation of continuity and momentum equations, the four-step development system is utilized:

(1) Solve for Ui from equation (3.2). The diffusion and convection terms are considered implicitly. The pressure is considered on the right-hand side of the equation. For simplicity, here p/ρ is considered as p.

(2) Find new velocities as $U'i = Ui + \Delta t \cdot p,i$ where Ui' is not specified.

(3) Solve for pressure from $p,ii = U'i,i/\Delta t$.

(4) Correct the velocities for incompressibility: $Ui = U'i - \Delta t \cdot p,i$

Step 2 eliminates the checkerboard pressure field when using equal order interpolation for velocity and pressure in the case of a finite difference method. The time step is calculated according to the Courant-Frederick-Lewis (CFL) number. The CFL number is kept to less than one; this gives time step around 0.01 units for most of the computation.

3.6 Problem geometry

The geometry of the dome and cube or prism for this study is illustrated in Figures 3.2(a)-(b). The counterclockwise rotating vortex travels along the *x*-axis with a constant velocity V_t. The vortex flow and free stream of a constant velocity is smoothly introduced into the

computational domain. The two cases of vortex-building interaction are analyzed, namely vortex-dome interaction and vortex-prism interaction. The free stream velocity magnitude and its direction are equal to the translational velocity of the vortex. To have one to one correspondence with respect to height and the projected area in the *z*-direction, the width of the dome and prism are assumed to be 20.0 m and 17.72 m, respectively. The height of dome and prism is assumed to be 10.0 m. Instead of taking the same projected area of the dome and prism, in future study, the same volume of the dome and prism also will be taken. In the current study, the focus is on same projected area in *z*-direction and same height. The numerical computations are conducted based on the non-dimensional value. The height of the dome and prism (*H*) is considered to be the reference value. The width of the dome and the prism (*D*) comes to be 2.0*H* and 1.77*H* in non-dimensional (ND) units. The translational velocity is considered to be the reference velocity and the density of air is set at 1.0 ND unit. Based on the reference value, The Reynolds number Re comes to be $Re=1.2\times10^{6}$.

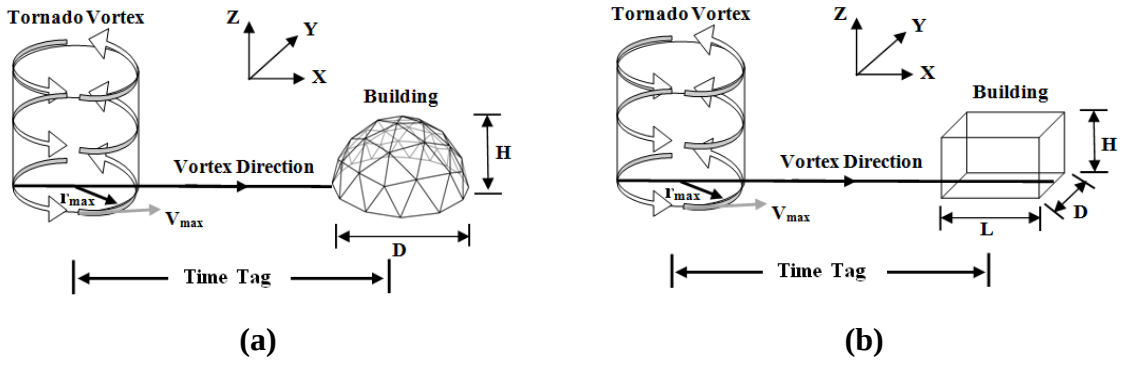

Figure 3.2: Problem geometry (a) Vortex-dome interaction and (b) Vortex-cube or prism interaction

3.7 Boundary conditions

The simulated flow is a consequence of time-dependent boundary conditions utilized over the simulation time on the domain boundaries, as illustrated in Figure 3.3. The building (e.g.

dome and cubic or prism) is located at a reasonable distance from the boundary of the computational domain. The velocities are considered to be zero on the surface of the rectangular prism and hemispherical dome (no-slip condition). The logarithmic law is used to model the boundary layer (Equation 3.10). The grid resolves the boundary layer of the building. Making an allowance for the starting point, both the *x*- and *y*- axis are located at the center of the building, and the *z*-axis is located on the ground. When the center of the tornado overlaps with center of the building, the time *t* is zero. The velocity components in the *x*- and *y*- directions are expressed as follows:

$$\left.\begin{aligned} U(_{x,y,z,t}) &= \left[(V_t - y)\times\alpha\right]z_f && for\ r \le r_{\max} \\ U(_{x,y,z,t}) &= \left[(V_t - y)\times\frac{\alpha r^2{}_{\max}}{r^2}\right]z_{fl} && for\ r > r_{\max} \end{aligned}\right\} \quad (3.8)$$

$$\left.\begin{aligned} V(_{x,y,z,t}) &= \left[(x - V_t t)\times\alpha\right]z_f && for\ r \le r_{\max} \\ V(_{x,y,z,t}) &= \left[(x - V_t t)\times\frac{\alpha r^2{}_{\max}}{r^2}\right]z_f && for\ r > r_{\max} \end{aligned}\right\} \quad (3.9)$$

Because the RCVM does not include any condition for the vertical velocity component, $w = 0$. In Eqs. (3.8)-(3.9), Z_f is applied to form the domain surface boundary layer based on the logarithmic law:

$$Z_f = \frac{u*}{k}\ln\left(\frac{z + z_0}{z_0}\right) \quad (3.10)$$

Where z is the height from the ground, $u*$ is the frictional velocity which is computed from the recognized velocities at known height, z_0, the surface roughness length, is considered to be 0.00375. $\kappa = 0.4$, on boundary faces the normal derivative of pressure is assumed to be zero, $p = 0$. The calculation is made on the orthogonal grid and the RCVM is transported to the Cartesian coordinates as:

$$r^2 = (x - V_t t)^2 + y^2 \quad (3.11)$$

More details about the derivation can be found in Selvam (1995). The NS equations are used for solving the interior velocities and pressures at each time step. The computational domain is a rectangular block with dimensions (L_D = 60.0H) x (D_D = 60.0 H) x (H_D = 45.0 H) units. The numerical computations are managed based on the non- dimensional values. The tornado parameters are stated in Table 3.1. Kosiba et al. (2014) discussed the dimensions of the simulated tornado vortex like tornado. The maximum vortex tangential flow velocity is equal to 3.0 units (30 m/s). The maximum vortex moves with a translational velocity of 1.0 unit (10 m/s). Consequently, the maximum horizontal flow velocity is 4.0 units (40 m/s) which is the sum of the translational velocity and the tangential velocity. The total simulation time is 60 units.

Table 3.1 Tornado Parameters

Units	α	r_{max}	V_t *(trans. Vel.)*	V_θ *(tang. Vel.)*	$V_{max} = V_t + V_\theta$
Non-dimensional	1.0	3.0	1.0	3.0	4.0
S.I. units	1.0 1/s	30 m	10 m/s	30 m/s	40 m/s

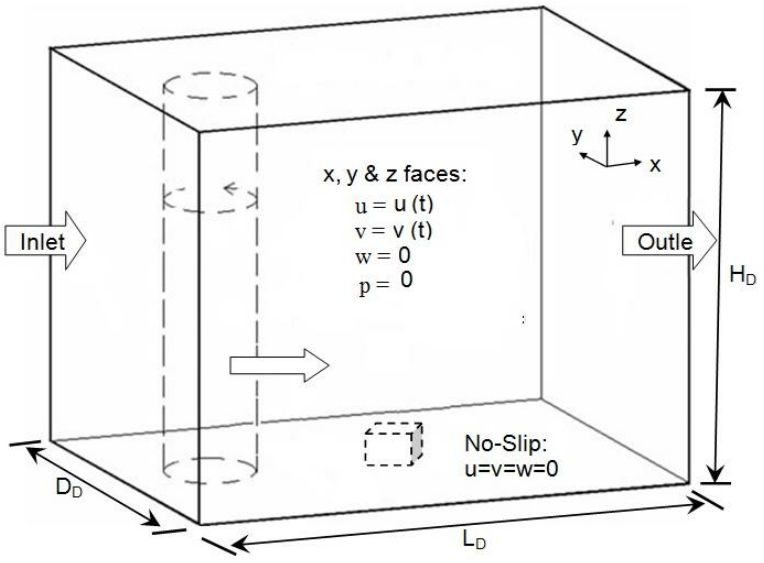

Figure 3.3: Boundary conditions for vortex-structure interaction

3.8 Computational domain size

Gorecki and Selvam (2015) studied the effects of domain dimensions and grid size on the simulation, individually.

3.8.1 Influence of side boundaries on vortex

Gorecki and Selvam (2015) studied the effect of the lateral size of the computational domain effects on vortex. They found that the simulated vortex exhibits similar characteristics in three domains as shown in Figure 3.4. They suggested that a domain width of 50 units (16.7 × r_{max}) is enough to prevent influencing the vortex characteristics. The difference in the minimum pressure drop between the simulations is at most 3%. The same is true with the maximum velocities. This means that the side boundary can be and kept about 8 × r_{max} away from the Rankine vortex center.

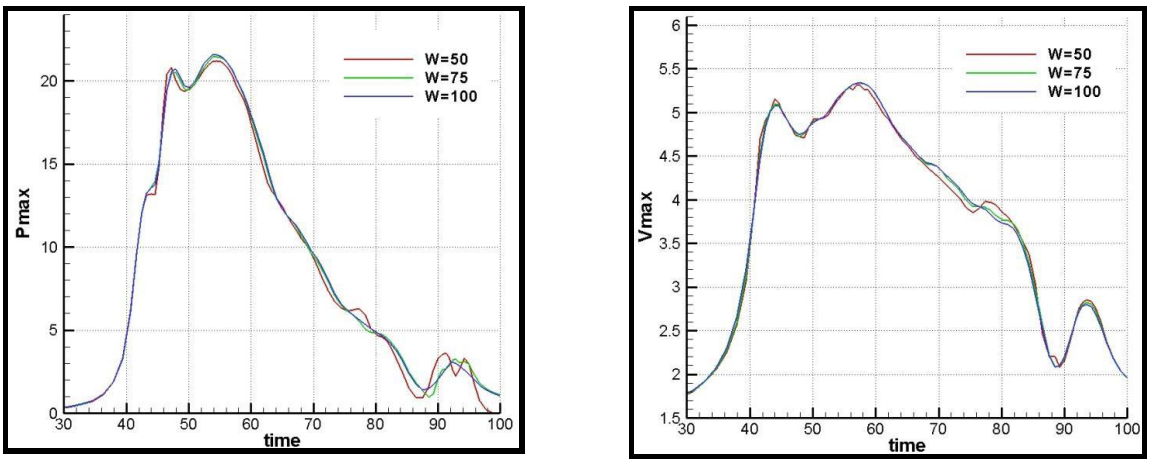

(a) (b)

Figure 3.4: Maximum absolute value of (a) the pressure drop and (b) velocity of the vortex for different widths of the domain (Gorecki and Selvam 2015)

3.8.2 Influence of upper boundary on vortex

Liu and Marshall (2004) noticed the importance of the computational domain height on the CFD vortex simulation, in the blade-vortex interaction (BVI) study. They concluded that the

height should be at least 2 times the blade chord. This was based on the force coefficients calculated on the blade. The Liu and Marshall's (2004) rule relates the size of the domain with the size of the structure (blade). Gorecki and Selvam (2015) also studied the influence of the computational domain height on the vortex as shown in Figure 3.5. They found that a domain height of 45 units is enough to prevent influencing the vortex characteristics. The velocity field most closely resembles the assumed Rankine-combined vortex parameters when the domain height is 45 units for their study. They suggested that the height of the domain must be at least 15 times greater that the vortex core radius (r_{max}) to maintain the vortex maximum velocities.

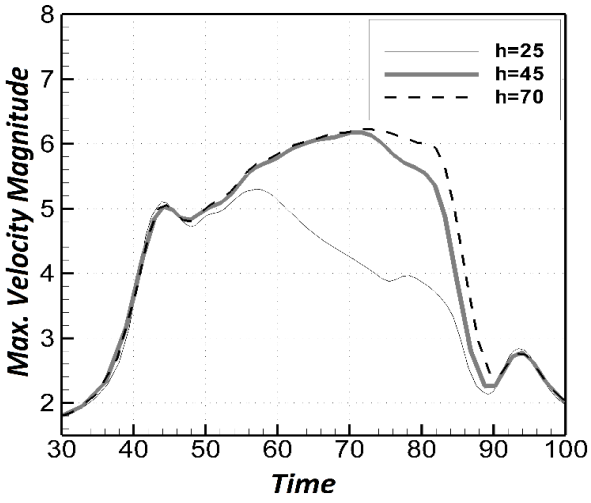

Figure 3.5: Maximum resultant velocity against simulation time for different computational domain heights (Gorecki and Selvam 2015)

3.9 Grid refinement

3.9.1 Grid refinement close to the structure

Selvam and Millett (2005) studied grid refinements near cubic building wall faces. They found that it has significant influence on the tornado forces on a building. The more they refined the grid the greater tornado forces they obtained. They suggested that the finest grid spacing, close to the structure, should be at least 0.005*H*, where *H* is a dimension of a cubic building.

Selvam and Millett (2002; 2003) refined their grid mostly around the building as illustrated in Figure 3.6. The grid spacing increases exponentially away from the cubic building walls. Near the building the grid is very fine. Due to the fluid flow around the building faces, the boundary layer is created close to the structural walls. In this layer, the flow is highly turbulent, which results in the generation of eddies of various sizes. To capture that effect using the large eddy simulation turbulence model (LES), a very fine grid is required. Selvam and Millett (2005) findings are applied for vortex-structure interaction problems.

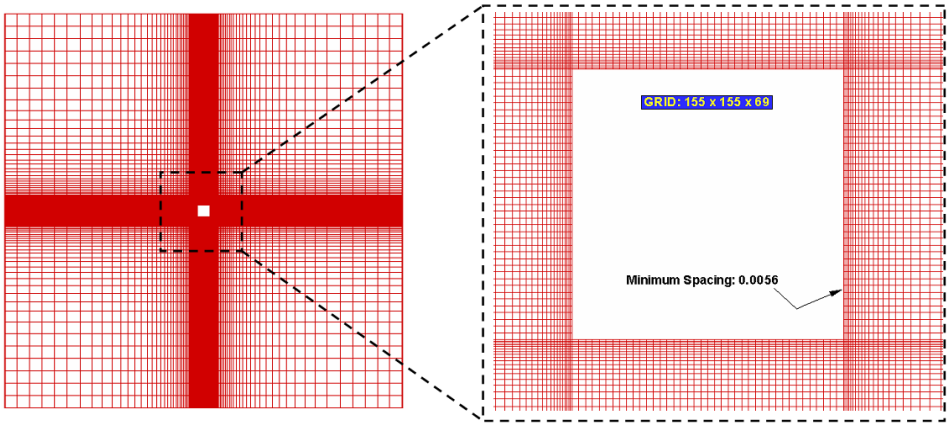

Figure 3.6: Grid refinement in domain and around a cubic building (Selvam & Millett 2003)

3.9.2 Grid refinement in the computational domain

Gorecki and Selvam (2015) studied grid refinement in the domain since the grid in the domain influences the strength of the simulated vortex. Three simulations were utilized to verify the grid size dependence on the simulated vortex. Each mesh is equally spaced in the entire domain. The grid size and the vortex core size are related by the ratio Δ/r_{max}, where Δ is a fine grid in the domain and r_{max} is the vortex core size. The finest grid includes 24 points across the vortex core. The computational resources limited refinement of the grid. They found that the finest grid (Δ/r_{max}= 0.083) produces the most accurate vortex parameters as shown in Figure 3.7.

The maximum tangential velocity is about 1% greater than the assumed. The simulated vortex core is 3% thinner than the assumed RCV model.

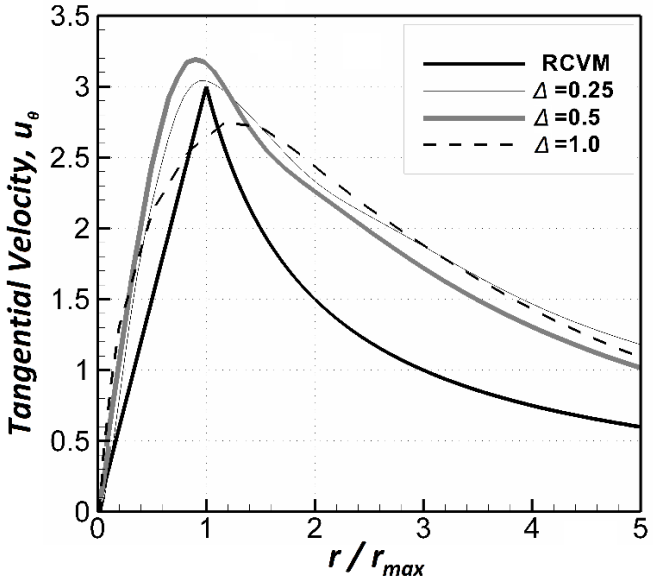

Figure 3.7: Tangential velocity distribution for different grid sizes (Gorecki and Selvam 2015)

3.9.3 Grid refinement on the vortex path

Gorecki and Selvam (2015) also investigated grid refinement on the vortex path. They found that the total number of grid points in the domain could be reduced by applying fine mesh only on the $6 \times r_{max}$ path of the vortex travel, where the high velocity gradients exist. This reduces the total number of the nodes by more than 30%, as shown in Figure 3.8.

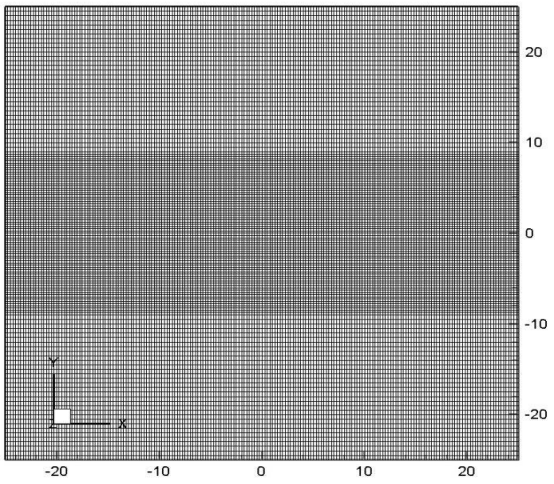

Figure 3.8: Grid refinements in any *xy*-plane (Gorecki and Selvam 2015)

3.10 Conventions used to present the data

The overall forces acting on the model were calculated by integrating the surface pressures. All force coefficients for the tornado cases were normalized using the respective maximum tangential velocity of a tornado and the area of the side or top face of the model as illustrated in Figure 3.9. The coefficients were calculated using the following equations where A_x and A_y is the projected areas in the *x and y* direction and A_z is the project area in the z direction:

$$Cx = \frac{F_x}{\left(0.5\rho V^2 A_X\right)} \tag{3.12}$$

$$Cy = \frac{F_y}{\left(0.5\rho V^2 A_y\right)} \tag{3.13}$$

$$Cz = \frac{F_z}{\left(0.5\rho V^2 A_z\right)} \tag{3.14}$$

$$Cp = \frac{\Delta p}{\left(0.5\rho V^2\right)} \tag{3.15}$$

Where *Cx*, *Cy* and *Cz* are the computed force coefficients in the *x*, *y*, and *z* respectively. *Fx, Fy* and *Fz* are respective forces in *x*, *y*, and z directions, ρ is the density of air, *V* is the reference

velocity and v is the kinematic viscosity of air. Cp is the mean pressure coefficient, Δp is the pressure difference, and P - Pref (Pref is equal to 0.0). The reference velocity in the tornado wind field is the maximum velocity, which is equal to V_θ+V_t. By integrating the pressure in each direction on the surface, the forces are computed.

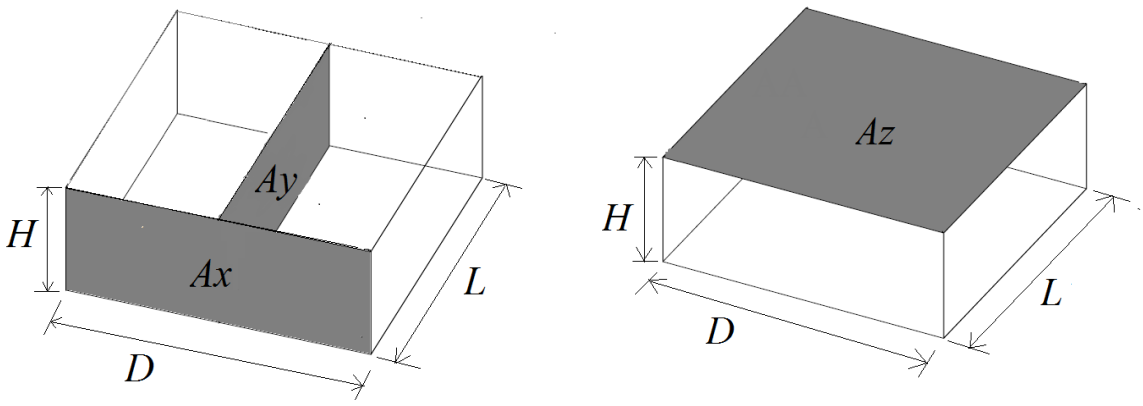

Figure 3.9: A_x and A_y are the projected area in the x and y-directions, A_z is the projected in z-direction

3.11 Summary and discussion

In the CFD vortex-structure simulation, the parameters of the simulated vortex and those applied in the boundary conditions are assumed to be similar to Selvam and Millet (2005) and Liu and Marshall (2004). The force and pressure coefficients are calculated using the maximum velocity at the height of the building ($V_{max} = V_t + V_\theta$). The dissipative and the convective effects change the vortex structure and strength over the simulation. Those effects are dependent on the quality of the computational domain grid and dimensions. Unless a properly resolved grid is used, the dissipative and dispersive error in modeling the convection term will be high. The simulations presented in this section are similar to those conducted by Gorecki and Selvam (2015). They verified the influence of the domain and mesh on the simulated vortex. The computational domain is a rectangular block with dimensions (L_D = 60.0H) x (D_D = 60.0H) x (H_D

= 45.0H) units. They suggested that the fine grid spacing of 0.25H is applied only on the 6 × r_{max} wide lane on the vortex path and around the dome and prism. Outside the path the grid spacing is equal to 0.5H. The dome and prism boundary layer is resolved by fine grid refinement. The first grid spacing next or close to the dome and prism buildings is assumed to be 0.0055H as suggested by Selvam and Millet (2005). Where, H is a structure's height, the computational grids for the dome and prism models in xy-plane are illustrated in Figs. 7(a)-(b).

The time step is kept in such a way that the CFL number is less than one. The time step is in the range of about 0.001 units. The velocity equations are solved by line iterations in the x-, y- and z-directions. In each time step, the velocities are calculated successively in the implicit method. The iterations are repeated to the convergence value. That value is defined to be IM × JM × KM × 10^{-5}, where IM, JM and KM are the number of grid points in the x-, y- and z-directions. The computation of the vortex-prism interaction takes about 20 days to conduct a single simulation for about 6.2 million grid points. The computation of the vortex-dome interaction takes about 5 days using 24 processors for approximately 7.5 million grid points. The output file is about 1.4 GB per time step. More details about parallel computing can be found in Ahmad and Selvam (2015).

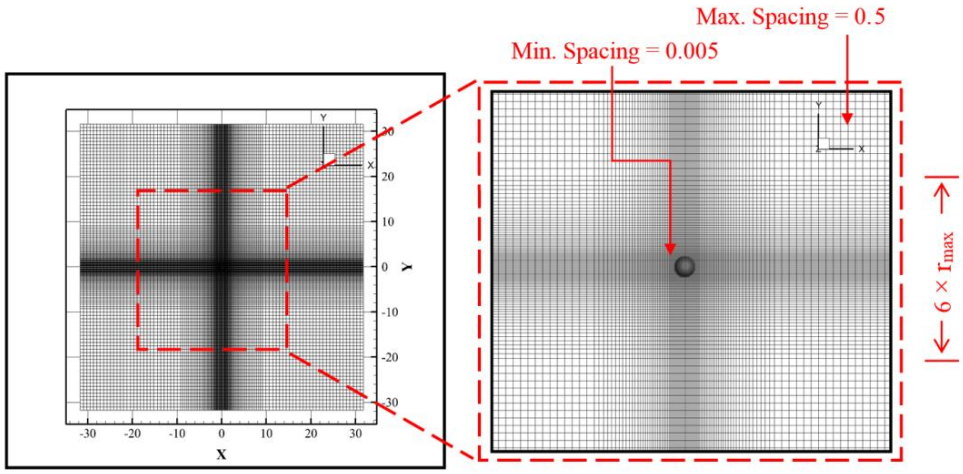

(a)

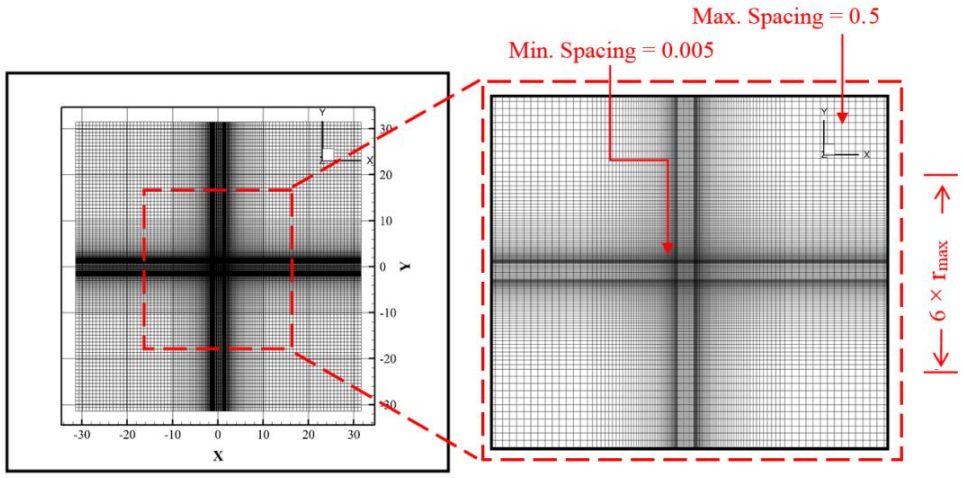

(b)

Figure 3.10: Computational grid in x-y plane (a) Vortex– dome building interaction and (b) Vortex-prism building interaction

CHAPTER 4: INVESTIGATE THE EFFECT OF SL WIND ON A DOME, CUBIC AND PRISM SHAPED BUILDINGS, USING ASCE 7-10 PROVISION AND A CFD MODEL

4.1 Introduction

The standards and wind tunnel testing are the tools available to engineers. The wind loading standards have been created based on data and experiments made in wind tunnel testing. For a preliminary design considering the shape of the structure, the wind force on a structure with variation of structural parameters should be known. The relationship between dome, cubic and prism models, considering height, surface area or volume, has never been clearly presented in the literature. First, the wind load on a dome, cube and prism are calculated using the ASCE 7-10 and compared with one another. Then to validate the CFD model, the wind load from the CFD model are compared with the ASCE 7-10 loads.

4.2 Objective

The present study is an effort to compare the influence of SL wind on dome, cube and prisms, primarily based on ASCE 7-10 provisions. Then, the calculated force and pressure coefficients for SL wind are compared with those from CFD to determine if computer model values are relevant to ASCE 7-10. Since it is not possible to have the dome, cubic and prism models with the same height, surface area or volume, height and projected area or height and volume are kept the same for comparison. The dome (DM) is assumed to be the reference model with constant dimensions as described in Table 1.1. The cube (CM2) and prisms (PM3, PM4, PM5 and MP6) consisted of five models with different dimensions: (1) cube and dome with the same height (2) prism and dome with the same surface and height (3) prism and dome with the same volume and height (4) prism and dome the same width and height (5) prism which can fit inside a dome (Table 1.1). The objective includes:

- The effect of SL wind on dome, cube and prism models were compared primarily based on ASCE 7-10 provisions.
- Comparison of the effect of SL wind on dome, cubic and prism models using a CFD model.
- The force and pressure coefficients due to SL wind that are calculated from ASCE 7-10 provisions are compared with those computed from the CFD model.

4.3 Wind loads on dome, cubic and prisms according to ASCE 7-10 provisions

In this section, the procedure for calculating force and pressure coefficients on a dome cubic and prisms using ASCE 7-10 provisions are presented. Then, the calculated coefficients with the main wind force resisting system (MWFRS) provisions and the components and cladding (C&C) provisions are discussed and compared.

4.3.1 Calculation of wind on dome building

Figure 4.1 illustrates the domed roof building used for a house in this example. Building data are as listed in Table 4.1.

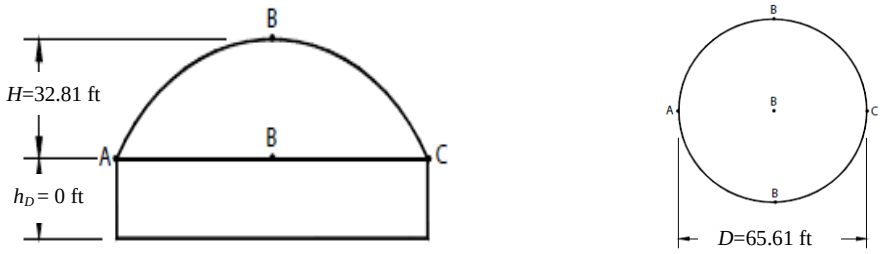

(a) **(b)**

Figure 4.1: Building characteristics for domed roof structure

Table 4.1 A dome building data

Model #	Unite	Dimensions	Plan area (A*x*-A*y*	Proj. area (*Az*)	Volume (*V*)
Model 1 (DM1)	m	*D* = 20, *H* = 10	157	314	2094
	ft	*D* = 65.61, *H*= 32.81	515.09	1030.18	6870.08

4.3.1.1 Analytical Procedure of model 1

Domed roofs are outside the scope of the Envelope Procedure of ASCE 7-10 since the roof shape does not comply with the restrictions of that procedure; therefore, the Directional Procedure of chapter 27, part 1, is used.

4.3.1.2 Building classification

Residential buildings can be in Risk Category II according to Table 1.5-1 of the Standard. The wind speed map associated with this risk category is Figure 26.5-1A of the Standard. The wind speed map for this Category of building is in Figure 26.5-1A of the Standard.

4.3.1.3 Basic wind speed

Selection of the basic wind speed is addressed in Section 26.5.1 of the Standard, and the wind map for Category II buildings is Figure 26.5-1A. The building is assumed to be located in Springdale, Arkansas. Therefore, the basic wind speed V_s = 115 mph (see Figure 26.5-1A of the Standard).

4.3.1.4 Exposure

The building is located in an open terrain area; according to Section 26.7 of the Standard, Exposure *C* is used.

4.3.1.5 Velocity Pressures

The velocity pressures are computed using the following equation:

$qz = 0.00256 \times K_z \times K_{zt} \times K_d \times V_s^2$ psf (Eq. 27.3-1 of ASCE 7-10)

Where:

Wind speed V_s= 115 mph (Figure 26.5-1A of ASCE 7-10)

Topography factor K_{zt} = 1.0 (Section 26.8 of ASCE 7-10)

Directionality factor K_d = 0.85 (for buildings) (Table 26.6-1 of ASCE 7-10)

$q_z = 0.00256\ K_z\ (1)\ (0.85)\ (115)^2 = 28.78\ K_z$ psf

Values for K_z and the resulting velocity pressures are given in Table 4.2.

Table 4.2 Velocity pressures

Height (ft)	K_z	q_z (psf)
0-15	0.85	24.463
20	0.9	25.902
25	0.94	27.053
30	0.98	28.20
32.8	0.987	28.406

4.3.1.6 Domed roof pressures

The roof pressure coefficients for a domed roof are taken from Figure 27.4-2 of the Standard. The height of the dome itself is from the spring line to the top of the dome, H = 32.8 ft. Determine *Cp* for a rise to diameter ratio, H/D = 32.8 /65.6= 0.50. Interpolation from Figure 27.4-2 of the Standard is required. Pressure coefficient values for H/D = 0.50 for points A, B, and C on the dome are given in Table 4.3. Two load cases are required for the MWFRS loads on domes: Cases A and B. Case A is based on linear interpolation of *Cp* values from point A to B and from point B to C (see Figure 4.1 of this guide for the locations of points A, B, and C). Case B uses the pressure coefficient at A for the entire front area of the dome up to an angle θ = 25°, then interpolates the values for the rest of the dome as in Case A.

Case A

For design purposes, interpolate the pressure coefficients at points at 8.2-ft intervals along the dome (see Table 4.4).

Case B

Determine the point on the front of the dome at which θ = 25°. The point is 23.93 ft from the center of the dome; therefore, 8.87 ft from point A. The pressure coefficient at A shall be used for the section from A to an arc 8.87 ft from A. The remainder of the dome pressures is

based on linear interpolation between the 25° point and point B; and then from point B to C (Table 4.5).

Table 4.3 Roof Pressure Coefficients for Domed Roof at $f/D = 0.50$

Point on dome in Figure 4.1	A	B	C
$h_D/D=0$	0.8	-1.2	0.0

Table 4.4 Interpolated Domed Roof Pressure Coefficients, Case A

Case A	Distance (ft)				
Segment	0	8.2	16.4	24.6	32.8
AB	0.8	0.3	-0.2	-0.7	-1.2
	32.8	41	49.2	57.4	65.6
BC	-1.2	-0.9	-0.6	-0.3	0

4.3.1.7 Internal pressure coefficient for domed roof

The building is not in a wind-borne debris region, so glazing protection is not required. The building is assumed to be an enclosed building. The net pressure on any surface is the difference in the external and internal pressures on the opposite sides of that surface:

$p = qGCp - qi\ (GCpi)$ (Eq. 27.4-1 of ASCE 7-10)

For enclosed buildings: $GCpi = +/-0.18$ (Table 26.11-1 of ASCE 7-10)

q_i is taken as q (f) = 28.4 psf

Design internal pressure:

$q_i\ (GCpi) = 28.4\ (0.18) = 5.1$ psf

4.3.1.8 Design wind pressures for domed roof

The design pressures for this building (shown in Figure 4.2) are obtained by the equation:

$p = qGCp - qi\ (GCpi)$ (Eq. 27.4-1 of ASCE 7-10)

Where

$q = q$ (f) = 28.4 psf (see Note 2 of Figure 27.4-2 of ASCE 7-10)

$G = 0.85$, the gust effect factor for rigid buildings and structures

Table 4.5 Interpolated Domed Roof Pressure Coefficients, Case *B*

Case *B*	Distance (ft)				
Segment	0.00	8.87	16.4	24.6	32.80
AB	0.8	0.80	-0.20	-0.70	-1.20
	32.8	41.0	49.2	57.4	65.60
BC	-1.2	-0.90	-0.60	-0.30	0.00

Cp = external pressure coefficient

q_i = *qh* for all surfaces since the building is enclosed

GCpi = +/- 0.18, the internal pressure coefficient for enclosed buildings

p = 28.4 (0.85) *Cp* – 28.4 (+/-0.18) = 24.14 *Cp* +/- 5.1

Values of design pressures for MWFRS are show in Tables 4.6 and 4.7

Table 4.6 Design pressure (psf) Case *A*

Segment	Distance (ft)				
	0.00	8.20	16.40	24.60	32.80
AB	19.31	7.20	-4.83	-16.89	-28.97
	32.80	41.0	49.20	57.40	65.60
BC	-28.97	-21.73	-14.48	-7.240	0.00

Table 4.7: Design pressure (psf) Case *B*

Segment	Distance (ft)				
	0.00	8.87	16.40	24.60	32.80
AB	19.31	19.31	-4.83	-16.89	-28.97
	32.80	41.0	49.20	57.40	32.80
BC	-28.97	-21.73	-14.48	-7.240	0.00

4.3.1.9 Design pressures for components and cladding (C&C)

Design pressure for C&C (Figure 4.3) is obtained by

$p = q_h [(GCp) - (GCpi)]$ (Eq. 30.4-1 of ASCE 7-10)

$q_h = q (h_D+H)$ = 28.406 psf for all domed roofs calculated at height h_D+H

$q_i = q (h_D+H)$ = 28.406 psf for positive and negative internal pressure

(*GCp*) = external pressure coefficient (see Figure 30.4-7 of the Standard)

(*GCpi*) = +/- 0.18 for internal pressure coefficient (see Table 26.11-1 of the Standard)

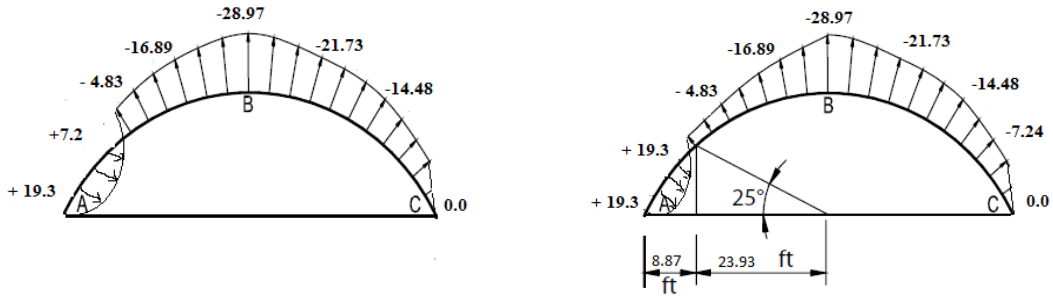

(a) **(b)**

Figure 4.2: MWFRS external pressures for domed roof (a) case A and (b) case B (Internal pressure of +/- 5.1 psf to be added)

Table 4.8 Roof external pressure coefficient for *C*& *C* (from Figure 30.4-7 of the Standard)

External pressure coefficient (*GCp*)		
Zone	Positive	Negative
0^0 to 60^0	+ 0.9	-0.9
60^0 to 90^0	+ 0.5	-0.9

4.3.1.10 Domed roof design pressures

The *C*&*C* domed roof pressure coefficients (Table 10) are given in Figure 30.4-7 of the Standard. This figure is valid only for domes of certain geometric parameters. The base height to diameter ratio, h_D/D = 0/32.8 = 0.0, which is in the range of 0 to 0.5 for Figure 30.4-7. The rise to diameter ratio, H/D = 65.6/32.8 = 0.50, which is in the range of 0.2 to 0.5 for Figure 30.4-7. Therefore, it is valid to use Figure 30.4-7 for this dome. The design pressures are the algebraic sum of external and internal pressures. Positive internal pressure provides controlling negative pressures, and negative internal pressure provides the controlling positive pressure. These design pressures act across the roof surface (interior to exterior).

P= 28.4 *GCp* – 28.4 (+/-0.18) = 28.4 *GCp* (+/- 5.1)

4.3.1.11 Design pressures are summarized in Table 4.9

These pressures are for the front half of the dome. The back half would experience only the negative value of – 30.7 psf. However, since all wind directions must be taken into account, and since each element would at some point be considered to be in the front half of the dome, each element must be designed for both positive and negative values.

4.3.1.12 Comment

The pressures determined are limit state design pressures for strength design. Section 2.3 of the Standard indicates load factor for the wind load to be 1.0D for loads determined in this example. If allowable stress design is to be used, the load factor for the wind load is 0.6D as shown in Section 2.4 of the Standard. Where D is a dome diameter or a cube and prism width.

Table 4.9 Roof design pressures

External pressure coefficient (*GCp*)		
Zone	Positive	Negative
0^0 to 60^0	+ 30.7	- 30.7
60^0 to 90^0	+ 19.3	-30.7

4.3.1.13 The maximum force coefficients on dome

The forces presented in Table. 4.10 are calculated by integrating pressure all over the building. Then, the forces used to calculate the force coefficients presented in Table 4.10 according to Equations (3-12 to 3-15) to allow comparison with CFD simulator results.

Table 4.10 Maximum Force coefficients of a hemispherical dome building due to SL Wind

Model #	*Fx-y* (Ib)	*Fz* (Ib)	*Cx*	*Cz*
Model 1	17,970	37,064	0.32	0.33

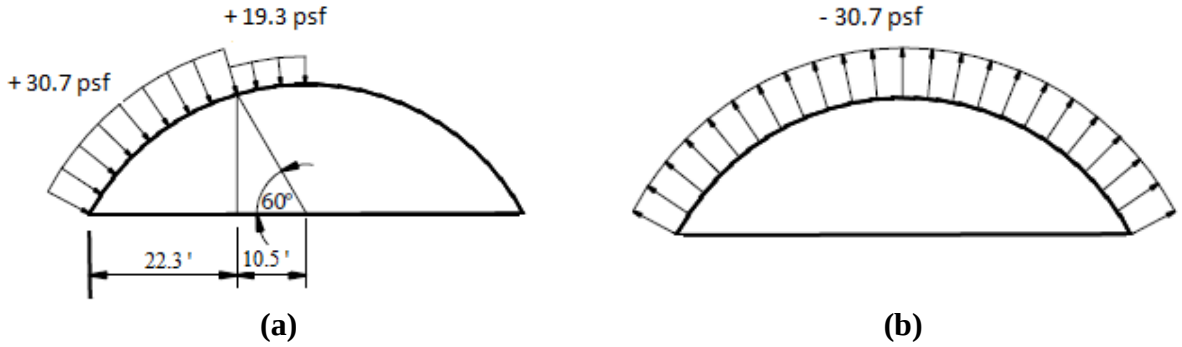

Figure 4.3: Component design pressures for domed roof (*C*&*C*): (a) Positive pressure and (b) Negative pressure

4.3.2 Calculation of wind on cube and prisms

Figure 4.4 illustrates the prism building used for a house in this example. Buildings data are as listed in Table 4.10.

Figure 4.4: (a) building characteristics for a prism building and (b) plan view of a prism building

Table 4.11 Prism models data

Model #	Unite	Dimensions	Plan area (Ax-Ay)	Projected area (Az)	Volume (V)
Model 2 (PM2)	m	L=D= 10.0, H=10.0	100	100	1000
	ft	L=D= 32.81, H=32.81	1076.5	1076.5	10764
Model 3 (PM3)	m	L=D= 17.72, H=10	177.2	314	3140
	ft	L=D= 58.14, H=32.81	1907.6	3380.3	110906
Model 4 (PM4)	m	L=D=14.47, H=10	144.7	209.38	2093.8
	ft	L=D= 47.47, H=32.81	474.74	1557.5	73935
Model 5 (PM5)	m	L=D=20, H=10	200	400	4000
	ft	L=D= 65.62, H =32.81	656.17	1312.34	13123.36
Model 6 (PM6)	m	L=D=13.4, H=7.5	100.5	179.56	1795.6
	ft	L=D=43.96, H=24.61	1932.5	1082	44558.4

4.3.2.1 Analytical Procedure of model 2-5

Analytical directional procedure for a building of any height given in chapter 27, part 1, is used to determine design wind pressure. Building Classification and wind load parameters that are used for calculating the pressure and force of model 2-4 are similar to the one that is used for model 1.

$q_z = 0.00256\, K_z\, (1)\, (0.85)\, (115)^2 = 28.78\, K_z$ psf

Values for K_z and the resulting velocity pressures are given in Table 4.2.

4.3.2.2 Wind loads

$p = qh\,(GCp) - qi\,(GCpi)]$ (Eq. 30.4-1 of ASCE 7-10)

Windward wall

Cp = 0.8 from Fig. 27.4.1 p.g 207 of ASCE 7-10

GCpi = +/- 0.18 from Table 27.4.1 p.g 201 of ASCE 7-10

Side wall

Cp = 0.8 from Fig. 27.4.1 p.g 207 of ASCE 7-10

Leeward wall

Cp = 0.8 from Fig. 27.4.1 p.g 207 of ASCE 7-10

Roof

From 0 to *h* the *Cp* = - 0.9, -0.18 from Figure 27.4.1 p.g 207 of ASCE 7-10

From *h* to 2*h* the *Cp* = - 0.5, -0.18 from Figure 27.4.1 p.g 207 of ASCE 7-10

External pressures are summarized in Table 4.12

Table 4.12 External pressures for MWFRS for wind normal to 32.8-ft Face

	Height (ft)	*qz* (psf)	*Cp*	External pressure (pdf)
Windward wall	0-15	24.463	0.8	16.63
	20	25.902	0.8	17.6
	25	27.053	0.8	18.4
	30	28.20	0.8	19.18
	32.8	28.406	0.8	19.32
Side Wall	All	28.406	-0.7	-16.90
Leeward wall	All	28.406	-0.5	-12.07
Roof	0 to 32.8	28.406	- 0.9	-21.73
	32.8 to 65	28.406	- 0.5	-12.07

4.3.2.3 Internal Pressure Calculation

Negative internal pressure = 28.406 × (−0.18) = − 5.1 psf

Positive internal pressure = 28.406× (0.18) = + 5.11 psf

4.3.2.4 Design Wind Load Cases

Section 27.4.6 of the Standard requires that any building whose wind loads have been determined under the provisions of Sections 27.4.1 and 27.4.2 shall be designed for wind load cases as defined in Figure 27.4-8. Case 1 includes the loadings determined in this example and shown in Figure 4.5.

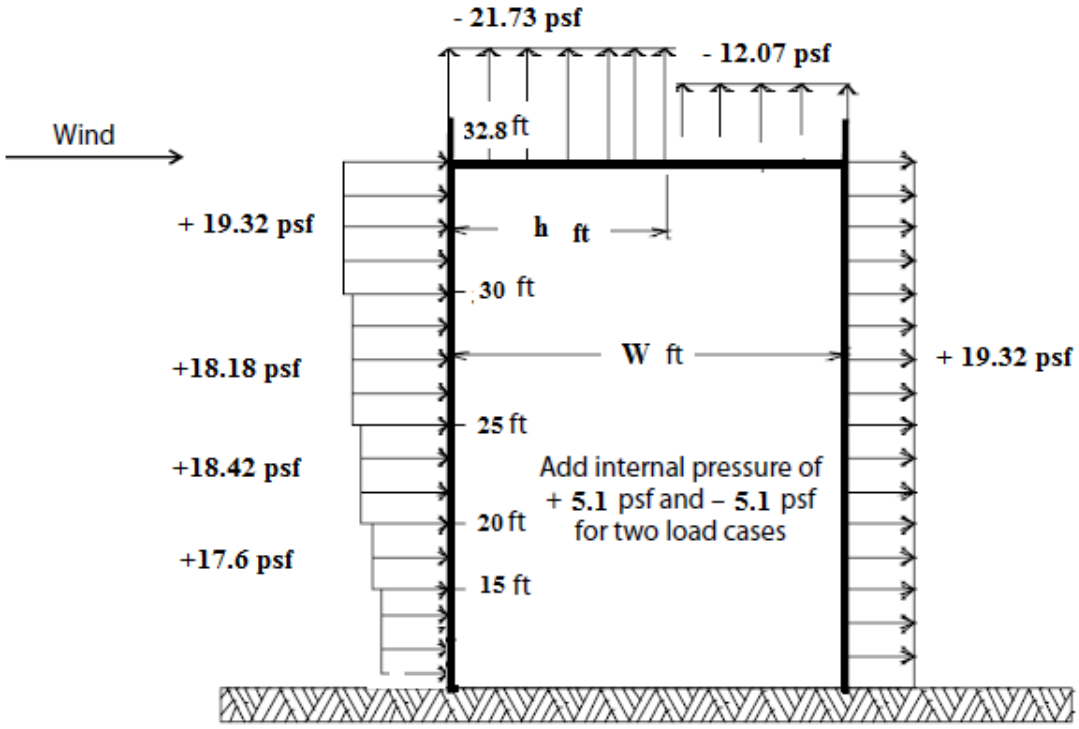

Figure 4.5: Design pressures for MWFRS for wind normal to the face

4.3.2.5 Design pressures for components and cladding (C&C)

Design pressure for *C*&*C* is obtained according to chapter 30, part 3. The equation is

$p = q\,(GCp) - qi\,(GCpi)$ (Eq. 30.6-1 of ASCE 7-10)

4.3.2.6 Wall Design Pressures

The pressure coefficients (*GCp*) are a function of the effective wind area (see Table 4.14).

The Effective wind area is assumed to be 10 ft^2, which is the worst case of the pressure on the wall and roof building.

Edge width of model 2 = 2a

a = min (0.1 b, 0.4 h) > max (0.04b, 3')

a = min (5.814, 13.12) > max (2.3, 3')

a= 5.814 ‘(Table 3.13)

2a=11.628’ (Figure 30.5.1)

Table 4.13 Edge width of model 2-4

	Model 2	Model 3	Model 4
A	5.8	4.7	6.6

Table 4.14 Wall Pressure coefficient

A (ft^2)	Zone 4 & 5 (+*GCp*)	Zone 4 (- *GCp*)	Zone 5 (-*GCp*)
10	1.0	-1.1	-1.4

4.3.2.7 Typical design pressure calculations

Design pressures for building are walls shown in Table 4.15

Zone 4

- Positive

P= 24.463×1.0 - 28.406× (-0.18) = 29.58

- Negative

P= 24.463× (-1.1)-28.406×0.18 = 32.02

Zone 5

- Positive

P= 24.463×1.0 - 28.406× (-0.18) = 29.58

- Negative

P= 24.463× (-1.4)-28.406×0.18 = - 39.36

Table 4.15 Controlling design pressures (psf)

	Zone 4		Zone 5	
Z (ft)	Positive	Negative	Positive	Negative
0-15	29.58	-32.02	29.58	-39.36
15-20	31.02	-33.61	31.02	-41.38
20-25	32.17	-34.87	32.17	-42.99
25-30	33.31	-36.13	33.31	-44.59
30-32.8	33.52	-36.36	33.52	-44.88

4.3.2.8 Roof design pressures

The *C*&*C* roof pressure coefficients are given in 30.6-1 of the Standard. The pressure coefficients (Table 4.16) are a function of the effective wind area. Since specific components of roofs are not identified, design pressures are given for various effective wind areas, A. The design pressures are the algebraic sum of external and internal pressures. Positive internal pressure provides controlling negative pressures. These design pressures act across the roof surface (interior to exterior):

Negative internal pressure = 28.406 × (−0.18) = − 5.11 psf

Positive internal pressure = 28.406× (0.18) = + 5.11 psf

Design pressures are summarized in Table 4.17.

P= 28.406× (-1) -28.406×0.18 = - 33.52

Table 4.16 Roof external pressure coefficient

A (ft^2)	Zone 1		Zone 2		Zone 3	
	GCp	*–GCp*	*GCp*	*–GCp*	*GCp*	*–GCp*
≤10	0.3	-1.0	0.3	-1.8	0.3	-2.8

Table 4.17 Roof External Pressure Coefficient

Design pressures negative (psf)			
A (ft^2)	Zone 1	Zone 2	Zone 3
≤10	-33.52	-56.24	-84.65

4.3.2.9 *The maximum Force of model 2-4*

The forces presented in Table. 4.18 are calculated by integrating pressure all over the building. Then, the forces used to calculate the force coefficients presented in Table 4.18 according to Equations (3-12 to 3-15) to allow comparison with CFD simulator results.

Table 4.18 Maximum Force coefficients of the hemispherical dome building due to SL Wind

Model #	F_X (Ib)	F_Z (Ib)	C_X	C_Z
Model 2	29,688	31,119	0.83	0.87
Model 3	52,607	97,713	0.83	0.87
Model 4	42,959	56,014	0.83	0.87
Model 5	59,376	124,476	0.83	0.87

4.3.2.10 Analytical Procedure of model 6

Analytical directional procedure for a building of any height given in chapter 27, part 1, is used to determine design wind pressure. Building Classification and wind load parameters used for calculating the pressure and force of model 5 are similar to the one used for models 1-4.

$qz = 0.00256\ K_z\ (1)\ (0.85)\ (115)^2 = 28.78\ K_z$ psf

Values for K_z and the resulting velocity pressures are given in Table 4.19.

Table 4.19 Velocity Pressures

Height (ft)	K_z	q_z (psf)
0-15	0.85	24.463
15-20	0.9	25.902
20- 24.6	0.937	26.967

4.3.2.11 Wind loads

$p = q_h\ (GCp) - qi\ (GCpi)]$ (Eq. 30.4-1 of ASCE 7-10)

Windward wall

Cp = 0.8 from Fig. 27.4.1 p.g 207 of ASCE 7-10

GCpi = +/- 0.18 from Table 27.4.1 p.g 201 of ASCE 7-10

Side wall

Cp = 0.8 from Fig. 27.4.1 p.g 207 of ASCE 7-10

Leeward wall

Cp = 0.8 from Fig. 27.4.1 p.g 207 of ASCE 7-10

Roof

From 0 to h the *Cp* = - 0.9, -0.18 from Fig. 27.4.1 p.g 207 of ASCE 7-10

From h to 2h the *Cp* = - 0.5, -0.18 from Fig. 27.4.1 p.g 207 of ASCE 7-10

External pressures are summarized in Table 4.20

Table 4.20 External pressures for MWFRS for wind normal to 32.8-ft Face

	Height (ft)	q_z (psf)	*Cp*	External pressure (pdf)
Windward wall	0-15	24.463	0.8	16.63
	20	25.902	0.8	17.6
	24.6	26.967	0.8	18.3
Side Wall	All	26.967	-0.7	-16.05
Leeward wall	All	26.967	-0.5	-11.46
Roof	0 to 24.6	26.967	- 0.9	-20.63
	24.6 to 43.96	26.967	- 0.5	-11.46

4.3.2.12 Internal Pressure Calculation

Negative internal pressure = 26.967× (−0.18) = − 4.9 psf

Positive internal pressure = 26.967× (0.18) = + 4.9 psf

4.3.2.13 Design pressures for components and cladding (C&C)

Design pressure for *C*&*C* is obtained according to chapter 30, part 3. The equation is

$p = q\,(GCp) - q_i\,(GCpi)$ (Eq. 30.6-1 of ASCE 7-10)

4.3.2.14 Wall Design Pressures

The pressure coefficients (*GCp*) are a function of effective wind area (see Table 4.20).

Effective wind area is assumed to be 10 ft^2, which is the worst case of the pressure on the wall and roof of the building.

Edge width of model 2 = 2a

a= minimum (0.1 b, 0.4 h) > maximum (0.04b, 3')

a = minimum (4.396, 9.84) > maximum (1.76, 3')

a= 4.396 ', 2a=8.792'

Table 4.21 Wall pressure coefficient

A (ft^2)	Zone 4&5 (+*GCp*)	Zone 4 (- *GCp*)	Zone 5 (-*GCp*)
10	1.0	-1.1	-1.4

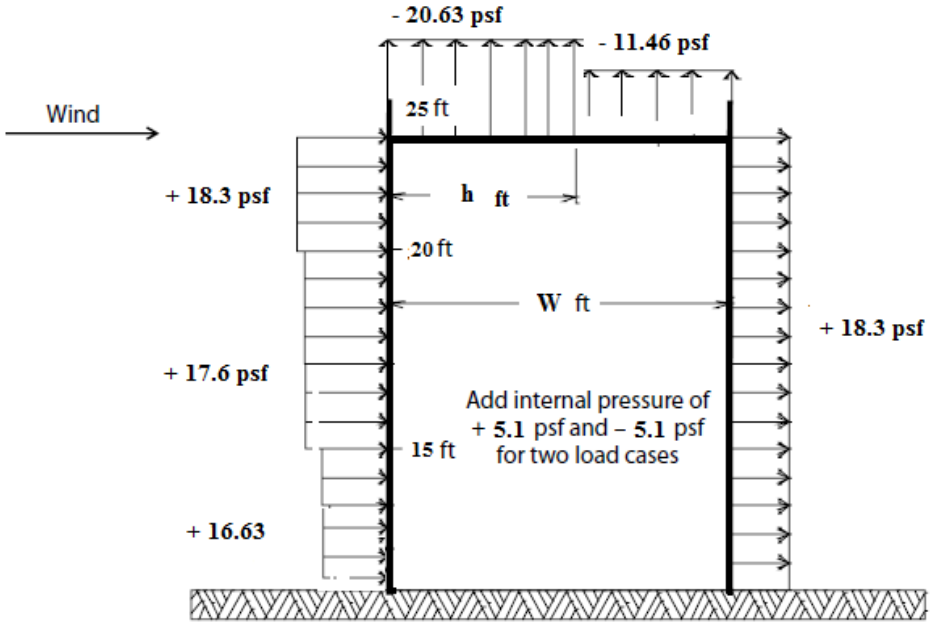

Figure 4.6: Design pressures for MWFRS for wind normal to the face

4.3.2.15 Typical design pressure calculations

Design pressures for building walls are shown in Table 4.21

Zone 4

- Positive

P= 24.463×1.0 - 26.967× (-0.18) = 29.32

- Negative

P= 24.463× (-1.1) - 26.967×0.18 = -31.76

Zone 5

- Positive

P= 24.463×1.0 - 26.967× (-0.18) = 29.32

- Negative

P= 24.463× (-1.4) - 26.967×0.18 = -39.10

Table 4.22 Controlling design pressures for model 5 (psf)

	Zone 4		Zone 5	
Z (ft)	Positive	Negative	Positive	Negative
0-15	29.32	-31.76	29.32	-39.10
15-20	30.76	-33.35	30.76	-41.12
20-24.6	31.82	-34.52	31.82	-42.61

Negative internal pressure = 28.406 × (−0.18) = − 5.1 psf

Positive internal pressure = 28.406× (0.18) = + 5.11 psf

Design pressures of roof are summarized in Table 3.24

P= 26.967× (-1) -26.967 ×0.18 = 31.82

4.3.2.16 *The maximum Force of model 6*

The forces presented in Table 4.25 are calculated by integrating pressure all over the building. Then, the forces are used to calculate the force coefficients presented in Table 4.25 according to Equations (3-12 to 3-15) to allow comparison with CFD simulator results.

T able 4.23 Roof External Pressure Coefficient

A (ft^2)	Zone 1		Zone 2		Zone 3	
	GCp	*–GCp*	*GCp*	*–GCp*	*GCp*	*–GCp*
≤10	0.3	-1.0	0.3	-1.6	0.3	-2.6

Table 4.24 Roof External Pressure Coefficient

Design pressures negative (psf)			
A (ft^2)	Zone 1	Zone 2	Zone 3
≤10	-31.82	-53.39	-80.32

Table 4.25 Maximum Force coefficients of rectangular prism building due to SL Wind

Model #	*Fx* (Ib)	*Fz* (Ib)	*Cx*	*Cz*
Model 6	36,906	50,863	0.77	0.79

4.3.3 Comparison of the coefficients on dome, cubic and prisms for SL wind from ASCE 7-10 provisions.

The force coefficient for each building shape as well as the total force acting on the building using the ASCE 7-10 standard is shown graphically in Figures 4.7 and 4.8. From the figures, one can see that the forces on prisms (PM2-PM5) are much higher than on the dome (DM1). The dome with no sharp windward edge is more effective in reducing the wind pressure coefficient than the prism shape with sharp windward edge. In brief, the dome shape is much better compared to the prism shape in terms of both wind force coefficient as well as total force. The wind force coefficients for the model2, model3 and model 4 (PM2, PM3, and PM4) are similar and higher than those for model 5 (PM5) as shown in Figure. 4.8. The wind forces in all models of prisms increase when square plan size increases as shown in Figure 4.7.

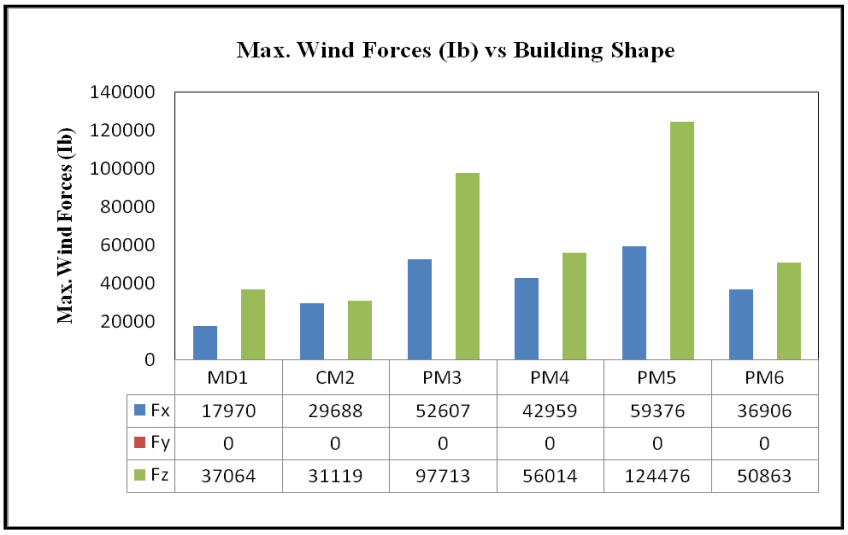

Figure 4.7: Maximum tornado forces (*Fx*, *Fy*, *Fz*) Vs Building shape

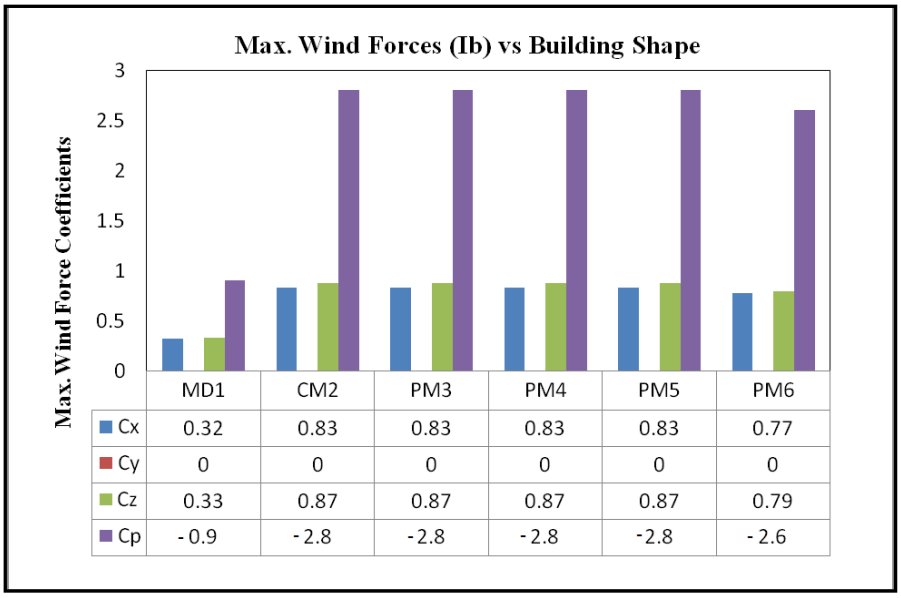

Figure 4.8: Maximum tornado force coefficients (*Cx*, *Cy*, *Cz*) vs Building shape

4.4 Wind loads on dome and prisms according to a CDF model

This section presents the computed forces and pressures due to SL wind for the dome, cubic and prisms (DM1, CM2, PM3, PM4, PM5 and PM6) using a CFD model. The three-dimensional contours of the minimum and maximum pressures for the dome and the prisms are

illustrated in Figures 4.9 - 4.14. The maximum negative and positive pressures on the dome (DM1) are - 0.8 and 0.5, respectively. The maximum effect of the negative pressure is seen close to the top of the dome and the positive pressure is seen closer to the ground. The maximum negative and positive pressures on the cubic (CM2) and prisms (PM3, PM4, PM5 and PM6) are – 2.5 and 0.7, – 2.5 and 0.7, – 2.4 and 0.9, – 2.6 and 0.7 and – 2.0 and 1.0, respectively. The maximum effect of the negative pressure is seen on the roof and walls of the cubic or prism close to the sharp edge and corners, and the positive pressure is seen more on the walls of the cubic or prism building. The cubic and prisms have higher maximum negative and positive pressure than the dome at least 150% and 40%, respectively (Table 25).

The force coefficients are calculated by integrating pressure all over the building (e.g. dome, cubic, prism). The maximum force values for the dome (DM1), cubic (CM2) and prisms (PM3, PM4, PM5, and PM6) are illustrated in Figure 4.15. For comparison, the cubic (CM2) and prisms (PM2, PM3, PM4, PM5) create at least 155 %, higher overall force in the *x*-direction, and 160 % higher overall suction force in the *z*-direction than the dome (DM1) (Table 26).

Table 4.26 Comparison of the absolute maximum values of *Cx, Cy, Cz,* $Cp_{neg.}$ and $Cp_{pos.}$ due to SL wind due to CFD

	DM1 vs CM2	DM1 vs PM3	DM1 vs PM4	DM1 vs PM5	DM1 vs PM6
Cx	175%	175%	170%	180%	155%
Cz	180%	190%	180%	180%	160%
$Cp_{neg.}$	210%	210%	200%	225%	150%
$Cp_{pos.}$	40%	40%	80%	40%	100%

4.5 The coefficients on the dome, cubic and prisms for SL wind due to ASCE 7-10 and CFD

In this section, the calculated coefficients on the dome, cubic and prisms from ASCE 7-10 SL wind are compared with those from the CFD model to determine if the computer model values are relevant to ASCE 7-10. The force coefficients were calculated from ASCE 7-10 provisions for low-rise buildings. The Main Wind Force Resisting Systems (MWFRS) provisions

were used for the force coefficient comparison. In addition, the Components and Cladding (C&C) provisions were applied for the pressures coefficients comparison. The building is assumed to be in open terrain (Exposure C) and with homogenous topography. An importance factor of 1.0 (Category 2) was considered for the present analysis with a design wind speed of 120 mph. Full-scale building dimensions were used for the force and moment calculation. Forces for the eight different building configurations given in the standard and the worst-case forces were normalized according to Equations (19) - (21) to compare with the CFD model results. The maximum ratios between the CFD model and the ASCE 7-10 are presented in Table 2.27. These data show that the maximum force and pressure coefficients on the dome, cubic and prisms from the ASCE 7-10 standard are close to those from the CFD model.

Table 4.27: Maximum ratios of force and pressure coefficients found from ASCE 7-10 and CFD Simulation under the influence of straight-line wind

Method	Shape	*Ax=Ay*	*Az*	*Cx*	*Cy*	*Cz*	*Cp*
ASCE 7-10	DM1	1.57	3.14	0.32	0.0	0.33	-0.9
CFD Model				0.29	0.0	0.30	-0.8
Maximum ratios (ASCE/CFD)				**1.03**	**------**	**1.06**	**1.1**
ASCE 7-10	CM2	1.0	1.0	0.83	0.0	0.87	2.8
CFD Model				0.80	0.0	0.84	2.5
Maximum ratios (ASCE/CFD)				**1.03**	**------**	**1.03**	**1.12**
ASCE 7-10	PM3	1.77	3.14	0.83	0.0	0.87	2.8
CFD Model				0.80	0.0	0.86	2.5
Maximum ratios (ASCE/CFD)				**1.03**	**------**	**1.01**	**1.12**
ASCE 7-10	PM4	1.44	2.09	0.83	0.0	0.87	2.8
CFD Model				0.79	0.0	0.84	2.4
Maximum ratios (ASCE/CFD)				**1.05**	**------**	**1.03**	**1.16**
ASCE 7-10	PM5	2.0	4.0	0.83	0.0	0.87	2.8
CFD Model				0.81	0.0	0.85	2.6
Maximum ratios (ASCE/CFD)				**1.02**	**------**	**1.02**	**1.07**
ASCE 7-10	PM6	1.34	1.0	0.77	0.0	0.82	2.6
CFD Model				0.74	0.0	0.79	2.0
Maximum ratios (ASCE/CFD)				**1.04**	**------**	**1.03**	**1.2**

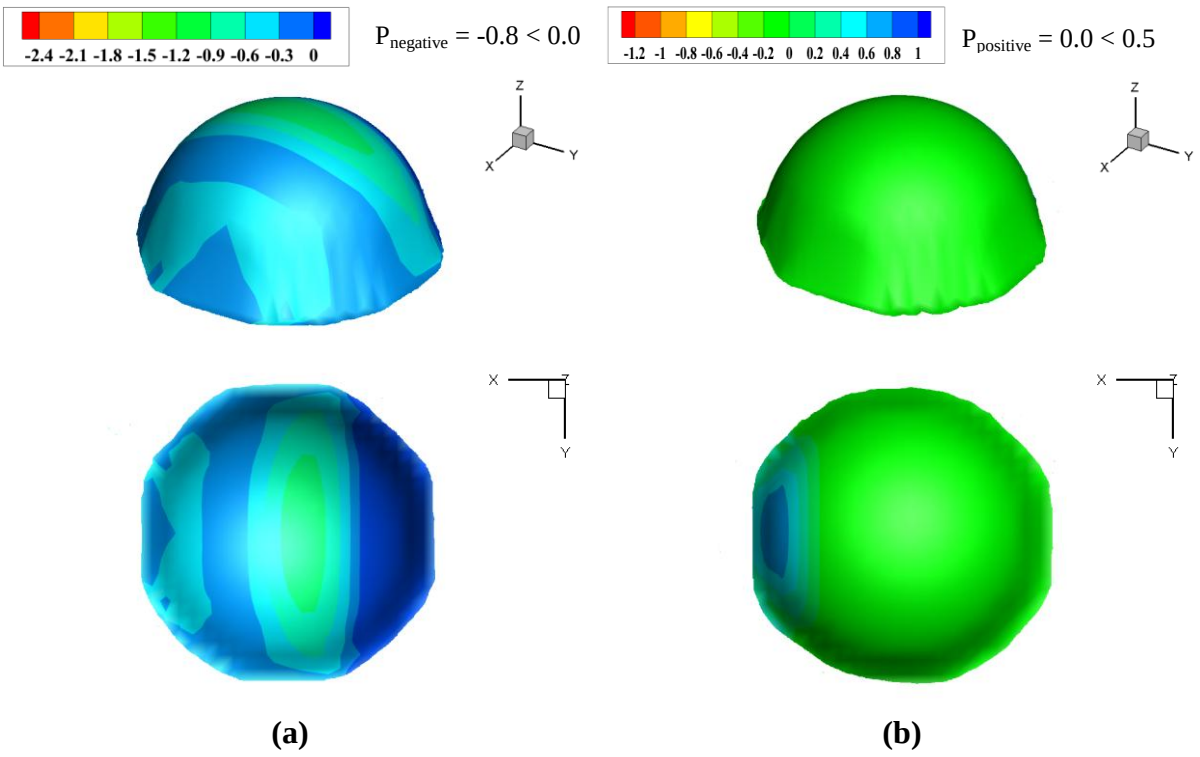

Figure 4.9: The maximum pressure coefficient contour plots due to SL wind on a dome (DM1) building (a) negative pressure (b) positive pressure

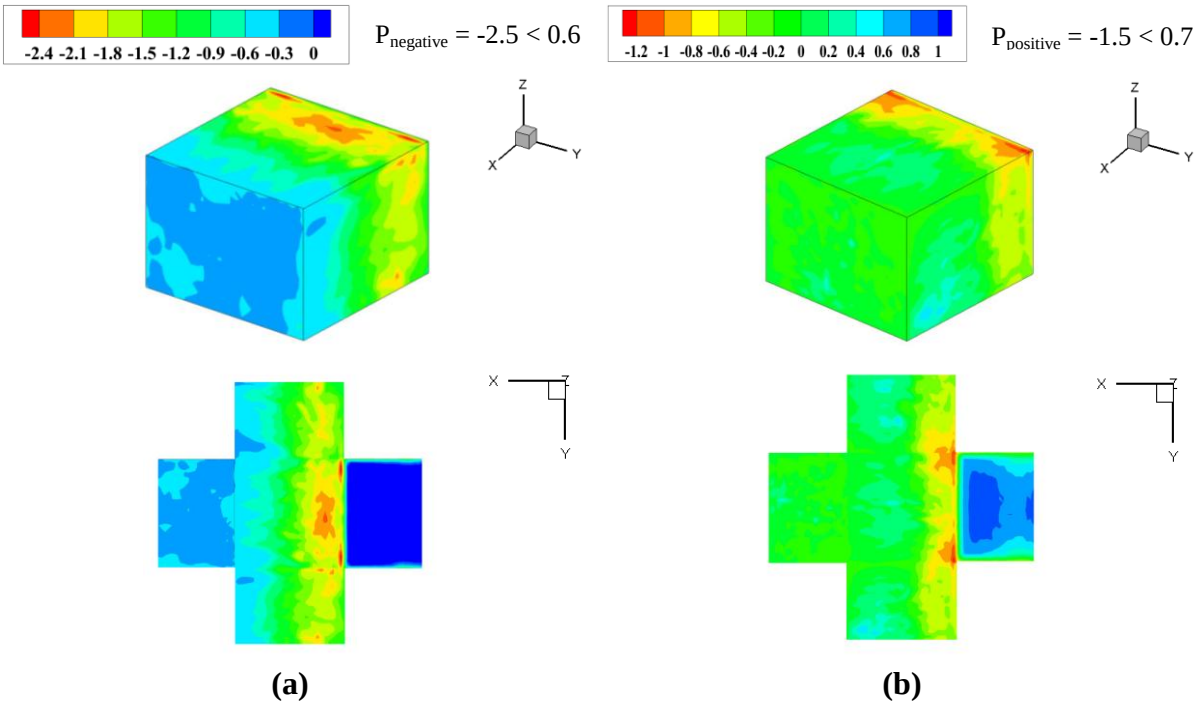

Figure 4.10: The maximum pressure coefficient contour plots due to SL wind on a cubic (CM2) building (a) negative pressure and (b) positive pressure

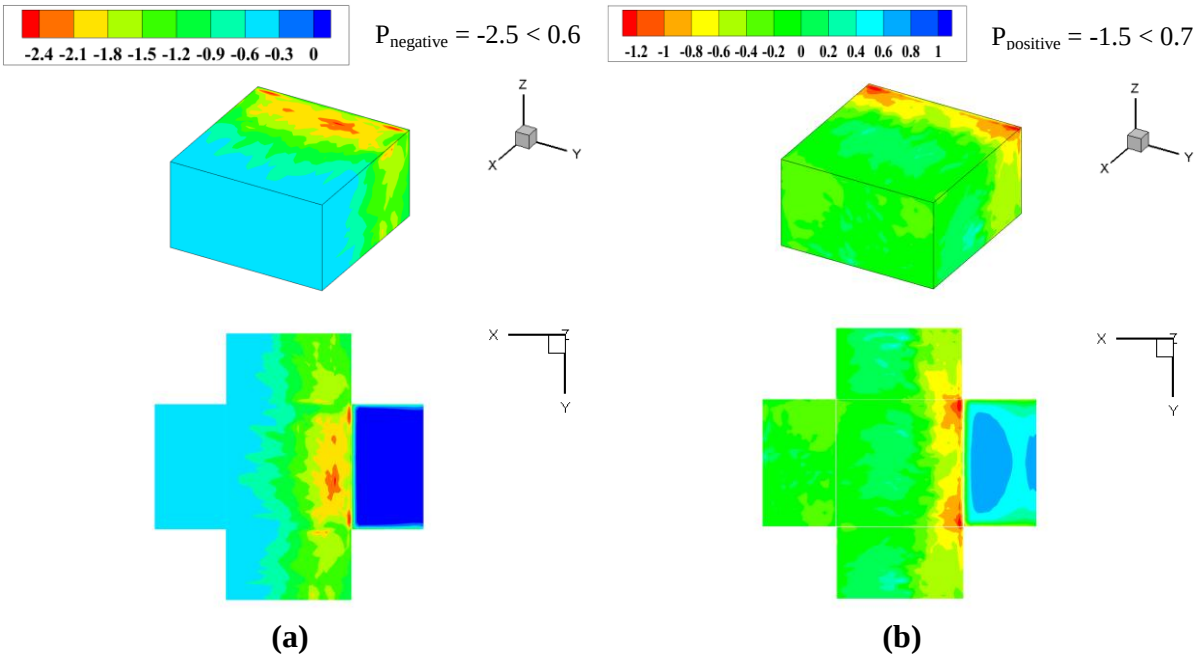

Figure 4.11: The maximum pressure coefficient contour plots due to SL wind for a prism (PM3) building (a) negative pressure and (b) positive pressure

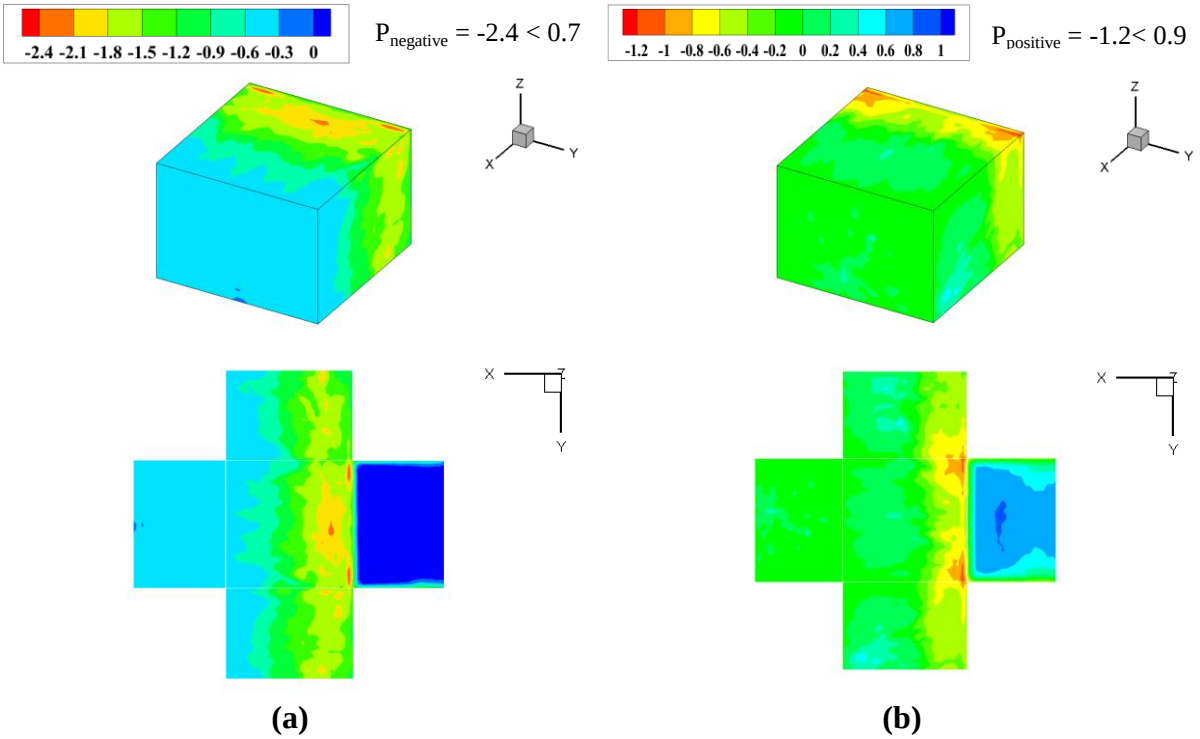

Figure 4.12: The maximum pressure coefficient contour plots due to SL wind for a prism (PM4) building (a) negative pressure and (b) positive pressure

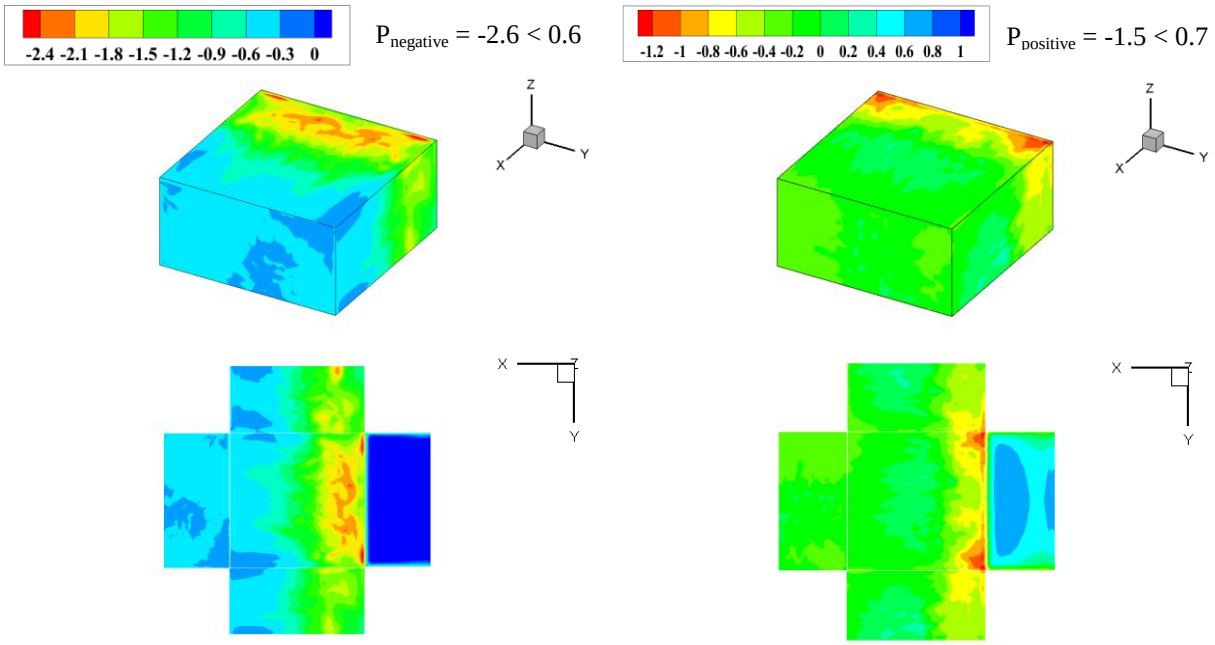

(a) **(b)**

Figure 4.13: The maximum pressure coefficient contour plots due to SL wind for a prism (PM5) building (a) negative pressure and (b) positive pressure

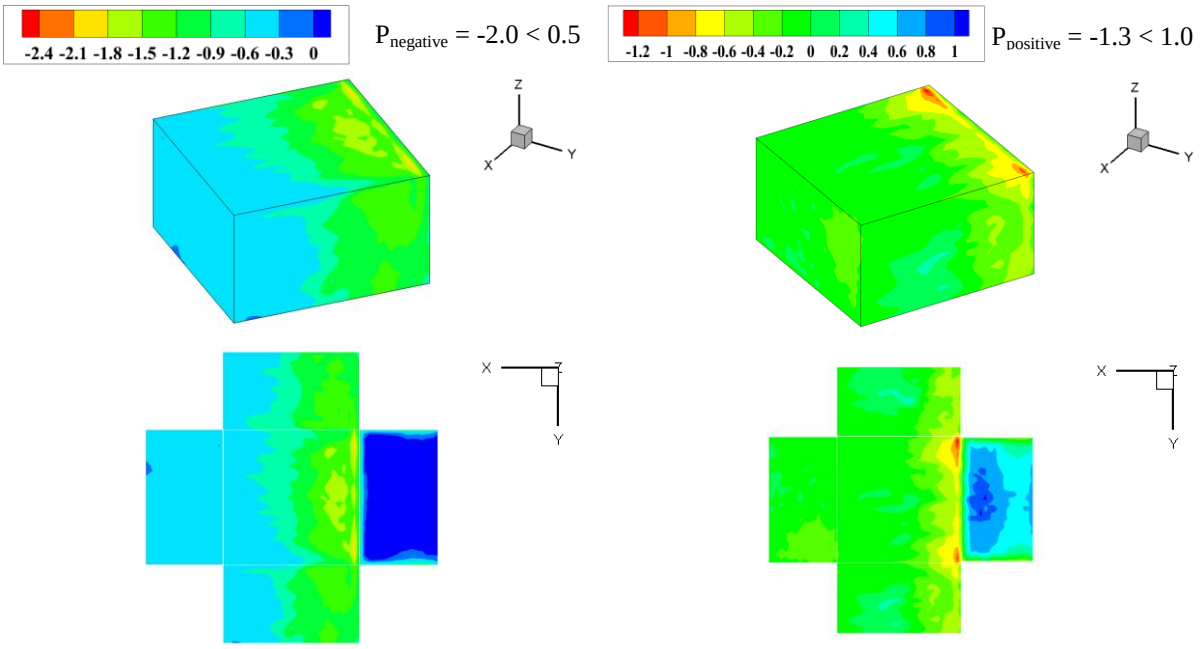

(a) **(b)**

Figure 4.14: The maximum pressure coefficient contour plots due to SL wind for a prism (PM6) building (a) negative pressure and (b) positive pressure

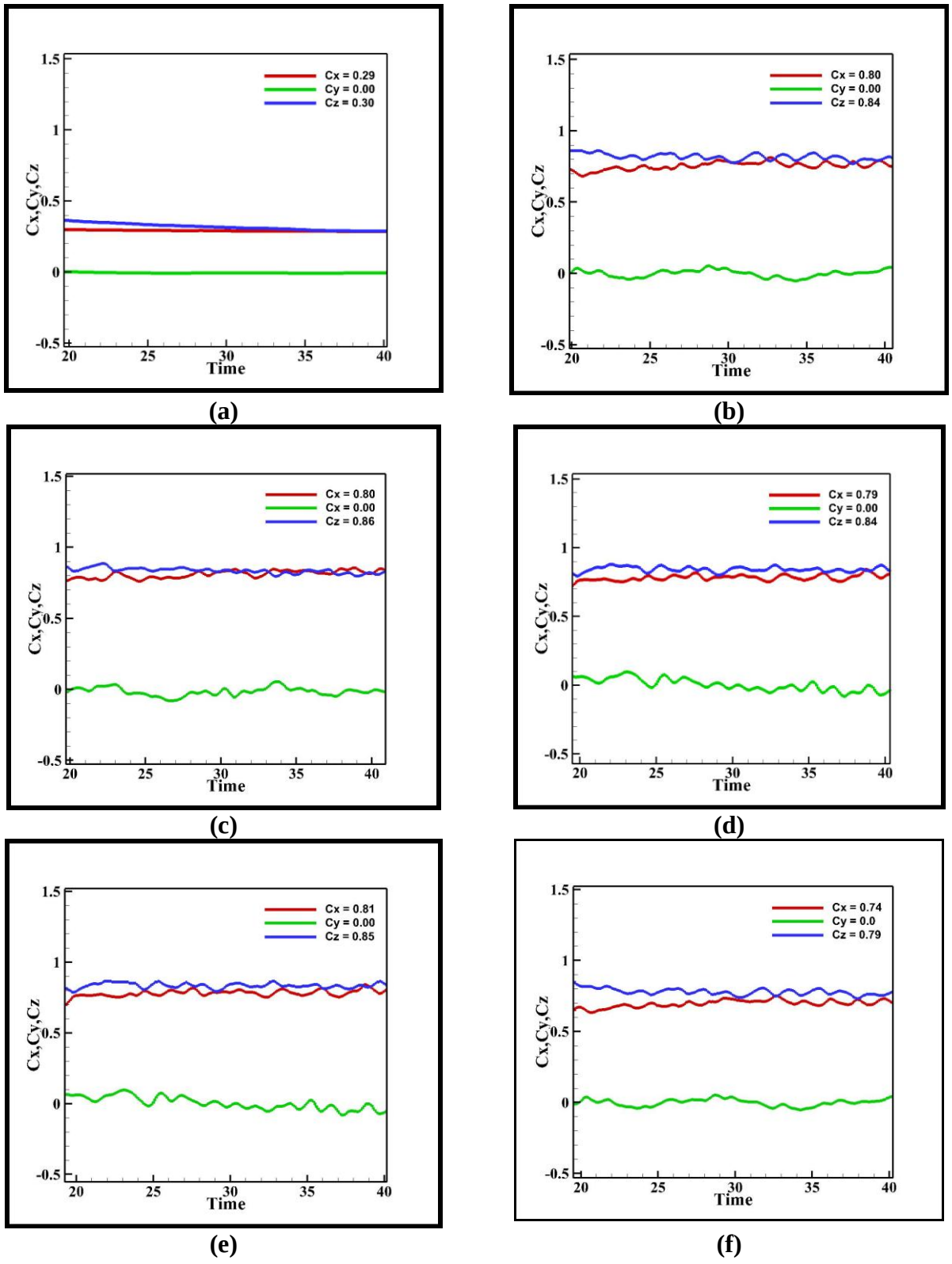

Figure 4.15: Maximum force coefficients on a building (a): DM1, (b): CM2, (c): PM3, (d): PM4 (e): PM5 and (f): PM6 due to SL wind.

4.6 Result and discussion

The force and pressure coefficients on the dome and prisms are compared using the ASCE 7-10 standard. Then, the calculated coefficients on the dome and prisms from ASCE 7-10 SL wind is compared with those from the CFD model to determine if the computer model values are relevant to ASCE 7-10. As a result, the SL wind produces higher maximum negative and positive pressure on prisms than the dome, at least 150% and 40%, respectively. The prisms create about 185%, 185%, 185%, 160%, higher force in the *x*-direction, and 220%, 190%, 220%, 170% higher force in the *z*-direction than the dome. In addition, the forces and pressures that were computed from the CFD model were compared with those calculated from the ASCE 7-10 provisions. It is noted that the values from both the ASCE 7-10 standard and the CFD model are very close. Therefore, the CFD model can be used with confidence.

CHAPTER 5: COMPARE THE EFFECT OF SL AND TORNADIC WIND ON A DOME, CUBIC AND PRISM SHAPED BUILDINGS,USING A CFD MODEL

5.1 Introduction

In the last four decades, tornado forces have been investigated and some comparisons have been made to distinguish between SL wind and tornado wind forces on structure. The interaction between a traveling tornado and various buildings is not yet thoroughly understood. Numerical and experimental tornado simulators are employed to compute tornado force coefficients on a circular cylinder, gable-roof and cubic buildings (e.g. Selvam and Millett 2003 and 2005; Sengupta et al. 2008; Yang et al. 2011; Mishra et al. (2008); Haan et al. 2010; Yang et al. 2010). However, little attention has been paid to tornado interactions with a dome building. According to the tornado damage observations, dome buildings have survived after a tornado event. In this chapter, the tornado forces on a dome were computed using CFD for tornadic and SL wind. Then, the interaction of a tornado on dome, cubic and prism shaped buildings were compared and analyzed.

5.2 Objective

The tornado wind effect on dome and cubic or prism buildings of the same height, surface area or volume were compared. The dome building was assumed to be a reference model with constant dimensions as described in Table 1.1. The difference between the cube and prism is only in the horizontal dimension. The height is kept the same. The length in the x & y direction are the same but not equal in height. The cubic (CM2) prisms (PM3, PM4, PM5 and MP6) consisted of five models with different dimensions: (1) cubic and dome with the same height (2) prism and dome with the same surface area (Az) and height (3) prism and dome with

the same volume and height (4) prism and dome the same width and height (5) prism, which can fit inside a dome (Table 1.1). These following tasks were performed:

- Flow visualizations were reported to understand the flow behavior around the dome, cubic and prism due to the tornado.
- Investigate the tornado force and pressure coefficients on dome, cubic and prism buildings.
- The force and pressure coefficients on dome, cubic and prism buildings were compared due to the SL and tornado wind effect.

5.3 Tornado vortex structure during the interaction with the dome and prisms

The primary advantage of CFD modeling of the tornado-structure interaction is the capability to investigate the wind characteristics for any building shape at any instant in time. The interaction of tornado wind with the dome, cubic and the prisms at various instances of non-dimensional times (t = 10, 24, 35) are illustrated in Figures 5.1-5.6. At the time of 10 units, the vortex is in front of the building (dome, cubic and prisms). At the time of 24 units, the low-level part of the vortex starts to interact with the building. As the vortex travels ahead, the vortex above the dome moves smoothly until it passes the building. However, the vortex over the cube and prism starts to separate until it passes the building. Since the cubic and prism buildings have angles, sharp corners and flat surfaces, they give the wind something to lift or push against. Therefore, the vortex separates when it travels over the cubic and prism buildings. However, the dome building does not have those features. The dome has smooth and rounded surfaces that make the vortex move smoothly over it. As the vortex moves away from the dome, cubic and the prism buildings at time t= 35, it starts to recover its initial cylindrical shape.

The x and the z plane velocities vector in pressure contours for dome (MD1), cubic (CM2) and prisms (PM3, PM4, PM5, PM6) at time 24 as illustrated in Figure 5.7. The tornado

vortex generates large amounts of vertical wind around each building. With the prism building interactions, the wind is changed from horizontal to vertical wind all around the roof of the buildings. As the high-pressure vertical wind flows past the corners of the prism building, flow separation occurs just above the entire roof surface as seen by the turbulent wake above the building. However, with the dome building interaction, the wind travels smoothly over the dome building, since the dome does not have multiple sharp corners like the prism building. As a result, the rotational wind of tornadoes creates higher forces on the prism than the dome.

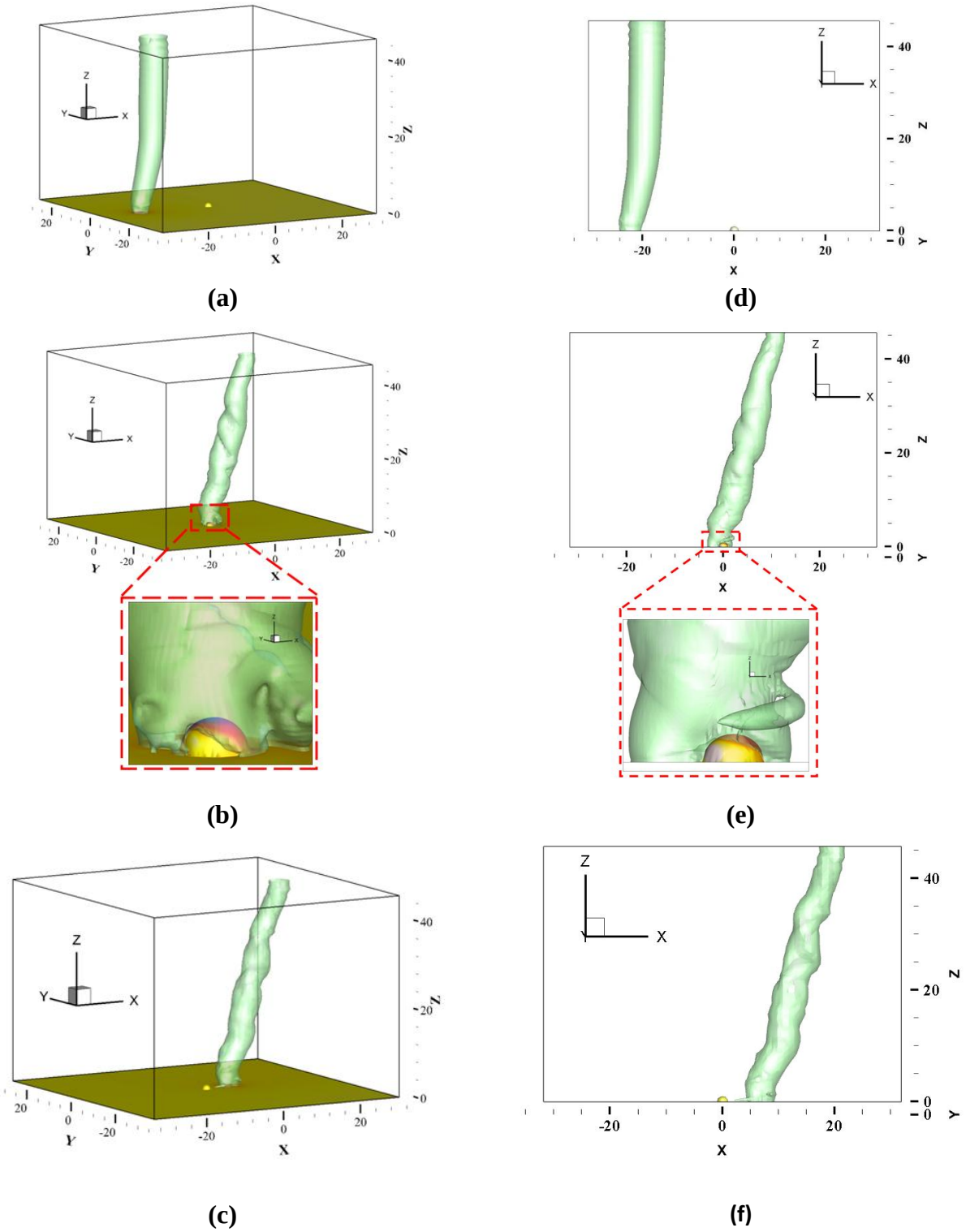

Figure 5.1: (Left) 3D Iso-pressure surfaces of the vortex-dome interaction (DM1) at (a) 10, (b) 24 and (c) 35 unite; (Right) *xz*-plane at (d) 10, (e) 24 and (f) 35 units for $V_\theta/V_t = 3$

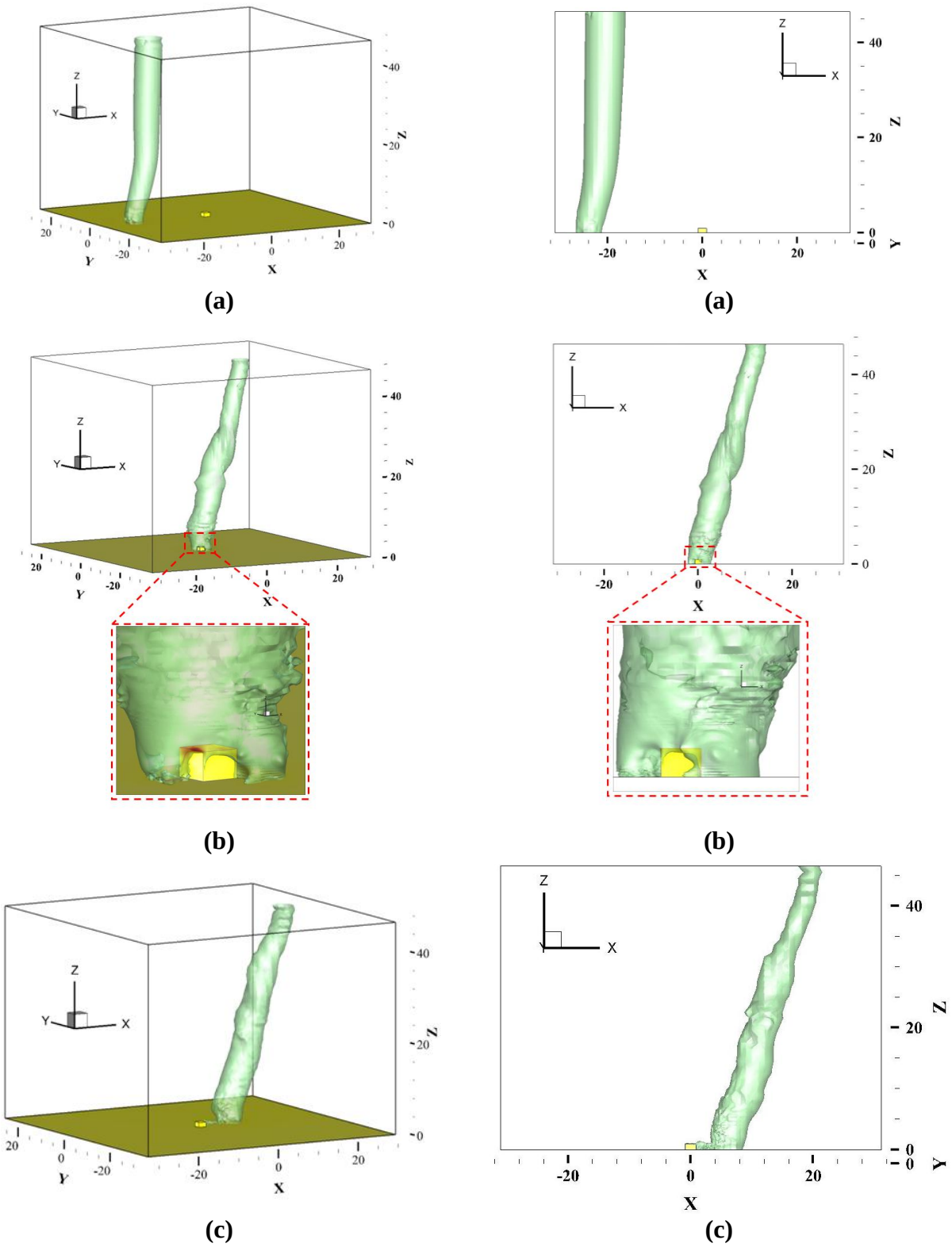

Figure 5.2: (Left) Iso-pressure surfaces of the vortex-cubic interaction (CM2) and (Right) *xz*-plane of tornado vortex-prism at (a) 10, (b) 24 and (c) 35 units for $V_\theta/V_t = 3$

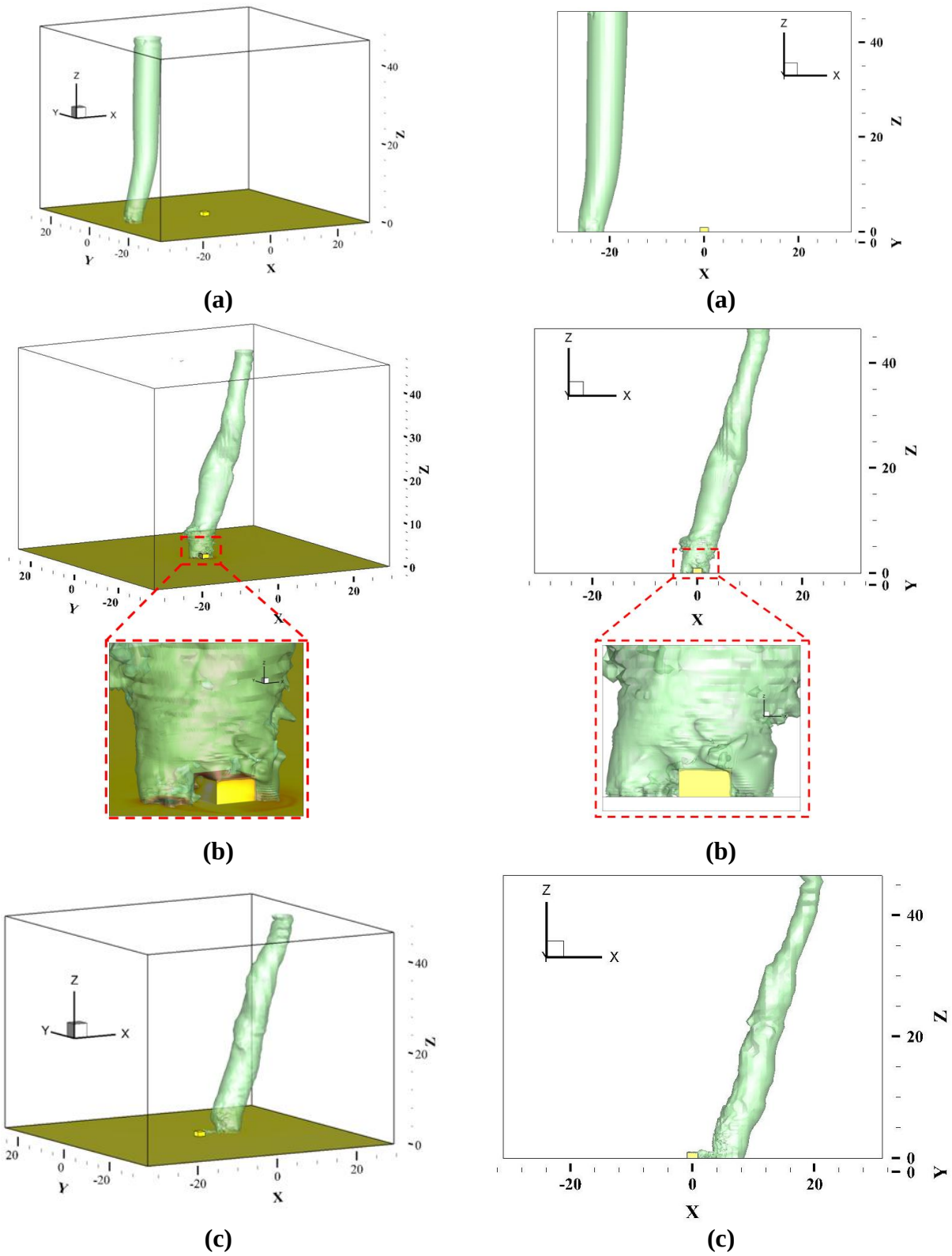

Figure 5.3: (Left) Iso-pressure surfaces of the vortex- prism interaction (PM3) and (Right) *xz*-plane of tornado vortex-prism at (a) 10, (b) 24 and (c) 35 units for $V_\theta/V_t = 3$

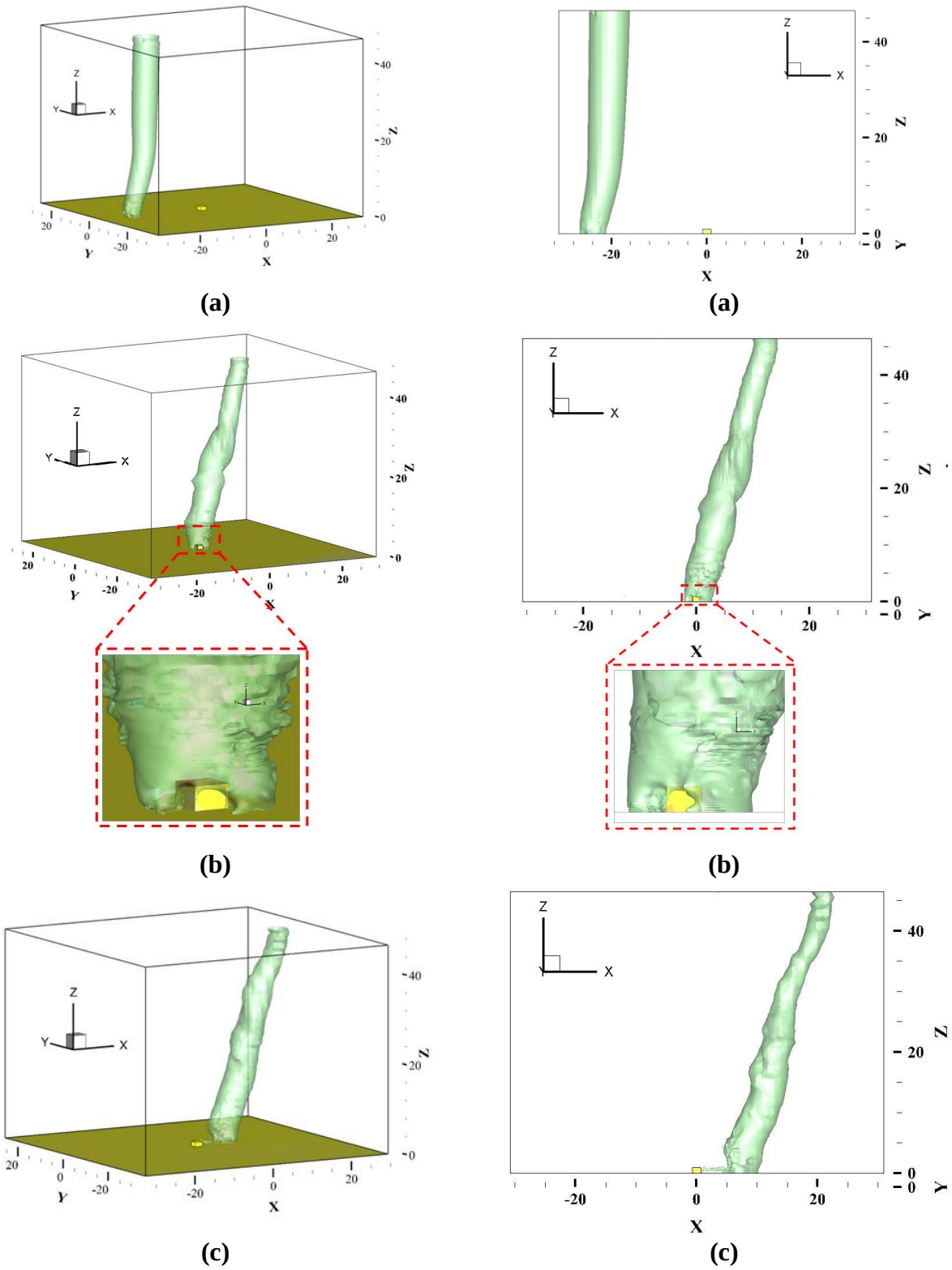

Figure 5.4: (Left) Iso-pressure surfaces of the vortex- prism interaction (PM4) and (Right) *xz*-plane of tornado vortex-prism at (a) 10, (b) 24 and (c) 35 units for $V_\theta/V_t = 3$

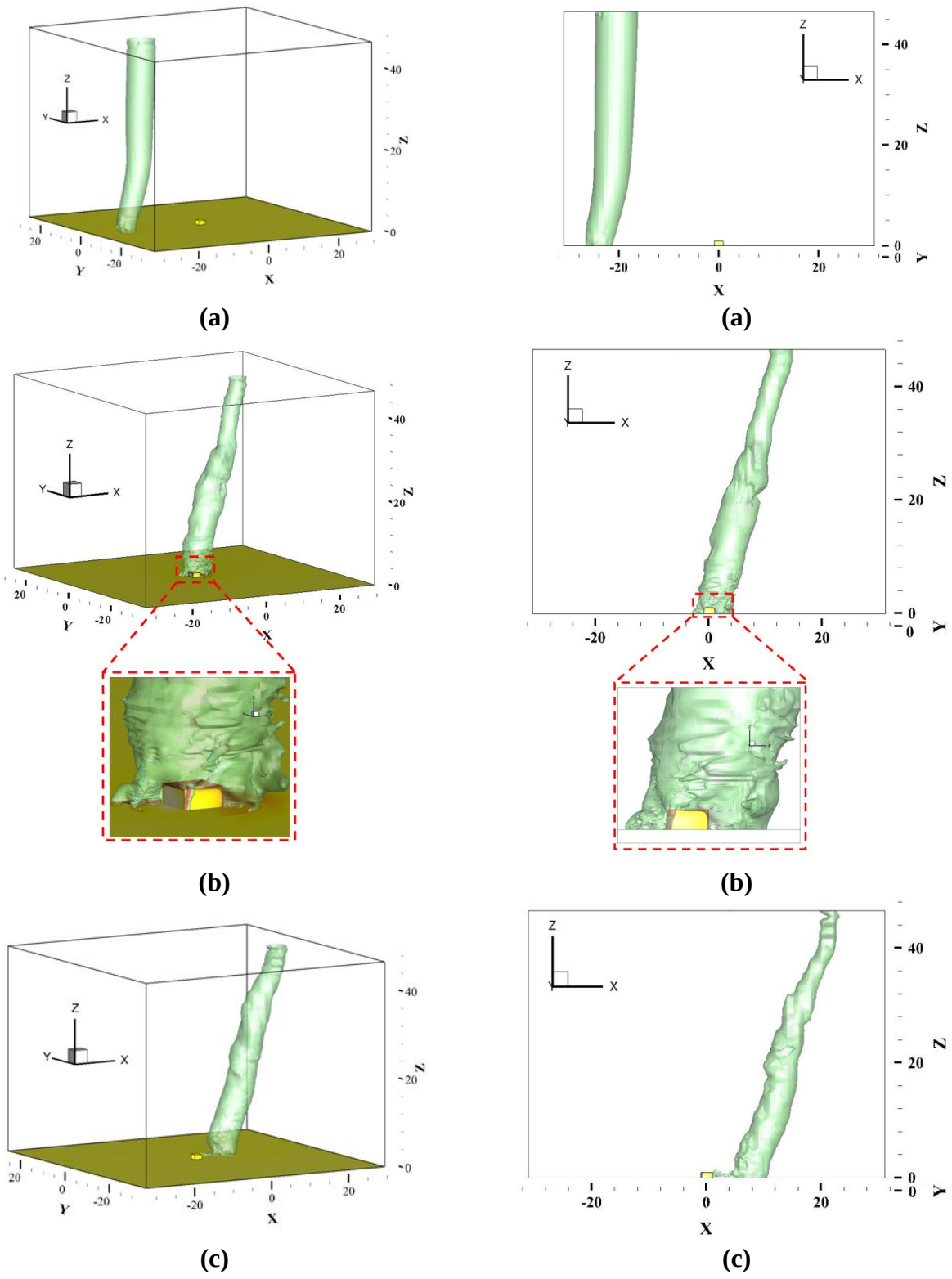

Figure 5.5: (Left) Iso-pressure surfaces of the vortex- prism interaction (PM5) and (Right) *xz*-plane of tornado vortex-prism at (a) 10, (b) 24 and (c) 35 units for $V_\theta/V_t = 3$

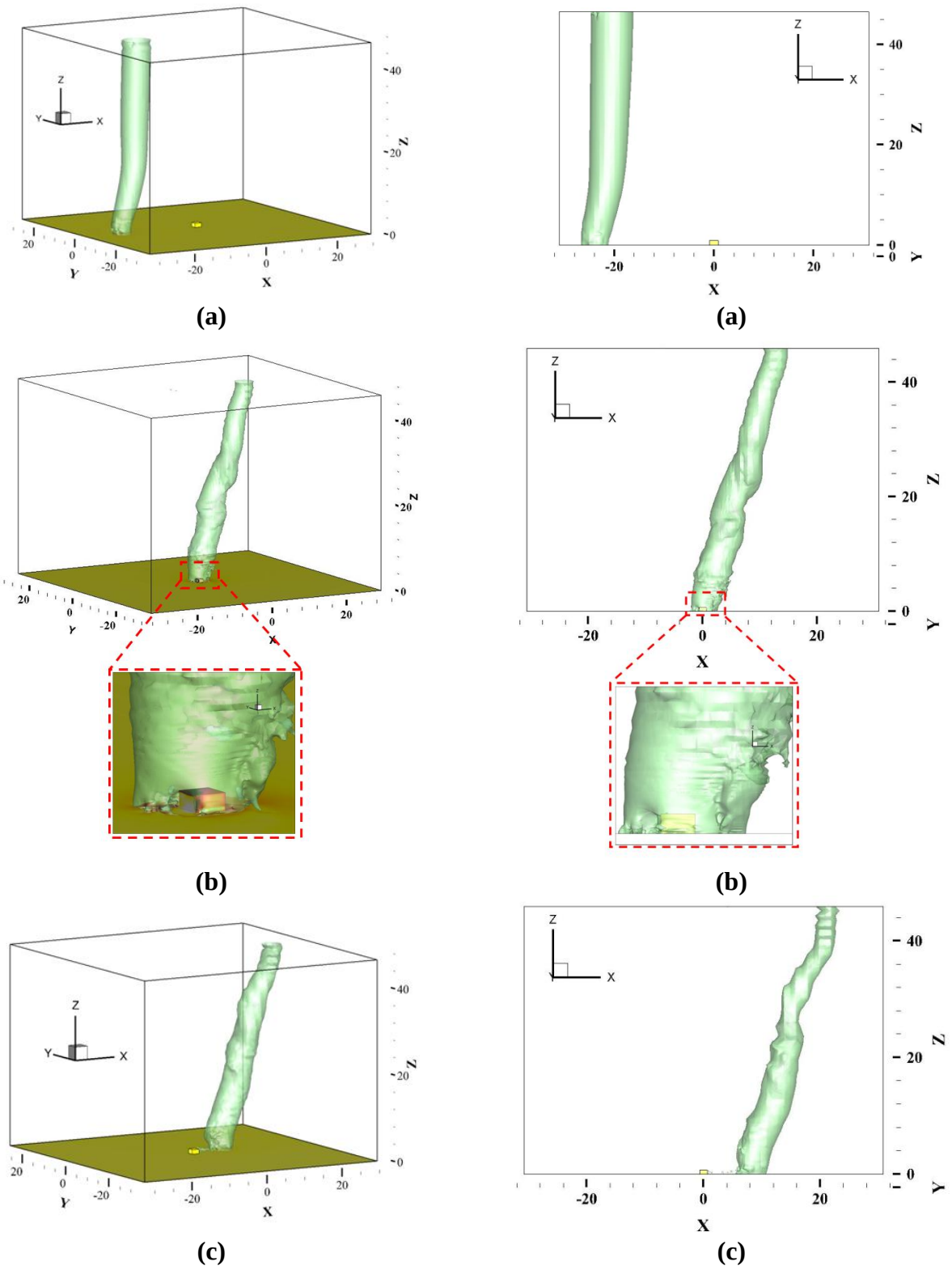

Figure 5.6: (Left) Iso-pressure surfaces of the vortex- prism interaction (PM6) and (Right) *xz*-plane of tornado vortex-prism at (a) 10, (b) 24 and (c) 35 units for $V_\theta/V_t = 3$

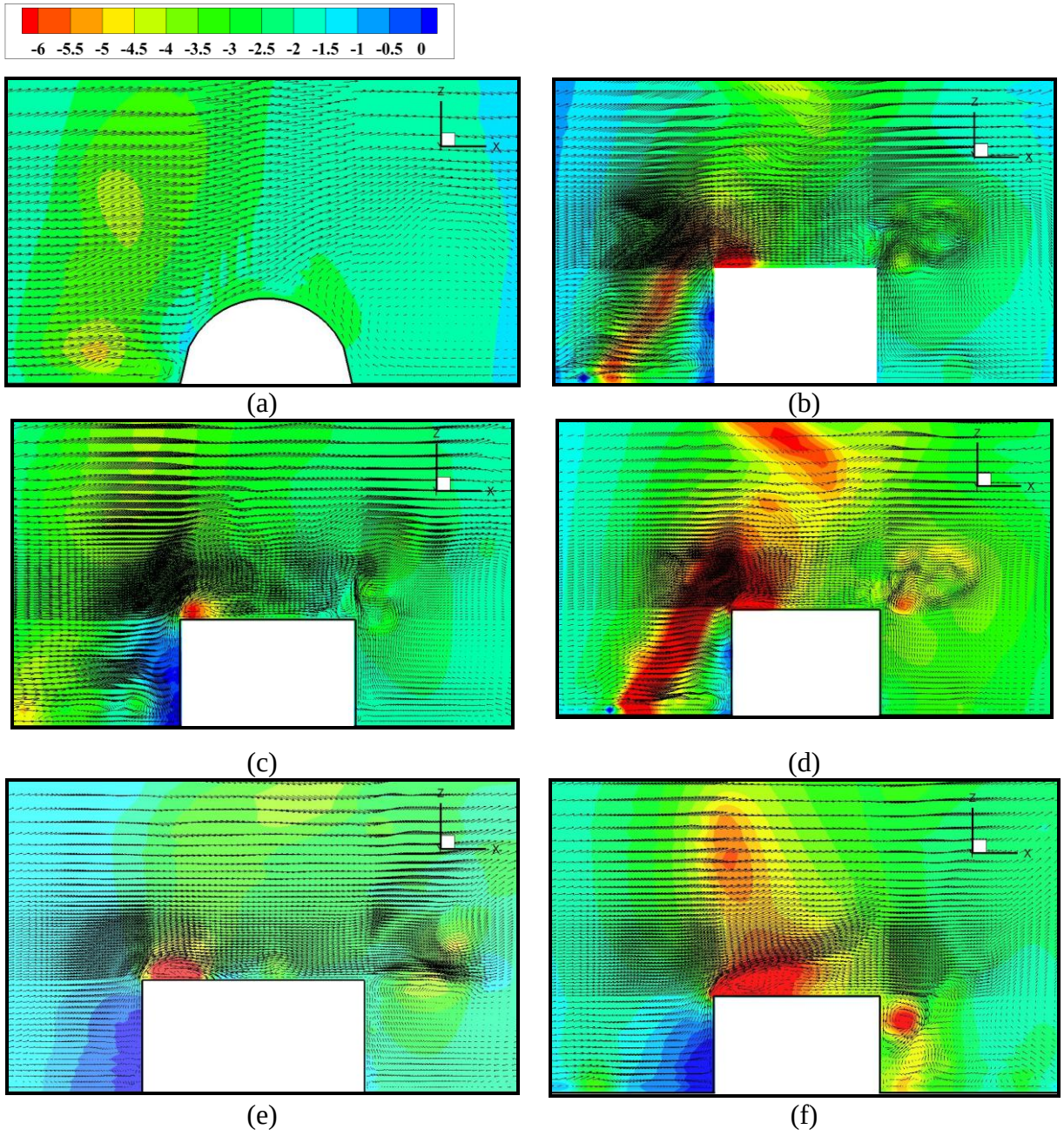

Figure 5.7: Close view of *xz*-plane of tornado vortex-building at time 24 unit (a): DM1, (b): CM2, (c): PM3, (d): PM4, (c): MP5 and (d): MP6 for $V\theta/Vt = 3$

5.4 Tornado coefficients on dome, cubic and prisms due to tornado wind

The three-dimensional contours of the minimum and maximum tornado pressures for the dome and the prisms are illustrated in Figures 5.8 - 5.13. The maximum negative and positive tornado pressures on the dome (DM1) are -2.0 and 0.6, respectively. The maximum effect of the

negative pressure is seen close to the top of the dome, and the positive pressure is seen closer to the ground. The maximum negative and positive pressures on the cubic (CM2) and prisms (PM3, PM4, PM5, and PM6) are -6.1 and 1.5, -6.0 and 1.4, -5.8 and 1.4, -6.8 and 1.3, -6.2 and 1.1, respectively. The maximum effect of the negative pressure is seen on the roof and walls of the cubic and prism close to the sharp edge and corners, and the positive pressure is seen more on the walls. The cubic (CM2) and prisms (PM3, PM4, PM5 and PM6) make, about 200%, 210%, 200%, 240% and 210% higher negative pressure than the dome model (DM1) as presented in Table 5.1. The pressure coefficients on the cubic and prisms due to the tornado wind were about two times larger than the force on the dome building. The cubic and prisms had a higher maximum positive pressure than the dome model, by about 200%, 180%, 180%, 160% and 120% more, respectively.

The tornado force coefficients on the dome and prisms were calculated by integrating pressure all over the dome and prisms. The maximum *Cx, Cy,* and *Cz,* values for dome, cubic and prisms are illustrated in Figure 5.14. The Cx and *Cz* were positive for the entire period of tornado-structure interaction, and *Cy* moved from positive to negative. Here positive value means the force coefficients were acting in the direction of the positive axis. Consequently, *Cz* was an uplifting force on the roof. The side forces could pull or push depending upon the tornado position with respect to the structure. Cubic (CM2) prisms (PM3, PM4, PM5 and PM6) had higher tornado force coefficients than the dome, about 190%, 150%, 175%, 90% and 210% more in the *x*- and *y*-directions and 260%, 180%, 260%, 140% and 280% more in the *z*-direction.

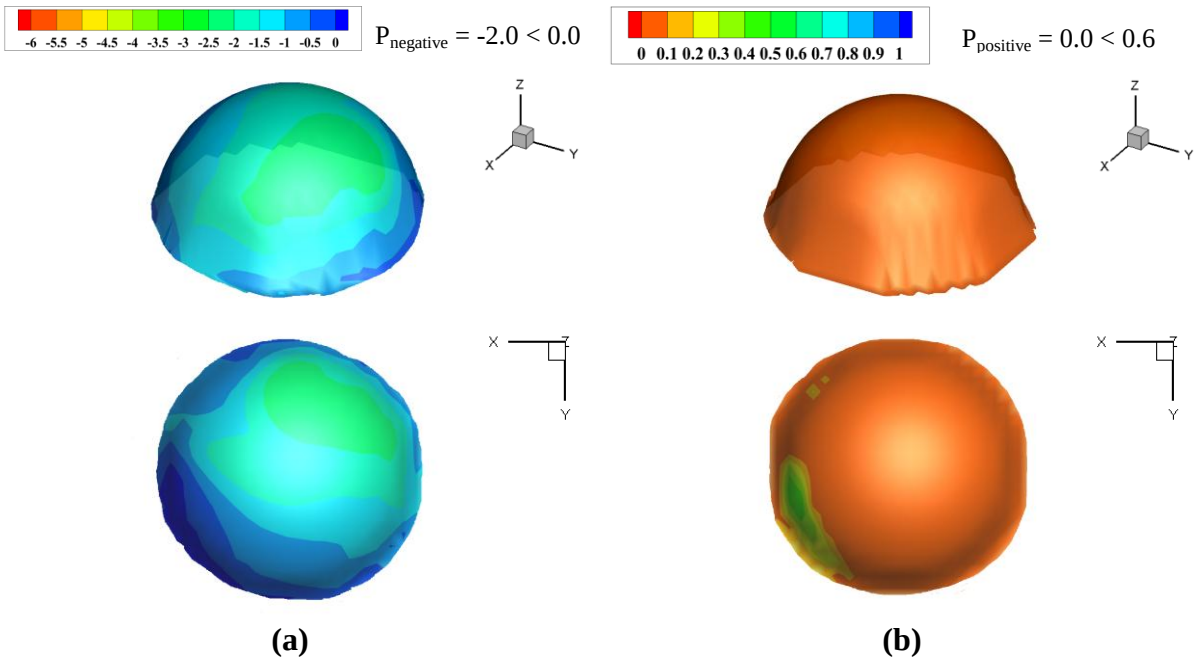

Figure 5.8: The max. Pressure coefficient contour plots due to SL wind for the dome (DM1) (a) negative pressure (b) positive pressure

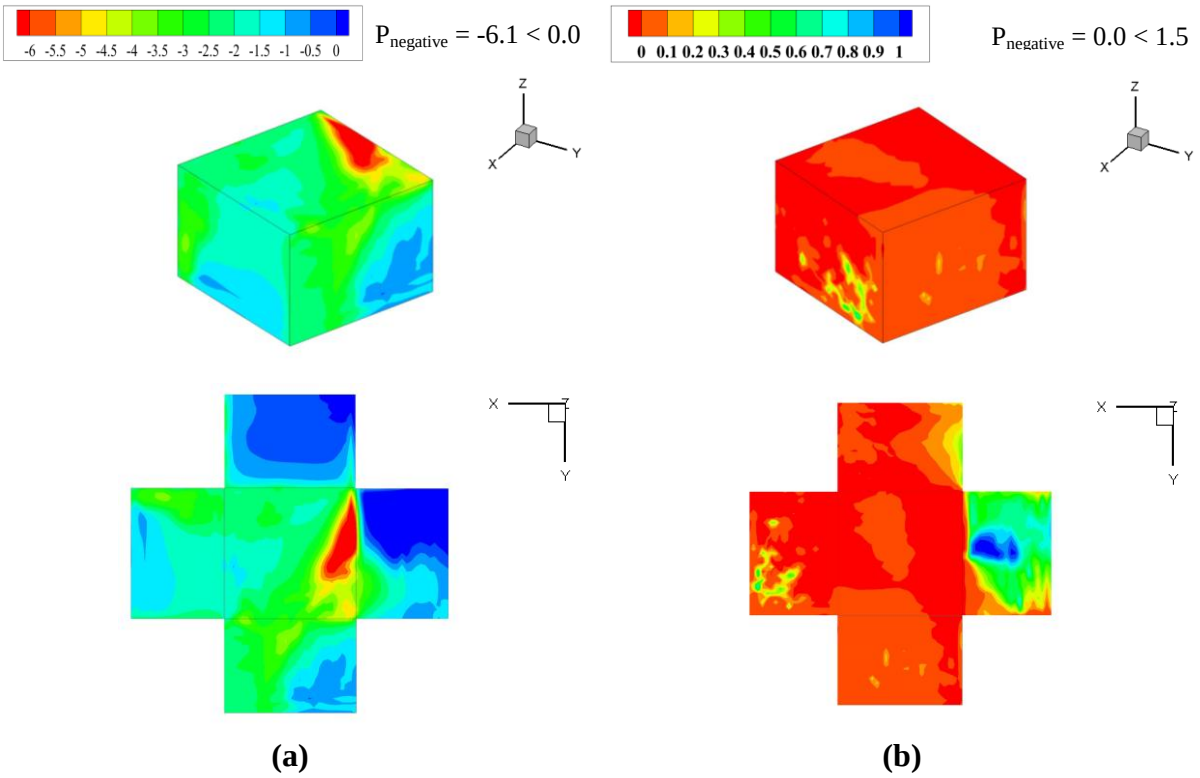

Figure 5.9: The maximum pressure coefficient contour plots due to SL wind for the cubic (CM2) building (a) negative pressure and (b) positive pressure

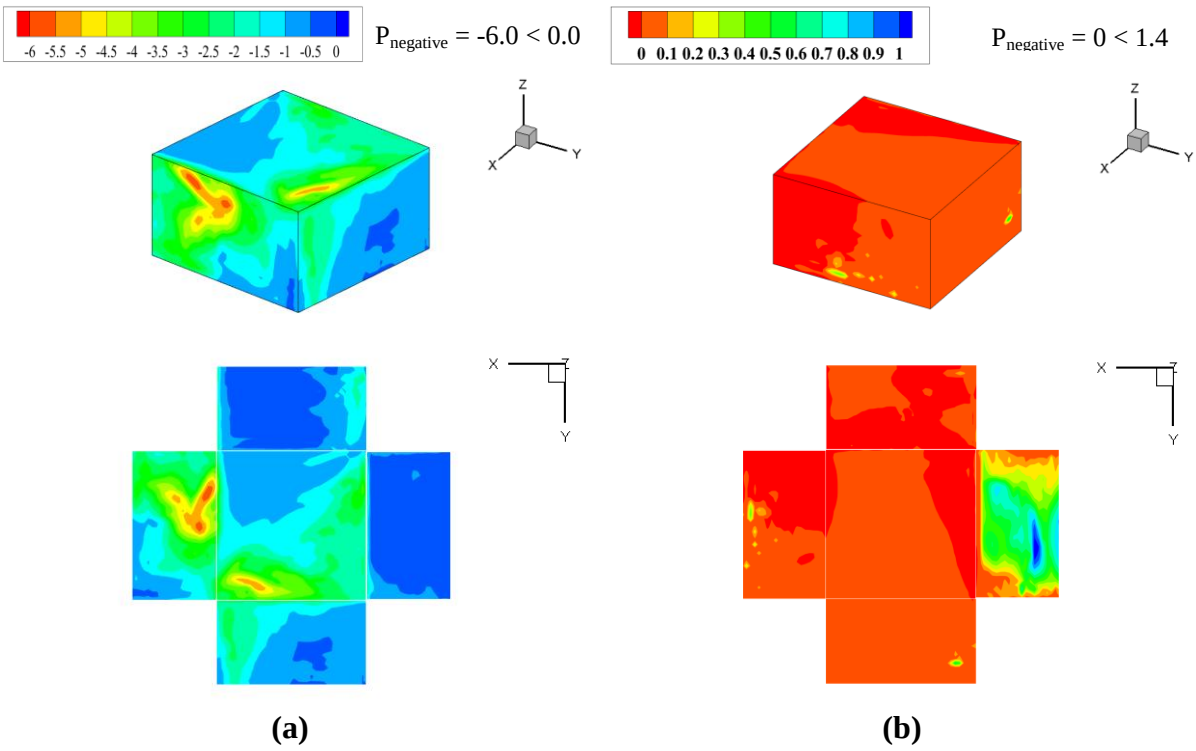

Figure 5.10: The maximum pressure coefficient contour plots due to SL wind for the prism (PM3) building (a) negative pressure and (b) positive pressure

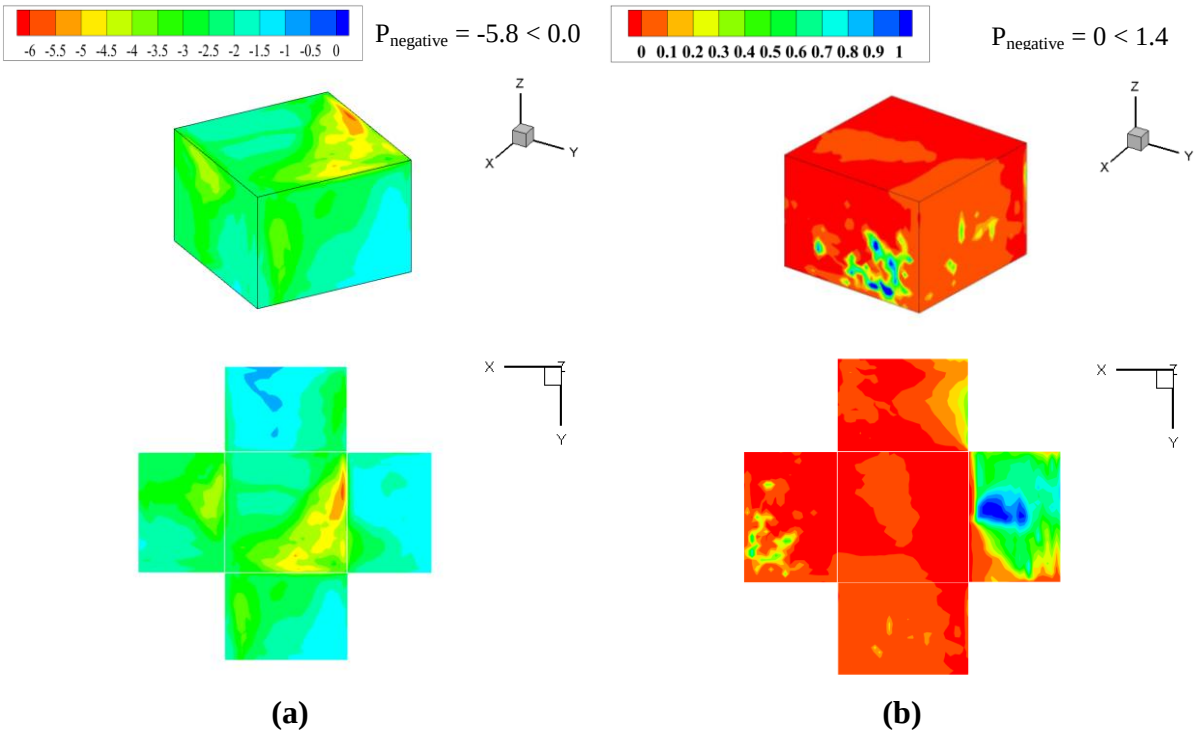

Figure 5.11: The maximum pressure coefficient contour plots due to SL wind for the prism (PM4) building (a) negative pressure and (b) positive pressure

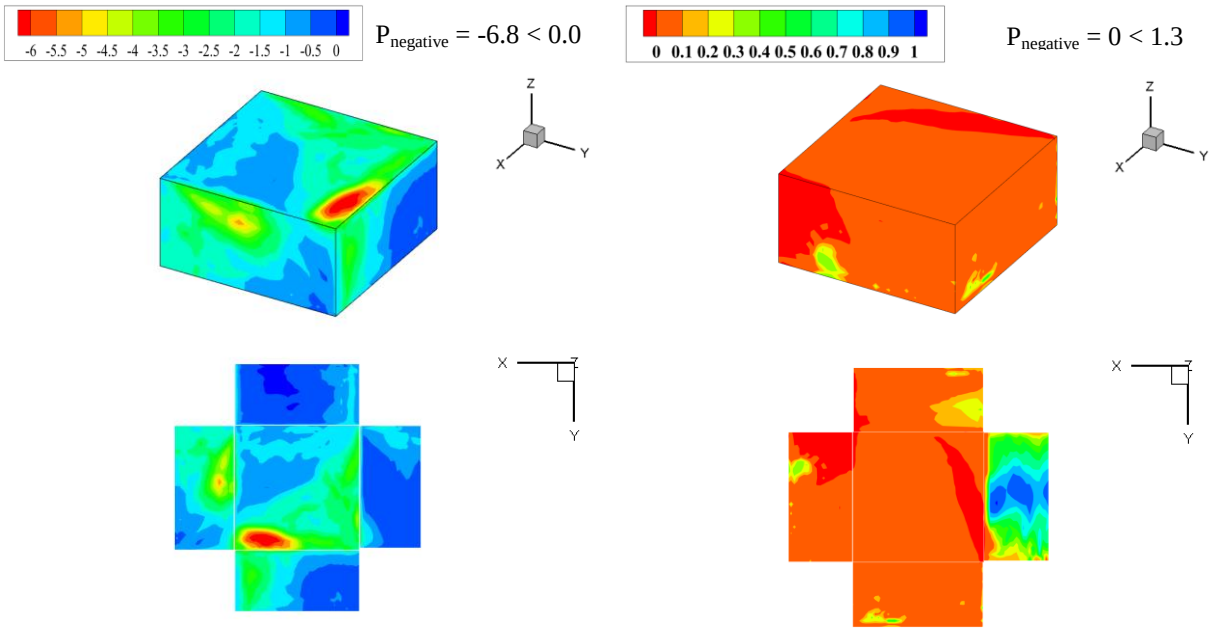

Figure 5.12: The maximum pressure coefficient contour plots due to SL wind for the prism (PM5) building (a) negative pressure and (b) positive pressure

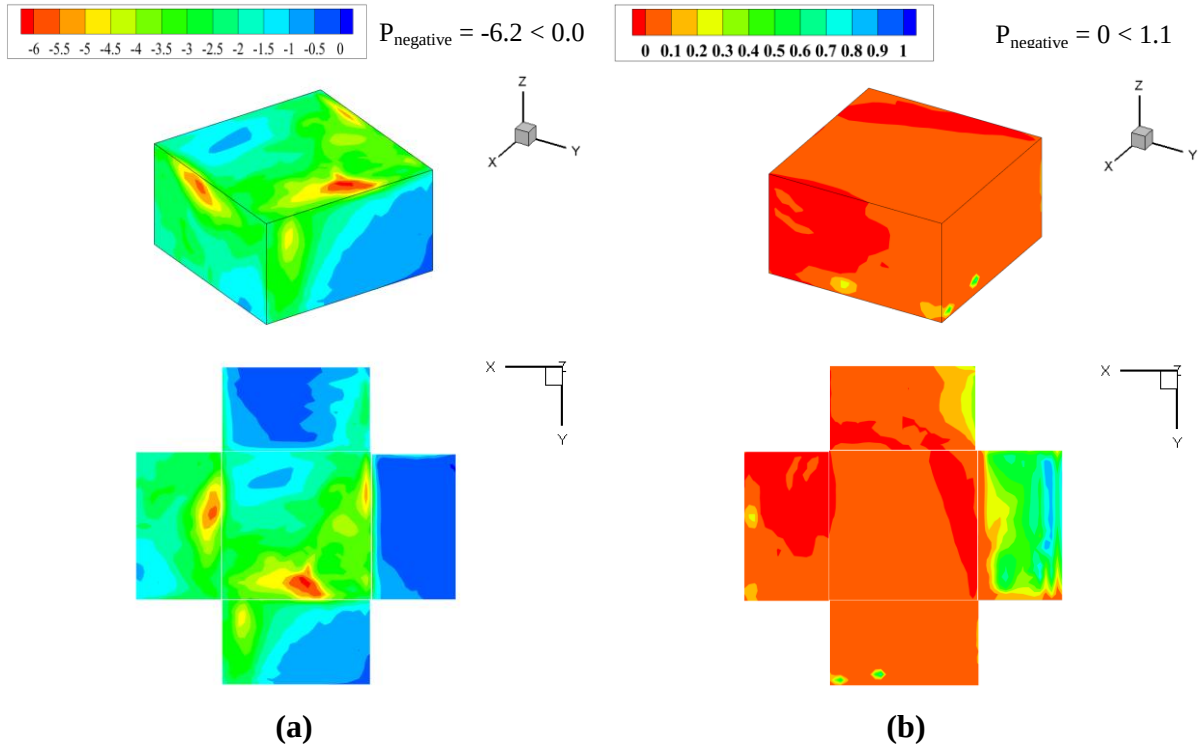

Figure 5.13: The maximum pressure coefficient contour plots due to SL wind for the prism (PM6) building (a) negative pressure and (b) positive pressure

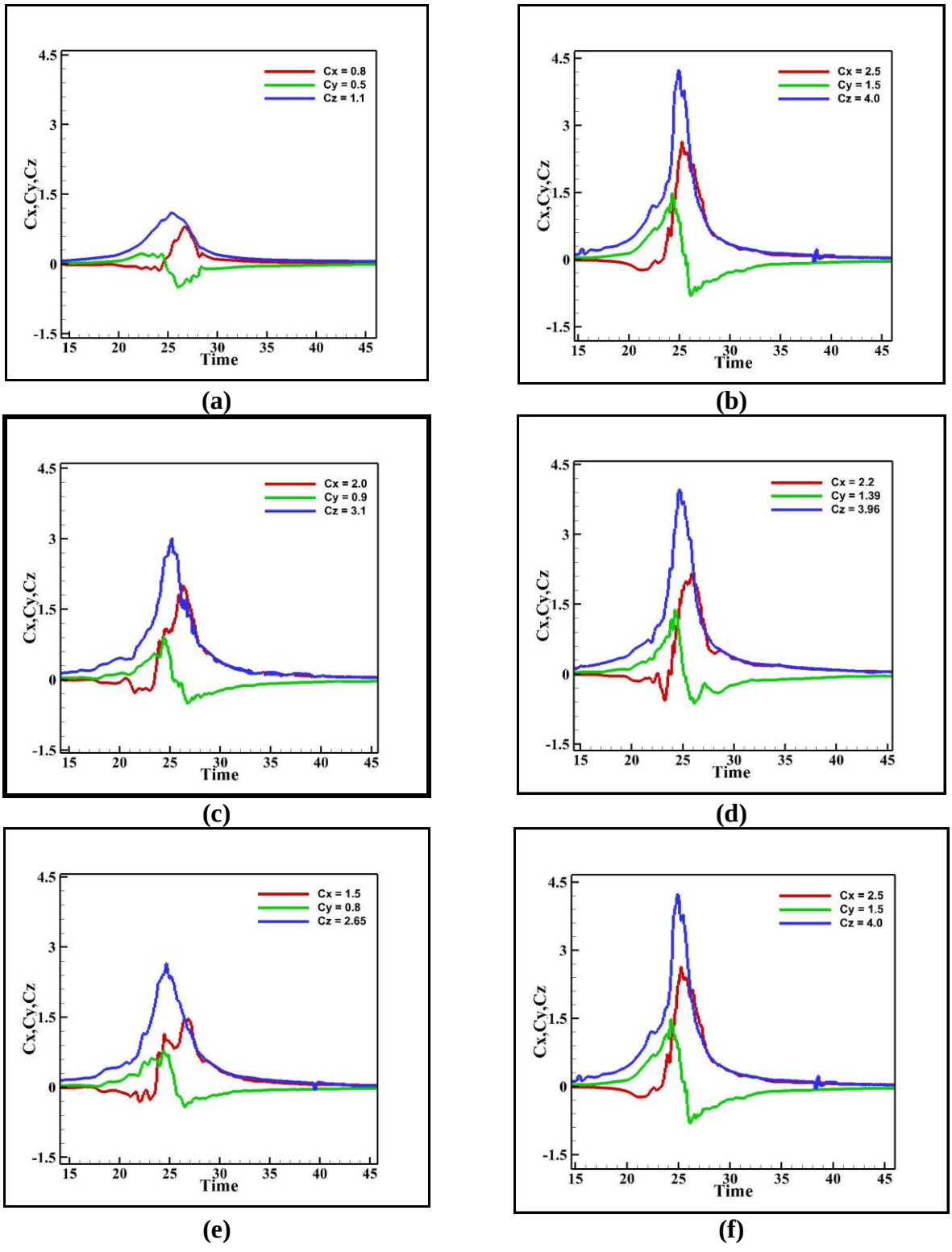

Figure 5.14: Maximum force coefficients on buildings (a): DM1, (b):CM2, (c): PM3, (d): PM4, (d) PM5 and (d) PM6 due to tornado wind for $V\theta/Vt = 3$

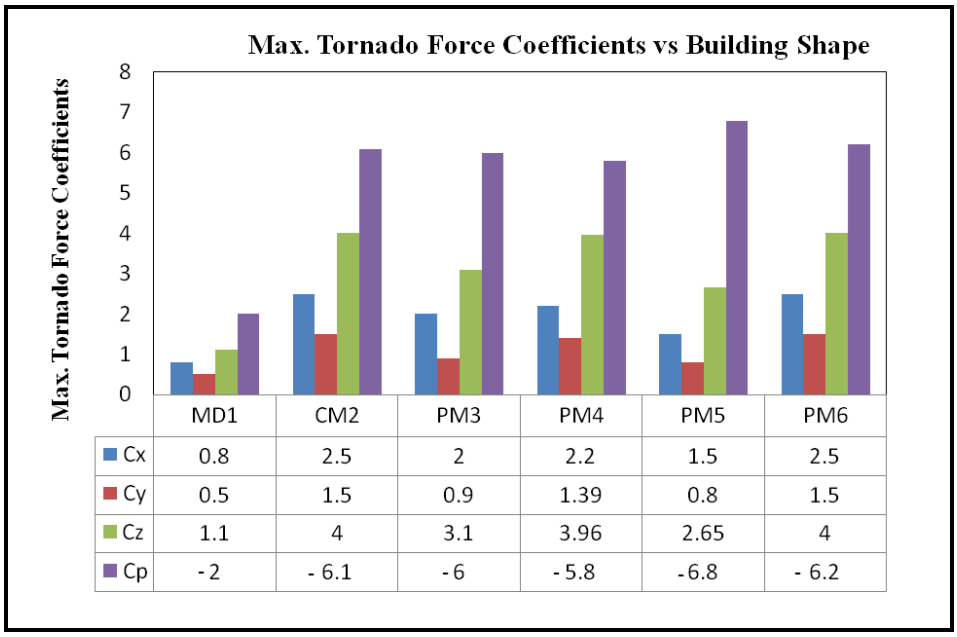

Figure 5.15: Maximum tornado force coefficients (*Cx, Cy, Cz*) vs Building shape

Table 5.1 Comparison of the absolute maximum values of *Cx, Cy, Cz, Cp* due to Tornado wind

	DM1 vs CM2	DM1 vs PM3	DM1 vs PM4	DM1 vs PM5	DM1 vs PM6
Cx	210%	150%	175%	90%	210%
Cy	200%	80%	180%	60%	200%
Cz	260%	190%	260%	150%	260%
Cp	200%	200%	190%	240%	210%

5.5 Comparison of the force and pressure coefficients due to SL and tornado wind

The maximum force and pressure coefficients due to tornado and SL wind were compared. From the comparison, one can see that the tornado forces were higher than SL wind. The side tornado forces on the dome were higher than the SL wind by 175%. The roof tornado force on dome was higher than the SL wind by 270%. The tornado pressure coefficients from the dome were higher than the SL wind by 150%. The side tornado forces on cubic (CM2) and prisms (PM3, PM4, PM5 and PM6) were higher than the SL wind by 190%, 150%, 180%, 85% and 240%, respectively. The roof tornado forces on cubic (CM2) and prisms (PM3, PM4, PM5 and PM6) were higher than the SL wind by 380%, 250%, 370%, 210% and 430%, respectively.

The tornado pressure coefficients were also greater, about 140%, 150%, 150%, 160% and 210% more. The comparison of the absolute maximum values of *Cx, Cy, Cz and Cp* due to Tornado and SL wind are listed in Table 5.2. In our comparison, the coefficients were calculated for the same maximum velocities and for the same maximum wind speed of the tornado wind. Consequently, the tornado wind field produced higher pressure coefficients.

Table 5.2 Comparison of the absolute maximum values of *Cx, Cy, Cz,Cp* due to Tornado and SL wind

Tornado vs SL	*Cx-y*	*Cz*	*Cp*
DM1	175 %	270%	150 %
CM2	190 %	380%	140%
PM3	150 %	250%	150%
PM4	180%	370%	150%
PM5	85%	210%	160%
PM6	240%	430%	210%

5.6 Results and Discussion

The tornado effect on dome, cubic and prism buildings were compared using a three-dimensional CFD simulation. The maximum force and pressure coefficients on the dome, cubic and prisms due to tornado and SL wind were compared. The following conclusions were derived from this study:

- The tornado force coefficients on the cube and prisms were larger than those on the dome building by at least two times in x-y directions and about three times in the z-direction.
- The tornado pressure coefficients on the cubic and prism buildings were at least two and half times more than those on the dome building.
- The tornado force coefficients on the dome building were larger than forces due to the SL wind, about 180% more in the x-direction and 270% more in the z- direction. The tornado pressure coefficients were also larger than pressure due to SL wind, about 150% more.

- The force coefficients on the cubic and prisms due to the tornado wind were larger than those due to the SL wind at least 85% in the x-y direction and about 210% more in z- direction. The tornado pressure coefficients also were greater by at least 140%.

CHAPTER 6: THE INFLUENCE OF TANGENTIAL TO TRANSLATIONAL VELOCITY RATIO OF TORNADO COEFFICIENTS ON STRUCTURES

6.1 Introduction

Tornados are a significant hazard for human lives and the economy. In recent years, extensive wind tunnel and computer modeling work has been done to understand the effect of tornado force on structures. Most of the work was on one or two tornado translation speed effects on building forces. The ratio of the tangential (V_θ) to translational velocity (V_t), ie V_θ/V_t , reported in recent studies by Sengupta et al. (2008), Yang et al. (2010), Haan et al. (2010) and Hu et al. (2011) is 10 or greater, which is larger than the field observation ratios. To quantify the loads on low-rise buildings due to realistic tornadoes, investigation of the pressures and forces on low-rise building models using several V_θ/V_t ratios is needed. Previously the tornado force and pressure coefficients on cubic buildings were compared using the University of Arkansas (UA) model for only one V_θ/V_t ratio of 2 (Selvam and Millet (2005) and Alrasheedi and Selvam (2011).

6.2 Objectives

The UA computer model based on the RCVM was used to calculate the effect V_θ/V_t ratio of tornado force coefficients on a dome cubic and prism buildings. The effect of grid resolution in the domain was considered. The force coefficients on a dome (DM1), cube (CM2) and prism (PM3) were compared in this chapter for V_θ/V_t ratios = 1, 3, 6 and 8. By using the computer model, the influence of four different V_θ/V_t ratios (i.e.1, 3, 6, 8) on tornado force coefficients were predicted and compared. These ratios are very much in agreement with field observation ratios. The V_θ/V_t ratio average from real tornados has been reported to be from 1.0 to 8.0 (Ahmed and Selvam, 2016).

6.3 Tornado vortex bending and displacement during the travel

The tornado is translated in the free stream direction (along x-axis) with a different impact speed, Vt (3, 1, 0.5, 0.375) toward the building, and the corresponding V_θ/V_t ratio are 1, 3, 6 and 8. The tangential velocity is kept constant, $V_\theta = 3$. The vortex core starts the travel outside the domain, and it is smoothly introduced inside the domain using the boundary conditions. The simulation begins with the free stream flow that slowly changes to the rotational wind field. This reduces any anomalies created by the superposition of the vortex flow over a free stream flow. According to the prescribed boundary conditions the center of the vortex is supposed to coincide with the center of the building at $t = 24$ units. Figures 6.1-6.3 illustrates the pressure field of the different tornado speed. It was noticed that as the tornado speed increases, the upper portion of the tornado inclines forward as shown in Figures 6.1-6.3. That may affect the position and value of tornado forces. The effect of different V_Θ/V_t ratio of tornado force coefficients on buildings will be disused V_Θ/V_t in the next section.

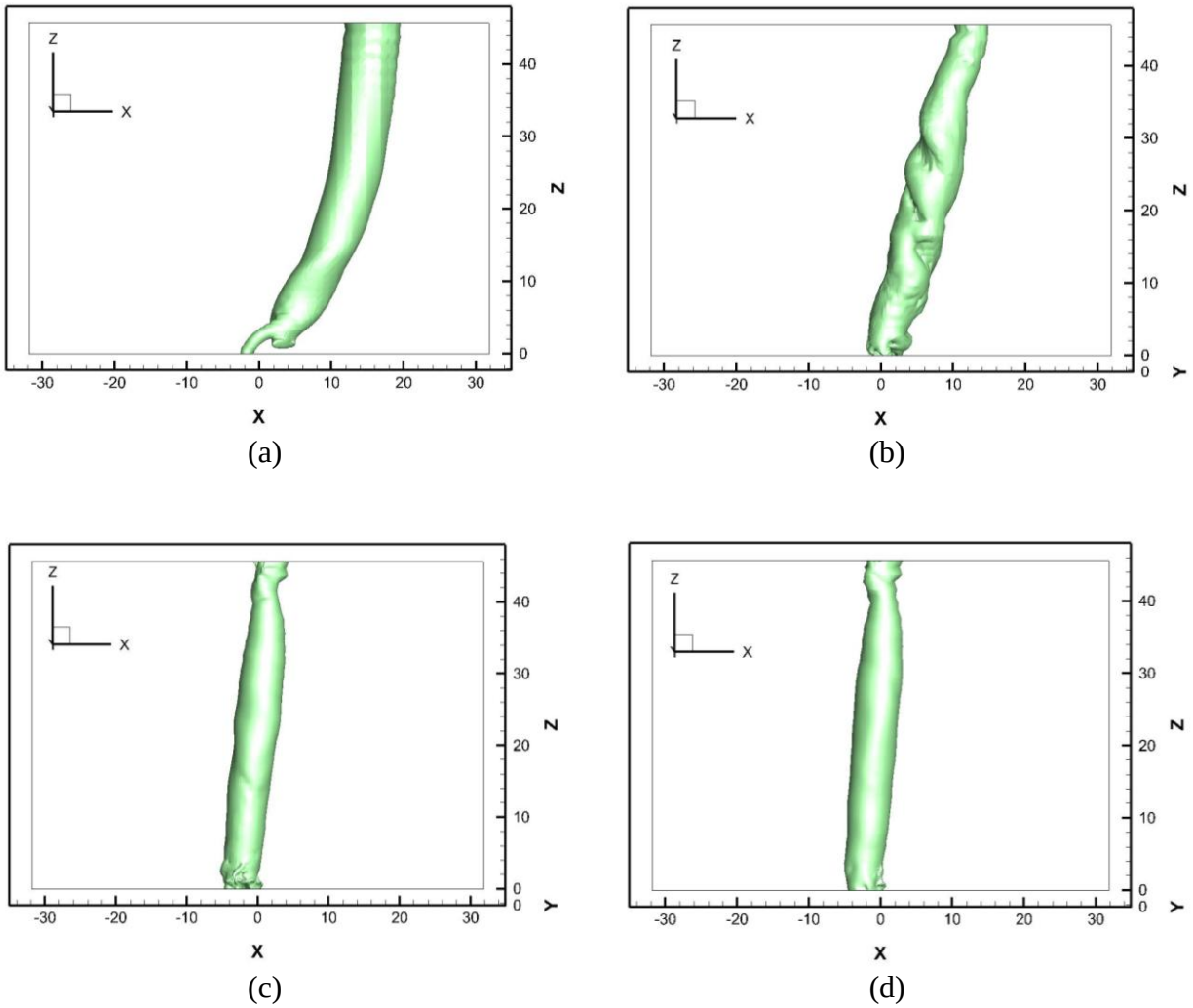

Figure 6.1: *xz*-plane of tornado vortex-dome at 24 units for (a) $V\theta/Vt$ = 1.0, (b) $V\theta/Vt$ = 3.0, (c) $V\theta/Vt$ = 6.0 and (d) $V\theta/Vt$ = 8.0.

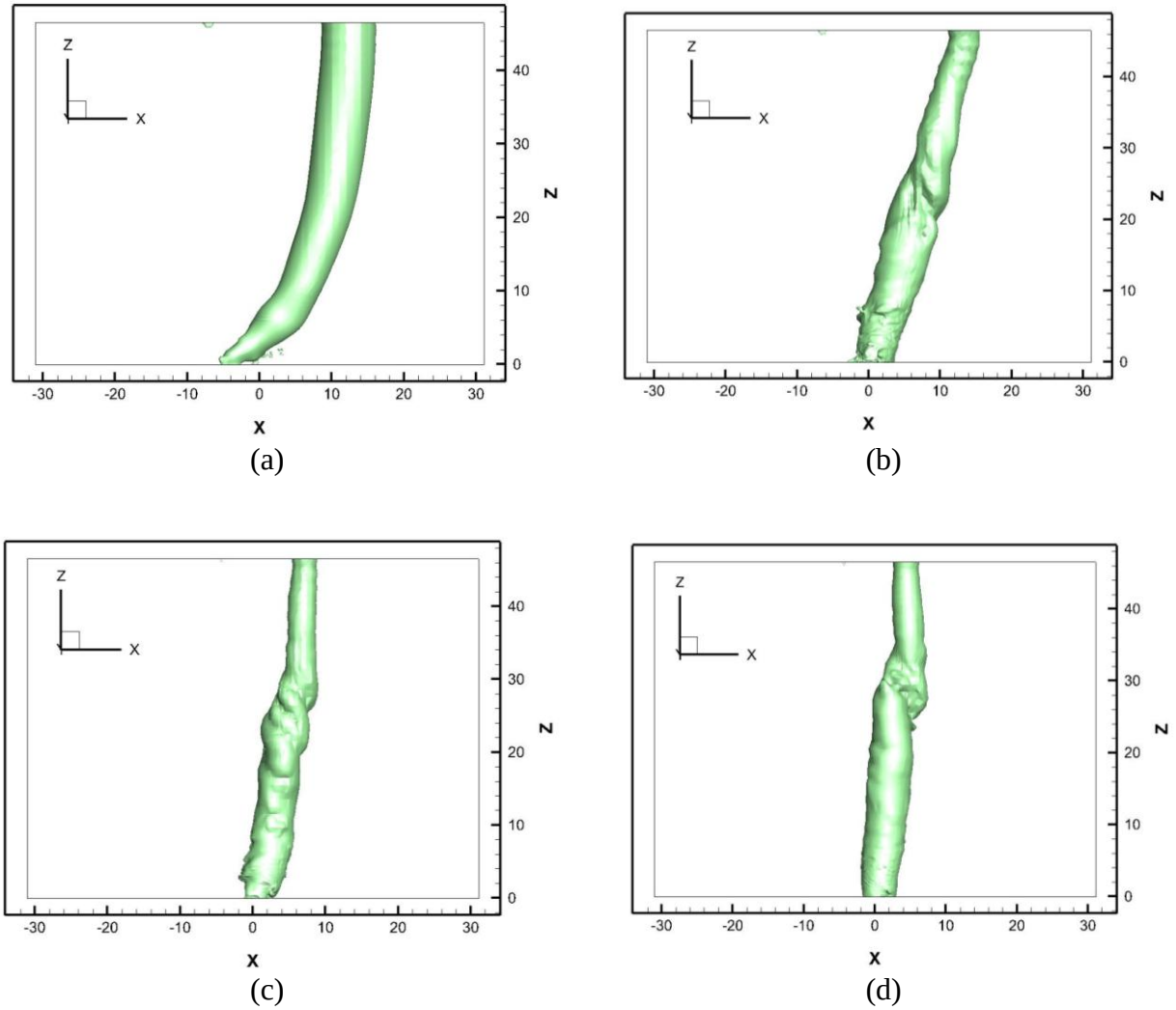

Figure 6.2: *xz*-plane of tornado vortex-cubic at 24 units for (a) $V\theta/Vt$ = 1.0, (b) $V\theta/Vt$ = 3.0, (c) $V\theta/Vt$ = 6.0 and (d) $V\theta/Vt$ = 8.0.

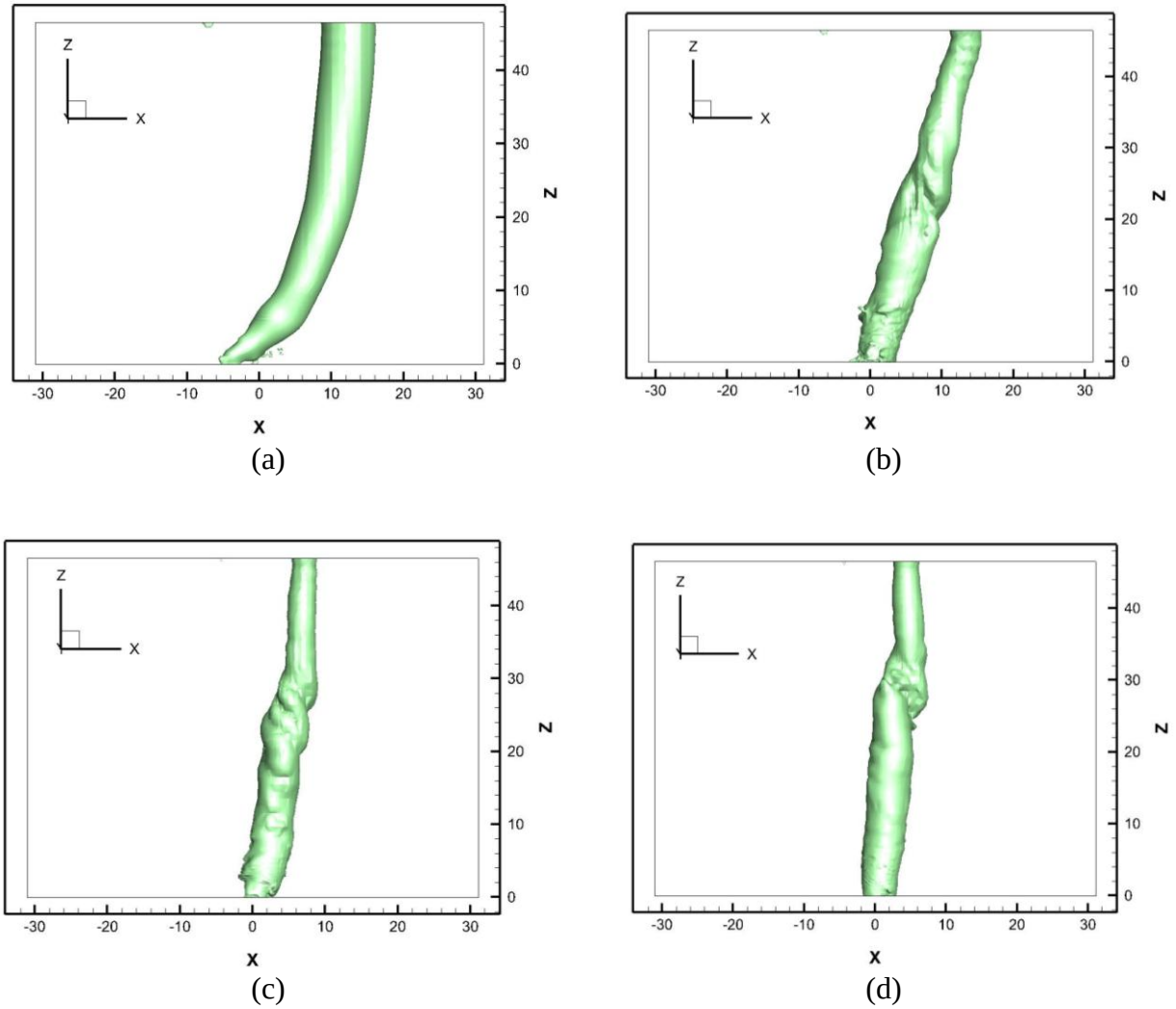

Figure 6.3: *xz*-plane of tornado vortex-prism at 24 units for (a) $V\theta/Vt$ = 1.0, (b) $V\theta/Vt$ = 3.0, (c) $V\theta/Vt$ = 6.0 and (d) $V\theta/Vt$ = 8.0.

6.4 Effect of the ratio of the tangential to translational velocity on tornado force coefficients

At each time step, large quantities of data were produced and the forces produced in the x, y and z-directions were calculated. The input data was taken from Table 1.1. The computed tornado force coefficients *Cx*, *Cy*, *Cz* were plotted against time. The forces were computed by integrating the pressure on a cubic and prism and dome building in the x, y and z directions, respectively.

6.4.1 The x-direction force coefficients

The *x*-direction force coefficient time histories of each model for V_Θ/V_t = 1, 3, 6, 8 are given in Figure 6.4. The *Cx* time histories of the three models (CM, PM, DM) were composed of several distinct parts. The time histories begin at a value close to zero and continue almost constantly until the tornado is close enough to begin affecting the pressure on the surface of the model. The second part causes a force in the negative *x*-direction (opposite of the direction of translation) as the tornado reaches the model, and the model begins to have negative surface pressures caused by the pressure drop due to the swirling winds. As the tornado passes over the building model, the force coefficient in the direction of translation returns to zero and then becomes increasingly positive until it reaches a peak and then returns to zero as the tornado continues past it.

For the V_Θ/V_t =1 case, the *Cx* changes from zero and then back to zero between the time values of 23 and 28 indicating that the loading of the building in the *x*-direction begins when the tornado is about a distance equal to one core diameter from the center of the building. For the ratio (V_Θ/V_t 3, 6 and 8), the tornado loading mainly occurs between the non-dimensional time of time from 18, 15, 12 units to 28, 30, 35 units. This was caused by the lagging behind of the lower portion of the tornado due to the faster translation speed. The low V_θ/V_t ratio, had faster translations speeds which shifted the entire time history with respect to the x-axis that measured the distance of the center of the vortex to the center of the building.

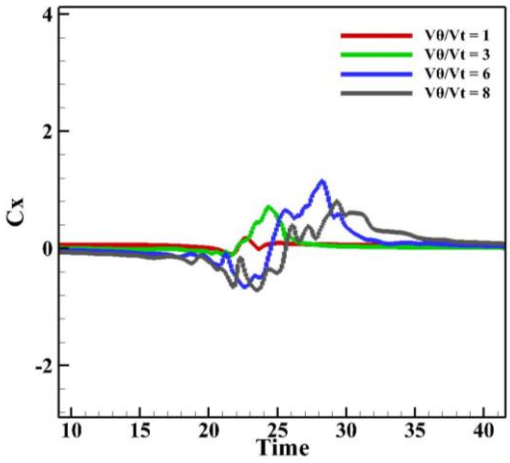

(a)

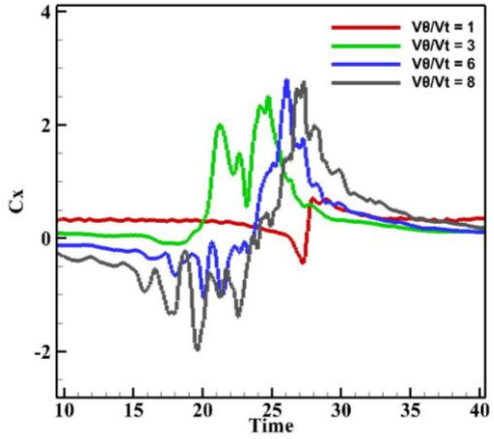

(b)

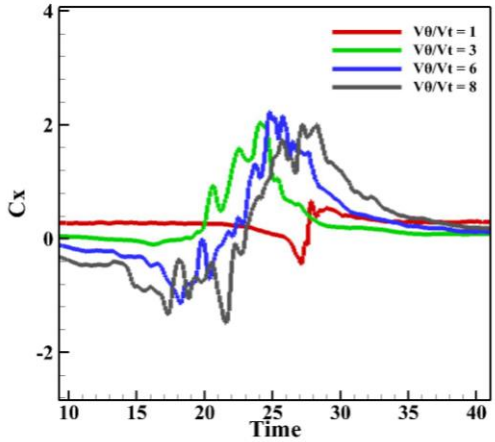

(c)

Figure 6.4: Tornado force coefficients in *x*-direction due to different V_θ/V_t (1, 3, 6 and 8) ratios on: (a) dome, (b) cubic and (c) prism

6.4.2 The y-direction force coefficients

The y-direction (perpendicular to the direction of translation) force coefficient time histories of each model for V_θ/V_t = 1, 3, 6, 8 are given in Figure 6.2. The *Cy* time histories also followed a distinct pattern. As the tornado approaches the building model, the tornado tangential velocity component is parallel to the positive y- axis. The positive pressures on the windward side of the building caused by the strong tangential velocity overcome the negative pressures due to the vortex causing the force coefficient to reach a positive peak. As the tornado moves over the center of the building, the tangential velocity component comes from the opposite direction causing the y- direction force coefficient to peak in the opposite direction.

The non-dimensional time histories for the cubic building considering all ratios (V_θ/V_t = 1, 3, 6, 8) reach their positive peak at a time t = 27, 24, 22, 20 units, respectively. Similar trends could be seen for the prism and dome models as shown in Figure 6.5. For faster translation speeds, or lower Vθ/Vt ratio, the maximum force coefficients shifted to the left of the time history. For all models considering all V_θ/V_t ratios the positive and negative peaks were symmetric around *Cy* = 0. The envelopes of the peak values are symmetric.

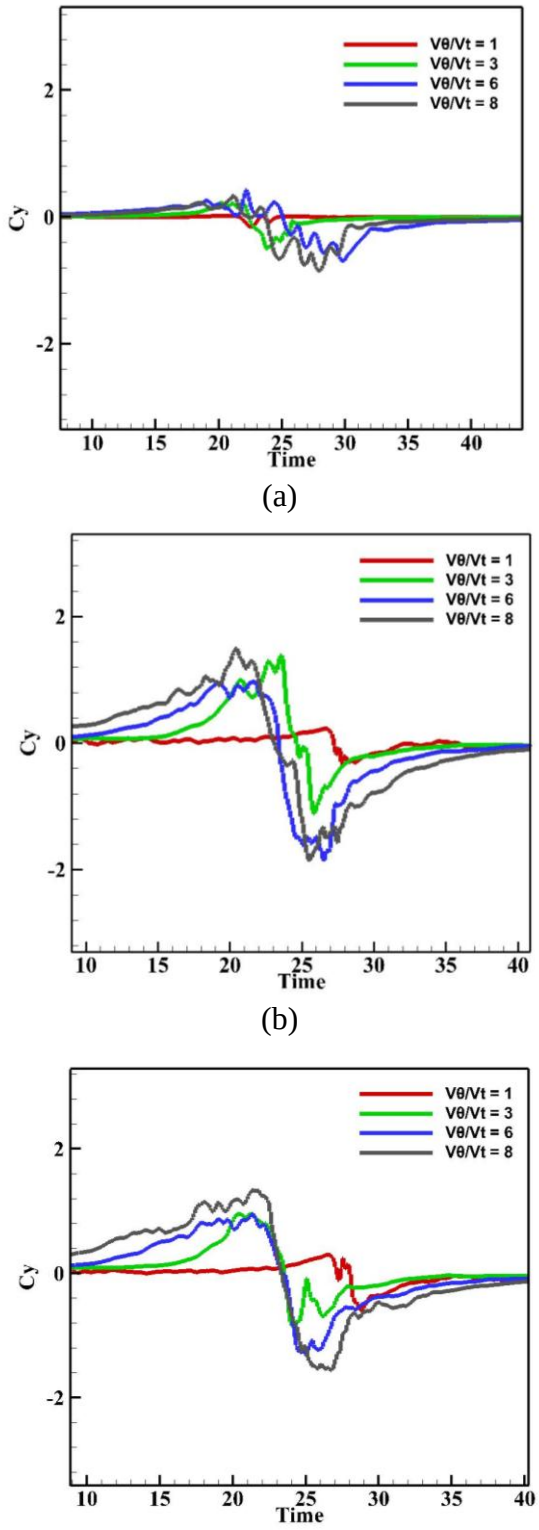

Figure 6.5: Tornado force coefficients in *y*-direction due to different V_θ/V_t (1, 3, 6 and 8) ratios on: (a) dome, (b) cubic and (c) prism

6.4.3 The z-direction force coefficients

The vertical (z) force coefficient time histories of the three models for the V_Θ/V_t = 1, 3, 6, 8 were shown in Figures 6.6. There are two important observations that should be made concerning the *Cz* coefficients. The first is that the *Cz* time histories peak at a much higher value than *Cx, Cy*. Where *Cx* and Cy never reached or exceeded *Cz* value. The second observation is that the pressures on the roofs of the models contributed to the tornado force in the vertical direction. In fact, only the vertical components of the pressures that act normal to the surface of the roof contribute to the vertical force. The time histories above clearly show two distinct peaks. This is most likely due to the high swirl ratio vortex simulated for this study. The valley between the two peaks does not drop to zero because even though the tangential velocity component of the swirling wind approaches zero at the center of the vortex, the pressures on the surface of the building are still affected by the pressure drop at the center of the tornado.

The duration of the loading on the roofs of the three models (CM, PM, DM) between the peaks for the ratios (VΘ/Vt = 1, 3, 6, 8) are about 1, 3, 7, 10 units, respectively. The cubic model has much higher peaks than the prism model that is geometrically the same except for the dimensions. The prism has a larger width and length than the cubic. The reason for the considerable difference between the tornado force coefficients on the cubic and prism model is that the relation between the tornado's diameter (td) and cubic and prism width (D) is not the same. The tornado's diameter is about 6 and 3.3 times larger than the width of the cubic and prism building, respectively. The maximum force coefficient on the building increases when the ratio between tornado and building' width increases. This observation is similar to the one reported by Alrasheedi (2011) and Yousef et al. (2016). A comparison of force coefficients

shows that for all models (CM, PM, DM) the slower moving tornado produces higher force coefficients.

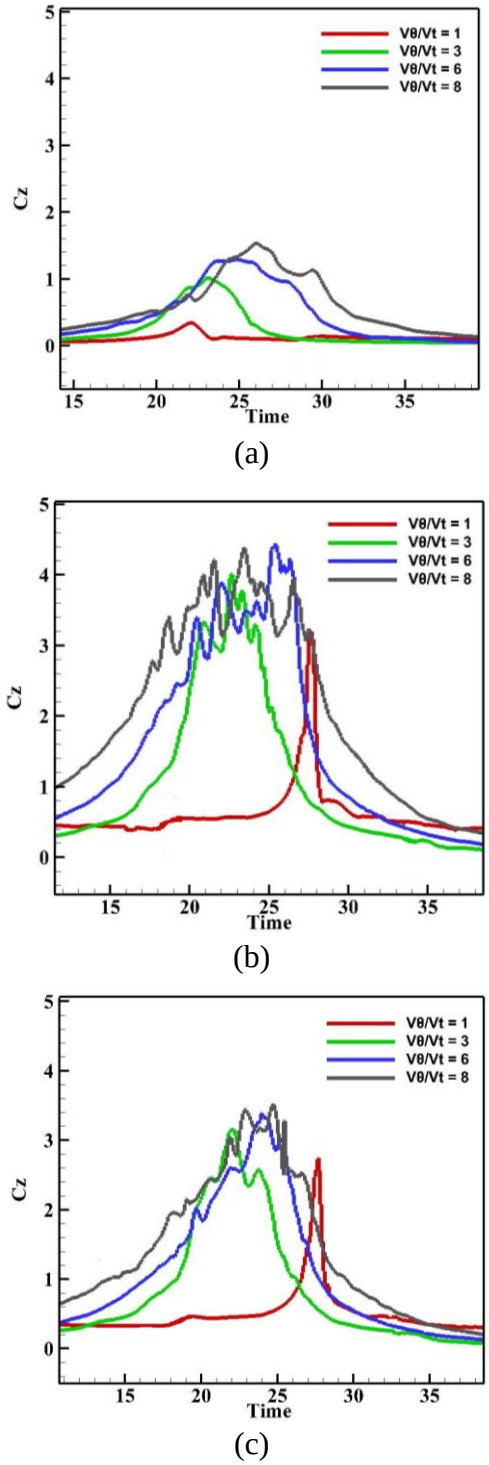

Figure 6.6: Tornado force coefficients in *x*-direction due to different V_θ/V_t (1, 3, 6 and 8) ratios on: (a) dome, (b) cubic and (c) prism

6.5 Results and discussion

The force coefficients on a dome (DM1), cubic (CM2) and prism (PM3) were compared in this chapter for *Vθ/Vt* ratios = 1, 3, 6 and 8. The conclusions arrived from this comparison are:

- When the tornado translation speed increases, the upper portion of tornado moves forward more than bottom part due to boundary layer interaction at the bottom part.
- The magnitudes of the forces were found to be larger for slower translation speeds, high *Vθ/Vt* ratio. These results are in agreement with the results reported in the recent studies as listed in Table 6.1.
- For faster translation speeds or, lower Vθ/Vt ratio, the maximum values shifted to the left of the time history

Table 6.1 The force coefficients on the dome, cube and prism due to different V_θ/V_t ratios

Referees	*Vθ/Vt*	Building Shape	Model	*Cx*	*Cy*	*Cz*
Selvam et al. (2005)	2.0	Cube	Num.	0.82	1.36	1.81
Sarkar et al. (2006)	35	Tall Cube	Exp.	2.01	2.01	1.77
	18			1.78	1.78	1.66
Sengupta et al. (2008)	40	Cube	Exp.	1.97	1.97	1.24
	20			1.82	1.82	1.22
Sengupta et al. (2008)	40	Tall Cube	Exp.	2.17	2.17	1.54
	20			1.75	1.75	1.78
Sengupta et al. (2008)	40	Tall Cube	Num.	2.01	2.01	1.77
	20			1.78	1.78	1.66
Sengupta et al. (2008)	40	Cube	Num.	1.57	1.57	1.09
	20			1.4	1.4	0.98
Hana et al. (2010)	80	Gable roof	Exp.	1.1	1.2	3.0
Hu et al. (2011)	18	Gable roof	Exp.	0.9	0.7	2.8
Case et al. (2011)	78	Gable roof	Exp.	0.75	1.20	2.4
	26			0.70	1.00	2.0
Yang et al. (2011)	24	Tall cube	Exp.	2.0	0.4	0.7
Zhao et al. (2016)	10	Dome	Num.	0.69	0.13	0.52
Current study	1.0	dome	Num.	0.2	0.2	0.4
	3.0			0.7	0.5	1.1
	6.0			1.0	0.7	1.3
	8.0			0.8	0.9	1.5
Current study	1.0	cube	Num.	0.7	0.3	3.0
	3.0			2.5	1.5	4.0
	6.0			2.6	1.8	4.3
	8.0			2.7	1.8	4.3
Current study	1.0	dome	Num.	0.65	0.6	2.7
	3.0			2.0	0.9	3.1
	6.0			2.2	1.2	3.4
	8.0			2.0	1.4	3.6

CHATER 7: SUMMARY AND CONCLUSIONS

7.1 Summary

For a regular straight wind, the forces on buildings are available from standards and wind tunnel testing whereas the tornado forces on buildings are not yet thoroughly understood. Experimental tornado simulators were employed to measure tornado force coefficients on multiple building shapes (e.g. circular cylinder, gable-roof and cubic building). However, few studies have been conducted to understand tornado interaction with a dome building. In this work, the effects of force coefficients on dome, cubic and prism buildings were compared. A three-dimensional CFD simulation, based on large eddy simulation, was applied to numerically simulate tornado-structure interaction using computational fluid dynamics. That model was also used to calculate the effect of V_θ/V_t ratios on tornado force coefficients for prism and dome buildings with systematic study. The V_θ/V_t ratios are completed considered to be 1, 3, 6 and 8 for comparison. The conclusions arrived from the work are listed below.

7.2 Conclusions

7.2.1 Objective 1: Investigate the effect of SL wind on dome, cubic and prisms using ASCE 7-10 provision and A CFD model

The force and pressure coefficients on dome, cube and prisms due to SL wind were compared using the ASCE 7-10 standard and CFD model. The SL wind produced higher maximum negative pressure on the cubic and prisms (CM2, PM3, PM4, PM5, and PM6) than the dome (DM1), about 210%, 210%, 200%, 225% and 150%. The cube and prisms also had higher maximum positive pressure than the dome, about 40%, 40%, 80%, 40% and 100% more. The cubic and prisms create about 175%, 175%, 170%, 180%, 155%, higher force in the *x*-direction, and 180%, 190%, 180%, 180%, 160% higher force in the *z*-direction than the dome. Then, the

calculated force and pressure coefficients on the dome, cube and prisms for ASCE 7-10 SL wind were compared with those from the CFD model to validate. The forces and pressures that were computed from the CFD model were compared with those calculated from ASCE 7-10 provisions. The results calculated from the ASCE 7-10 standard and CFD model were very close. Therefore, the CFD model can be used with confidence.

7.2.2 Objective 2: Compare the effect of tornado on dome and prisms building using a CFD model

The tornado force and pressure coefficients on buildings (dome, cube and prism) for only one V_θ/V_t ratio of 3 was investigated using the University of Arkansas (UA) model. The calculated maximum negative and positive pressures on the dome, cube and prisms were compared. The cube and prisms (CM2, PM3, PM4, PM5, and PM6) made about 200%, 210%, 200%, 240% and 210% higher negative pressure than the dome model (DM1). The pressure coefficients on the cube and prisms due to the tornado wind were about two larger than the force on dome building. The cube and prisms made higher maximum positive pressure than the dome, about 150%, 130%, 130%, 130% and 80% more, respectively. The tornado forces on the dome, cube and prisms were compared using a CFD model. The cube and prisms (CM2, PM3, PM4, PM5, and PM6) made higher tornado force coefficients than the dome, about 190%, 150%, 175%, 90% and 210% more in the *x*- and *y*-directions and 260%, 180%, 260%, 140% and 280% more in the *z*-direction.

The tornado force coefficients on the dome building were larger than SL wind forces about 180% more in the x-direction and 270% more in the z- direction. The tornado pressure coefficients were also larger than pressure due to SL wind, about 150% more. The force coefficients on the cube and prisms (CM2, PM3, PM4, PM5, and PM6) due to the tornado wind

were larger than those due to the SL wind, about 190% ,150%, 180%, 85% and 240% more in *x*-direction and about 380%, 250%, 370%, 210% and 430%, more in *z*-direction, respectively. The tornado pressure coefficients were also greater, about 140%, 150%, 150%, 160% and 210% more.

7.2.3 Objective 3: Investigate the influence of tangential to translational velocity ratio on tornado coefficients on structures, using a CFD model

The UA computer model based on RCVM was used again to calculate the effect V_θ/V_t ratio on tornado force coefficients on a dome, cube and prism building. The effect of grid resolution in the domain was considered. The force coefficients on a dome (DM1), cube (CM2) and prism (PM3) for V_θ/V_t rations (1, 3, 6 and 8) were compared. It was noticed that when the tornado translation speed increases, the upper portion of tornado moves forward more than the bottom part due to boundary layer interaction at the bottom part. The magnitudes of the forces were found to be larger for slower translation speeds, or higher V_θ/V_t ratio. For faster translation speeds, or lower V_θ/V_t ratio, the maximum force coefficients shifted to the left of the time history.

7.3 Primary Contributions

The first contribution to the scientific community was that tornadoes produced higher force coefficients, about three times, on dome buildings than those of SL wind. In addition, the tornado force coefficients on a dome building were about three or four times less than those on cubic and prism buildings. This observation is in agreement with the field observations. The pressure and force coefficients in the x-direction on the cube and prisms due to SL wind were similar to those on the dome due to the tornado. However, force coefficients in the z-direction on the cube and prisms due to SL were higher than those on the dome due to the tornado by 30%. One can say that the dome shape can reduce the tornado forces. Therefore, the people who live in

Tornado Alley should build beautiful, safe dome buildings as shown in Figure 7.1 and get on with living healthy, happy, safe lives.

(a) **(b)**

Figure 7.1: Dome house (a) exterior (b) interior

7.4 Limitations of the present study

Like most of the numerical model, UA numerical model has some limitations and disadvantages. The vertical velocity is not considered in the RCVM that was used in the UA model; only the tangential velocity profile is represented. Grid independency is another limitation that it is hard to achieve due to high computational cost and the huge storage space required. In addition, there are different numerical errors caused by approximation of governing equations and repetition of the error.

7.5 Suggested future work

There are still many interesting and important studies that were observed during the conduction of this study but were not considered due to the time limit. This section addresses most of the suggested research areas.

- Tornado force on dome building needs to be compared with a greater variety of structures, such as dome on cylinder, mansard roof, hip- and gable-roof, Gambrel roof (Dutch Colonial) and shed roof as shown in Figure 7.2. With more data collected, our findings are likely to

provide new results of tornado effects on any type of buildings.

- Effect of different surroundings on tornado wind loads on domed structures
- The influence of the ratio of tornado radius to the dome's height has not been explored.

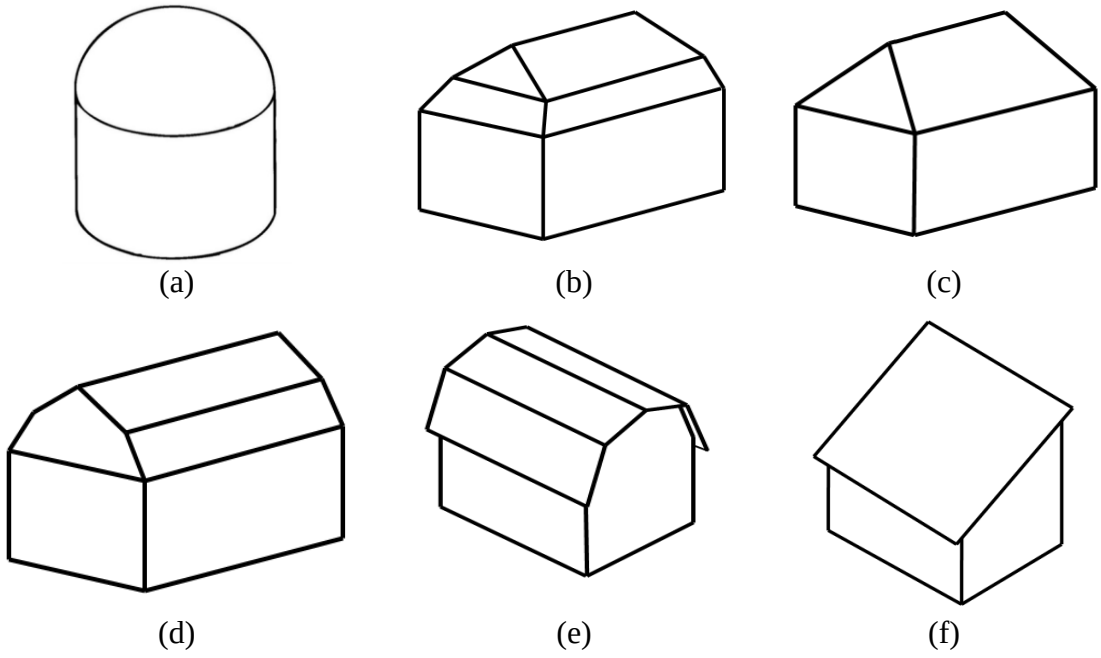

Figure 7.2: Building models (a) dome on cylinder (b) mansard roof (c) Hip and gable roof (d) Gambrel roof (e) gambrel (Dutch Colonial) roof (f) Shed roof

REFERENCES

Ahmed, S.N., & Selvam, R.P. (2015). Ridge effects on tornado path deviation. *International Journal of Civil and Structural Engineering Research*, *3*(1), 273-294.

Alrasheedi, N.H., & Selvam, R.P. (2011). Computing tornado forces on different building sizes. *In Proceedings of the 13th International Conference on Wind Engineering (ICWE13)*, Amsterdam, Netherlands.

Alrasheedi, N.H. (2012). Computer modeling of the influence of structure plan areas on tornado forces. *PhD dissertation, University of Arkansas*, Fayetteville, USA.

Armstrong, G. (2013). Storm Shelter Survives EF-5 Tornado. Retrieved from https://www.fema.gov/media-library/assets/images/70975.

Bagwell, N. (2014). Build Me a Dome: Dreaming of a Monolithic Dome House. Retrieved from http://www.noelbagwell.com/personal-views/build-me-a-dome.

Castro, I.P., & Robins, A.G. (1977). The flow around a surface-mounted cube in uniform and turbulent streams. *Journal of Fluid Mechanics, 79,* 307–335

Cermak, J.E. (1975). Applications of fluid mechanics to wind engineering - a Freeman Scholar Lecture. *Journal Fluid Engineering, 97,* 9–38.

Chang, C.H., & Meroney, R.N. (2001). The effect of surroundings with different separation distances on surface pressures on low-rise buildings. *Journal of Wind Engineering and Industrial Aerodynamics, 91,* 1039-1050.

Church, C., Burgess, D., Doswell, C., & Davies-Jones, R. (1993). Tornado vortex theory, in: the tornado: its structure, dynamics, prediction, and hazards. *Geophysics Mono, American Geophysical Union*, *79*, 19-39.

Church, C., Snow, J.T., Baker, G.L., & Agee, E.M. (1979). Characteristics of tornado-like vortices as a function of swirl ratio: A laboratory investigation. *Journal of the Atmospheric Sciences, 36*(9), 1755-1776.

de Sampio, P.B, Lyra, P.M., Morgan, K. & Weatherill, N.P. (1993). Petro-Galerkin solutions of the incompressible Navier-Stokes equations in primitive variables with adaptive remeshing. *Computer Methods in Applied Mechanics and Engineering, 106,* 143-178.

Diamond, C.J., & Wilkins, E.M. (1984). Translation effects on simulated tornadoes. *Journal of the Atmospheric Sciences*, *41*(17), 2574-2580.

Dutta P.K., Ghosh A.K., & Agarwal B.L. (2002). Dynamic response of structures subjected to tornado loads by FEM. *Journal of Wind Engineering and Industrial Aerodynamics, 90,* 55-69.

Filippone, A., & Afgan, I. (2008). Orthogonal blade-vortex interaction on a helicopter tail rotor. *AIAA Journal, 46* (6), 1476-1489.

Gomes, M.G, Rodrigues, A.M, & Mendes, P. (2005). Experimental and numerical study of wind pressures on irregular-plan shapes. *Journal of Wind Engineering and Industrial Aerodynamics*, 93, 741–756.

Gorecki, M.P., & Selvam, R.P. (2015a). Rankine combined vortex interaction with a rectangular prism. *International Journal of Computational Fluid Dynamics, 29* (1), 120-132.

Gorecki, M.P., & Selvam, R.P. (2015b). Visualization of tornado-like vortex interacting with wide tornado-break wall. *Journal of Visualization,18* (2), 393-406.

Haan, F.L., Balaramudu, V.K., & Sarkar, P.P. (2010). Tornado-induced wind loads on a low-rise building. *Journal of Structural Engineering, 136,* 106-16.

Holmes, J.D. (1993). Wind load on low-rise building—a review. CSIRO. *Division of Building Research,* Highett

Hoxeya, R.P., Robertsona, A.P., Basarab, B., & Younisb, B.A. (1993). Geometric parameters that affect wind loads on low-rise buildings: full-scale and CFD experiments. *Journal of Wind Engineering and Industrial Aerodynamics 50,* 243-252.

Horr, A.M., Safi, M., & Alavinasab, S.A. (2003). Computational wind tunnel analyses for large dome using CFD theory. *International Journal of Space Stru*ctures, *18,* 85-104.

Hunt, J.R, Abell C.J., Peterka J.A., & Woo H. (1978). Kinematical studies of the flows around free or surface-mounted obstacles: applying topology to flow visualization. *Journal of Fluid Mechanics, 86* (1), 179–200.

Hu, H., Yang, Z., Sarkar, P., & Haan, F. (2011). Characterization of the wind loads and flow fields around a gable roof building model in tornado-like winds. *Experiments in fluids, 51*(3), 835-851.

Ishihara, T., Oh, S., & Tokuyama, Y. (2011). Numerical study on flow fields of tornado-like vortices using the LES turbulence model. *Journal of Wind Engineering and Industrial Aerodynamics, 99*(4), 239-248.

Jischke, M.C, & Light, B.D. (1983). Laboratory simulation of tornadic wind loads on a rectangular model structure. *Journal of Wind Engineering and Industrial Aerodynamics, 13*, 371-382.

Kanda, M., & Maruta, E. (1993). Characteristics of fluctuating wind pressure on long low-rise buildings with gable roofs. *Journal of Wind Engineering and Industrial Aerodynamics 50*, 173–182.

Kim, K.C., Ji, H.S. & Seong S.H. (2003). Flow structure around a 3-D rectangular prism in a

turbulent boundary layer. *Journal of Wind Engineering and Industrial Aerodynamics*, *91*, 653–669.

Kosiba, K.A., & J. Wurman, (2013). The three-dimensional structure and evolution of a tornado boundary layer. *Weather and Forecasting*. doi:10.1175/WAF-D-13-00070.1

Kosiba, K.A., Robinson, P, Chan P.W., & Wurman, J. (2014). Wind field of a non-mesocyclone anticyclonic tornado crossing the Hong Kong International Airport. *Advances Meteorology*, *2014*, 1-7.

Krajnovicm, S., & Davidson, L. (1999). Large-eddy simulation of the flow around a surface-mounted cube using a dynamic one-equation sub grid model. *In the First Int. Symp. On Turbulence and Shear Flow Phenomena*, Begell House, Inc, New York.

Kringen, A. (2014). Dome shaped buildings gaining ground in Oklahoma. Retrieved from http://kfor.com/2014/08/14/dome-shaped-buildings-gaining-ground-in-oklahoma-considered-tornado-proof/.

Kuo, H.L. (1971). Axisymmetric flow in the boundary layer of a maintained vortex. *Journal of the Atmospheric Sciences*, *28*(1), 20-41.

Leslie, F.W. (1977). Surface roughness effects on suction vortex formation: A laboratory simulation. *Journal of the Atmospheric Sciences, 34*(7), 1022-1027.

Lewis, K. (2013). Oklahoma School Says Its Buildings Are Tornado Proof. Retrieved from http://www.monolithic.org/in-the-media/oklahoma-school-says-its-buildings-are-tornado-proof.

Lewellen, W. S. (1993). Tornado Vortex Theory. *In the Tornado: Its Structure, Dynamics, Prediction, and Hazards*, C. Church, D. Burgess, C. Doswell, and R. Davies-Jones, Geophysical Monograph 79, American Geophysical Union, 19-39.

Liu, X., & Marshall, J.S. (2004). Blade Penetration into a Vortex Core with and Without Axial Core Flow. *Journal of Fluids Mechanics, 519*, 81–103.

Liu, Z., Prevatt, D.O, Aponte-Bermudez, L.D., Gurley, K.R., Reinhold, T.A. & Akins, R.E. (2009). Field measurement and wind tunnel simulation of hurricane wind loads on a single family dwelling. *Engineering Structures*, *31* (10), 2265–2274.

Martinuzzi R., & Tropea C., (1993). The flow around surface-mounted, prismatic obstacles placed in a fully developed channel flow. *Journal Fluid Engineering, 1158*, 5–92.

Mehta, K. C., Minor, J.E., & McDonald, J. R. (1976). Wind speed analysis of April 3-4 tornadoes. *Journal of the Structural Division*, 102, 1709-1724.

Meroney, R. N. (2000). Comparison of numerical and wind tunnel simulation of wind loads on smooth, rough and dual domes immersed in a boundary layer. *Proceedings of CWE 2000*.

Meroney R.N., Letchford C.W. and Sarkar P. P. (2002). Comparison of numerical and wind tunnel simulation of wind loads on smooth, rough, and dual domes immersed in a boundary layer. *Wind and Structures, 5*, 347-358.

Millett, P.C. (2003). Computer Modeling of the Tornado-Structure Interaction: Investigation of Structural Loading on a Cubic Building. *Master's Thesis, University of Arkansas,* Fayetteville, AR.

Monolithic (2009). Monolithic Dome Shapes. Retrieved from http://www.monolithic.org/monolithic-dome-shapes.

NOAA (2012). Enhanced F Scale for Tornado Damage. Retrieved from http://www.spc.noaa.gov/faq/tornado/ef-scale.html

NWS (2011). Tuscaloosa-Birmingham Tornado. Retrieved from http://www.srh.noaa.gov/bmx/?n=event_04272011tuscbirm.

New Age Dome Construction (2015). Tornado Shelters/Domes in Disasters. Retrieved from http://newagedomeconstruction.com/services/tornado-shelters/.

Parker, F. (2009). Surviving Hurricanes and Tornadoes. Retrieved from http://www.monolithic.org/benefits/benefits-survivability/surviving-hurricanes-and-tornadoes.

Parker, F. (2011). A Testament to the Dome Shape. Retrieved from http://www.monolithic.org/benefits/benefits-survivability/a-testament-to-the-dome-shape

Parker, F. (2013). Domers respond to Moore, Oklahoma. Retrieved from http://www.monolithic.org/testimonials/domers-respond-to-moore-oklahoma.

Rajasekharan, S.G., Matsui, M., & Tamura, Y. (2013). Characteristics of internal pressures and net local roof wind forces on a building exposed to a tornado-like vortex. *Journal Wind Engineering and Industrial Aerodynamics*, *112*, 52-57.

Sabareesh, G.R., Matsui, M., & Tamura, Y., (2013). Ground roughness effects on internal pressure characteristics for buildings exposed to tornado-like flow. *Journal Wind Engineering and Industrial Aerodynamics*, *122*, 113-117.

Sarkar, P. P., Haan, F. L., Balaramudu, V., & Sengupta, A. (2006). Laboratory simulation of tornado and microburst to assess wind loads on buildings. Proc., ASCE Structures Congress, ASCE, Reston,Va.

Peterka, J.A, Hosoya, N., Dodge, S., Cochran, L. & Cermak J.E. (1998). Area average peak

pressures in a gable roof vortex region. *Journal of Wind Engineering and Industrial Aerodynamics*, 77–78 (1), 205–215.

Selvam, R.P. (1985). Applications of the boundary element method for tornado forces on buildings. *Ph.D. dissertation, Texas Tech University*, Lubbock.

Selvam, R. P., (1993). Computer modeling of tornado forces on buildings. *In Proceedings of the 7th US National Conference on Wind Engineering*, Gary C. Hart, Los Angeles, June, 27-30, 605-613.

Selvam, R.P. (1997). Computation of pressures on Texas Tech building using Large Eddy Simulation. *Journal of Wind Engineering and Industrial Aerodynamics, 67-68*, 647-657.

Selvam, R.P., (1998). Computational procedures in grid based computational bridge aerodynamics. *In Bridge Aerodynamics*, Larsen, A. and Esdahl (eds), Balkema, Rotterdam, 327-336.

Selvam, R.P., & Peng, Y., (1998). Issues in computing pressure around buildings. *In Structural Engineering World Wide 1998*, N.K. Srivastava (eds), Elsevier, New York, 941.

Selvam, R. P., & Millett, P. (2003). Computer modeling of tornado forces on buildings. *Wind and Structures, 6*, 209-220.

Selvam, R. P., & Millett, P. (2005). Large eddy simulation of the tornado-structure interaction to determine structural loadings. *Wind and Structures, 8* (1), 49-60.

Selvam, R.P., & Paterson, D.A. (1993). Computation of Conductor Drag Coefficients. *Journal of Wind Engineering and Industrial Aerodynamics*, **50**, 1-8.

Selvam, R. P., Roy, U. K., Jungl, Y., & Mehta K. C. (2002). Investigation of tornado forces on a 2D cylinder using computer modeling. *In Wind Engineering*, by K. Kumar (Ed), Phoenix Publishing House, New Delhi, India, 342-353.

Selvam, R.P., & Qu, Z.Q. (2002). Adaptive p-finite element method for wind engineering. *Wind and Structures, 5*, 301-316.

Sengupta, A., Haan, F.L., Sarkar, P.P, & Balaramudu, V. (2008). Investigation of tornado transient loads on buildings in microburst and tornado winds. *Journal of Wind Engineering and Industrial Aerodynamics*, 96, 2173-2187.

Sevalia, J.K, Desai, A.K, & Vasanwala, S.A. (2012). Effect of geometric plan configuration of tall building on wind force coefficient using CFD. *International Journal of Advanced Engineering Research and Studies, I*, 127-130.

Shah K.B., & Ferziger J.H. (1997). A fluid mechanicians view of wind engineering: large eddy

Simulation of flow past a cubic obstacle. *Journal of Wind Engineering and Industrial Aerodynamics, 67*(68), 211–224.

Sousa, J. (2002). Turbulent flow around a surface-mounted obstacle using 2D–3C DPIV. *Experiments in Fluids*, 33, 854–862.

Sousa J., M.M., & Pereira J.C.F (2004). DPIV study of the effect of a gable roof on the flow structure around a surface-mounted cubic obstacle. *Experiments in Fluids, 37*, 409–418.

Stathopoulos, T., Wank, K., & Wu, H. (2001). Wind pressure provisions for gable roofs of intermediate roof slope. *Wind and Structures International Journal, 4*, 119–130.

Tamura, T., Itoh, Y., Wada, A., & Kuwahara, K. (1995). Numerical study of pressure fluctuations on a rectangular cylinder in aerodynamic oscillation. *Journal of Wind Engineering and Industrial Aerodynamics, 54*, 239-250.

Tamura, T. (1999). Reliability on CFD estimation for wind-structure interaction problems. *Journal of Wind Engineering and Industrial Aerodynamics*, 81(1), 117-143.

Ward, N.B. (1972). The exploration of certain features of tornado dynamics using a laboratory model. *Journal of the Atmospheric Sciences, 29*(6), 1194-1204.

Wen Y., (1975). Dyamic tornadic wind loads on tall buildings. *Journal of structural Division. 101*, 169-185.

Wen, Y.K., & Chu, S.L. (1973). Tornado Risks and Design Wind Speed. *Journal of the Structural Division, 99*, 2409-2421.

Wolchover, N. (2011). Why Aren't There Tornado Safety Building Codes? Retrieved from http://www.livescience.com/13962-tornado-safety-building-codes.html.

Wurman, J., Kosiba, K., & Robinson, P. (2013). In situ, Doppler radar and video observations of the interior structure of a tornado and the wind-damage relationship. *Bulletin of the American Meteorological Society, 94*(6), 835-846.

Yakhot, A., Anor, T., Liu, H., & Nikitin N. (2006). Direct numerical simulation of turbulent flow around a wall mounted cube: spatiotemporal evolution of large-scale vortices. *Journal Fluid Mechanics, 566*, 1–9.

Yang Z., Sarkar P. and Hu H. (2011). An experimental study of a high-rise building model in tornado-like flows. *Journal Fluids and Structure, 27*, 471-486

Yang Z., Sarkar P. and Hu H. (2011). Visualization of the flow structures around a gable-roofed building model in tornado-like winds. *Journal Visualize, 13* (4), 285-288.

Yousef, M.A., & Selvam, R.P. (2016). Effect of equivalent height, surface area and Volume of

the dome to prism on tornado forces using CFD. *Proceeding: 8th International Colloquium on Bluff Body Aerodynamics and Applications (BBAA VIII),* Boston, Massachusetts, June.

Zhao, Y., Yan, G., Zu, J., Yuan, F., Kakkattukuzhy, M. and Isaac, K. (2016). Comparison on wind effects of tornadic and straight-line wind fields on spherical dome structures. *Proceeding: 8th International Colloquium on Bluff Body Aerodynamics and Applications (BBAA VI*II)" Boston, Massachusetts, June.

APPENDIX A: Calculation of Wind Loads on Structures according to ASCE 7-10

- Table 27.2-1 Steps to determine MWFRS wind loads for enclosed partial and open building of heights

The design wind loads for buildings and other structures, including the MWFRS and component and cladding elements thereof, shall be determined using one of the procedures as specified in the following section. An outline of the overall process for the determination of the wind loads, including section references, is provided in Figure A.1.

Main Wind-Force Resisting System (MWFRS) Wind loads for MWFRS shall be determined using one of the following procedures:

(1) Directional Procedure for buildings of all heights as specified in Chapter 27 for buildings meeting the requirements specified therein.

(2) Envelope Procedure for low-rise buildings as specified in Chapter 28 for buildings meeting the requirements specified therein'

(3) Directional Procedure for Building Appurtenances (rooftop structures and rooftop equipment) and Other Structures (such as solid freestanding walls and solid freestanding signs, chimneys, tanks, open signs, lattice frameworks, and trussed towers) as specified in Chapter 29.

(4) Wind Tunnel Procedure for all buildings and all other structures as specified in Chapter 31.

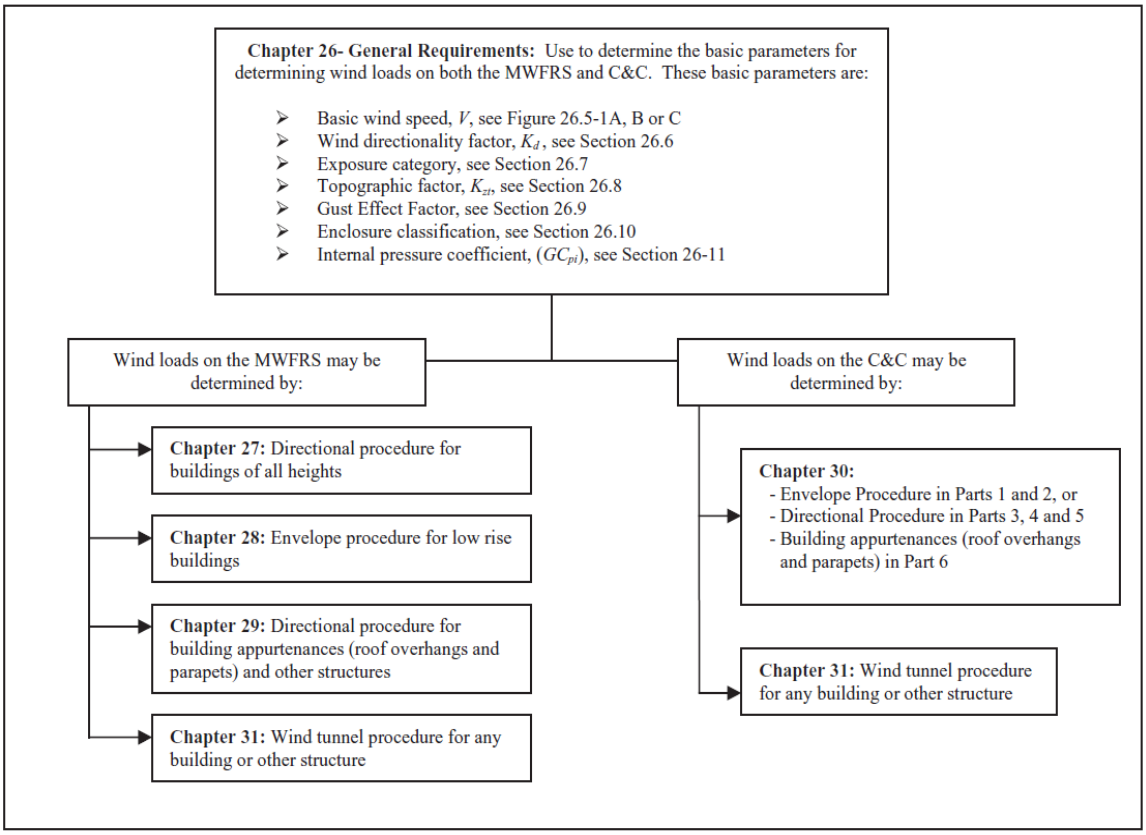

Figure A.1: Determination of Wind Loads

Step 1: Determine risk category of building or other structure, see Table 1.5-1 in **(P.g 2)**

Table 1.5-1 Risk Category of Buildings and Other Structures for Flood, Wind, Snow, Earthquake, and Ice Loads

Use or Occupancy of Buildings and Structures	Risk Category
Buildings and other structures that represent a low risk to human life in the event of failure	I
All buildings and other structures except those listed in Risk Categories I, III, and IV	II
Buildings and other structures, the failure of which could pose a substantial risk to human life.	III
Buildings and other structures, not included in Risk Category IV, with potential to cause a substantial economic impact and/or mass disruption of day-to-day civilian life in the event of failure.	
Buildings and other structures not included in Risk Category IV (including, but not limited to, facilities that manufacture, process, handle, store, use, or dispose of such substances as hazardous fuels, hazardous chemicals, hazardous waste, or explosives) containing toxic or explosive substances where their quantity exceeds a threshold quantity established by the authority having jurisdiction and is sufficient to pose a threat to the public if released.	
Buildings and other structures designated as essential facilities.	IV
Buildings and other structures, the failure of which could pose a substantial hazard to the community.	
Buildings and other structures (including, but not limited to, facilities that manufacture, process, handle, store, use, or dispose of such substances as hazardous fuels, hazardous chemicals, or hazardous waste) containing sufficient quantities of highly toxic substances where the quantity exceeds a threshold quantity established by the authority having jurisdiction to be dangerous to the public if released and is sufficient to pose a threat to the public if released.[a]	
Buildings and other structures required to maintain the functionality of other Risk Category IV structures.	

[a]Buildings and other structures containing toxic, highly toxic, or explosive substances shall be eligible for classification to a lower Risk Category if it can be demonstrated to the satisfaction of the authority having jurisdiction by a hazard assessment as described in Section 1.5.2 that a release of the substances is commensurate with the risk associated with that Risk Category.

Step 2: Determine the basic wind speed, V_s, for the applicable risk category, see Figure 26.5-1A, B or C **(P.g 191)**

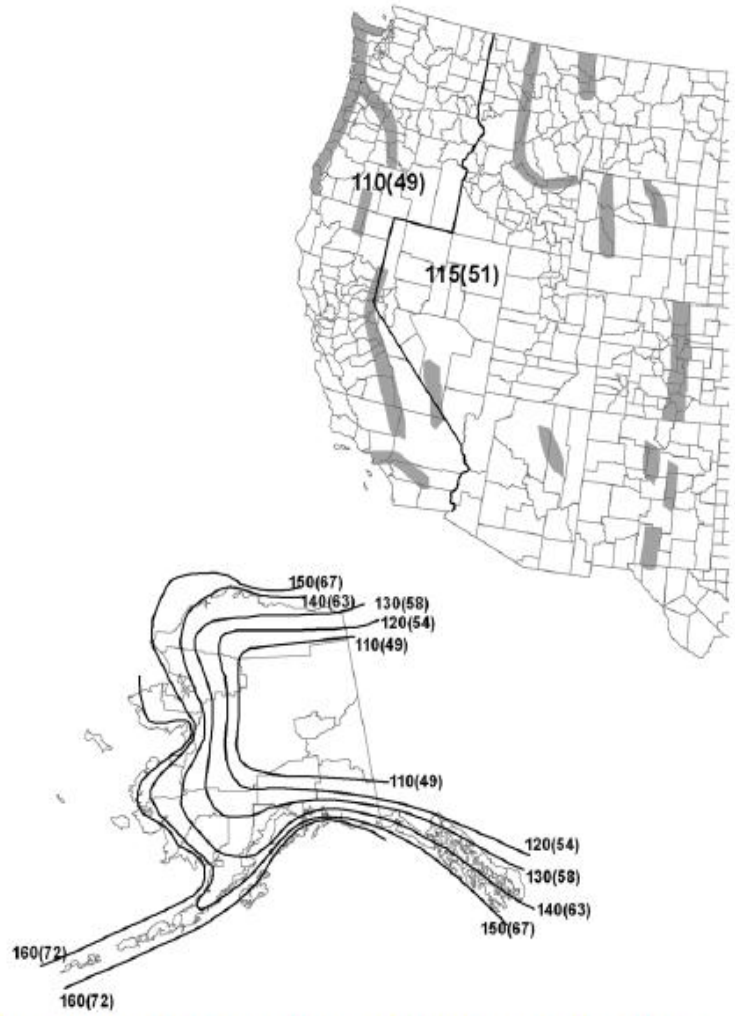

Figure 26.5-1A Basic Wind Speeds for Occupancy Category II Buildings and Other Structures.

Notes:

1. Values are nominal design 3-second gust wind speeds in miles per hour (m/s) at 33 ft (10m) above ground for Exposure C category.
2. Linear interpolation between contours is permitted.
3. Islands and coastal areas outside the last contour shall use the last wind speed contour of the coastal area.
4. Mountainous terrain, gorges, ocean promontories, and special wind regions shall be examined for unusual wind conditions.
5. Wind speeds correspond to approximately a 7% probability of exceedance in 50 years (Annual Exceedance Probability = 0.00143, MRI = 700 Years).

Step 3: Determine wind Load parameters:

- Wind directionality factor, K_d, see Section 26.6 and Table 26.6-1 (**P.g 194**)

Wind Directionality Factor, K_d

Table 26.6-1

Structure Type	Directionality Factor K_d*
Buildings	
Main Wind Force Resisting System	0.85
Components and Cladding	0.85
Arched Roofs	0.85
Chimneys, Tanks, and Similar Structures	
Square	0.90
Hexagonal	0.95
Round	0.95
Solid Freestanding Walls and Solid Freestanding and Attached Signs	0.85
Open Signs and Lattice Framework	0.85
Trussed Towers	
Triangular, square, rectangular	0.85
All other cross sections	0.95

*Directionality Factor K_d has been calibrated with combinations of loads specified in Chapter 2. This factor shall only be applied when used in conjunction with load combinations specified in Sections 2.3 and 2.4.

- Exposure category, see Section 26.7 **(P.g 195)**

- Topographic factor, K_{zt}, see Section 26.8 and Figure 26.8-1 **(P.g 198)**

Topographic Factor, K_{zt}

Figure 26.8-1

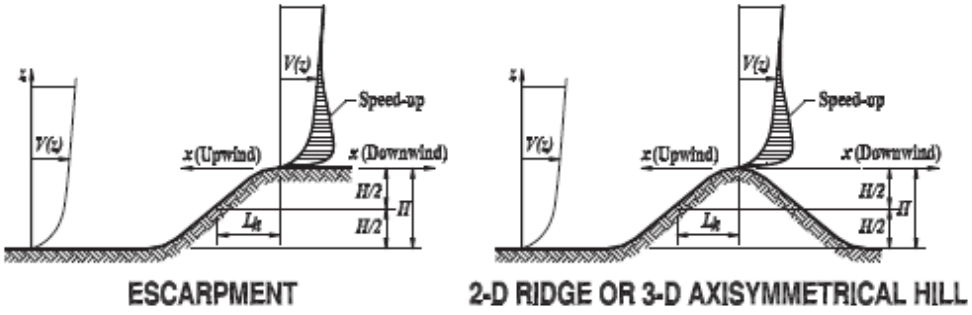

Topographic Multipliers for Exposure C

H/L_h	K_1 Multiplier			x/L_h	K_2 Multiplier		z/L_h	K_3 Multiplier		
	2-D Ridge	2-D Escarp.	3-D Axisym. Hill		2-D Escarp.	All Other Cases		2-D Ridge	2-D Escarp.	3-D Axisym. Hill
0.20	0.29	0.17	0.21	0.00	1.00	1.00	0.00	1.00	1.00	1.00
0.25	0.36	0.21	0.26	0.50	0.88	0.67	0.10	0.74	0.78	0.67
0.30	0.43	0.26	0.32	1.00	0.75	0.33	0.20	0.55	0.61	0.45
0.35	0.51	0.30	0.37	1.50	0.63	0.00	0.30	0.41	0.47	0.30
0.40	0.58	0.34	0.42	2.00	0.50	0.00	0.40	0.30	0.37	0.20
0.45	0.65	0.38	0.47	2.50	0.38	0.00	0.50	0.22	0.29	0.14
0.50	0.72	0.43	0.53	3.00	0.25	0.00	0.60	0.17	0.22	0.09
				3.50	0.13	0.00	0.70	0.12	0.17	0.06
				4.00	0.00	0.00	0.80	0.09	0.14	0.04
							0.90	0.07	0.11	0.03
							1.00	0.05	0.08	0.02
							1.50	0.01	0.02	0.00
							2.00	0.00	0.00	0.00

Notes:

1. For values of H/L_h, x/L_h and z/L_h other than those shown, linear interpolation is permitted.
2. For $H/L_h > 0.5$, assume $H/L_h = 0.5$ for evaluating K_1 and substitute $2H$ for L_h for evaluating K_2 and K_3.
3. Multipliers are based on the assumption that wind approaches the hill or escarpment along the direction of maximum slope.
4. Notation:
   - H: Height of hill or escarpment relative to the upwind terrain, in feet (meters).
   - L_h: Distance upwind of crest to where the difference in ground elevation is half the height of hill or escarpment, in feet (meters).
   - K_1: Factor to account for shape of topographic feature and maximum speed-up effect.
   - K_2: Factor to account for reduction in speed-up with distance upwind or downwind of crest.
   - K_3: Factor to account for reduction in speed-up with height above local terrain.
   - x: Distance (upwind or downwind) from the crest to the building site, in feet (meters).
   - z: Height above ground surface at building site, in feet (meters).
   - μ: Horizontal attenuation factor.
   - γ: Height attenuation factor.

- Gust Effect Factor, *G*, see Sections 26.9 **(P.g 198)**

- Enclosure classification, see Section 26.10 **(P.g 201)**

- Internal pressure coefficient, (GCpi), see Section 26.11 and Table 26.11-1 (**P.g 201)**

Main Wind Force Resisting System and Components and Cladding		All Heights
Table 26.11-1	Internal Pressure Coefficient, (GC_{pi})	Walls & Roofs
Enclosed, Partially Enclosed, and Open Buildings		

Enclosure Classification	(GC_{pi})
Open Buildings	0.00
Partially Enclosed Buildings	+0.55 -0.55
Enclosed Buildings	+0.18 -0.18

Notes:

1. Plus and minus signs signify pressures acting toward and away from the internal surfaces, respectively.
2. Values of (GC_{pi}) shall be used with q_z or q_h as specified.
3. Two cases shall be considered to determine the critical load requirements for the appropriate condition:
   (i) a positive value of (GC_{pi}) applied to all internal surfaces
   (ii) a negative value of (GC_{pi}) applied to all internal surfaces

✓ For dome **C&C**

Components and Cladding		All Heights
Figure 30.4-7	External Pressure Coefficients, GC_p	Domed Roofs
Enclosed, Partially Enclosed Buildings and Structures		

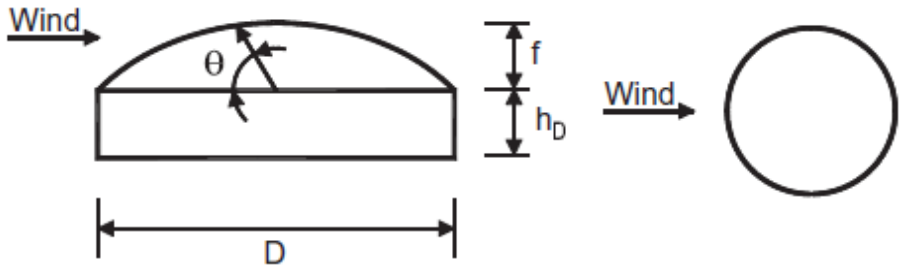

External Pressure Coefficients for Domes with a Circular Base			
θ, degrees	Negative Pressures	Positive Pressures	Positive Pressures
	0 – 90	0 – 60	61 – 90
GC_p	-0.9	+0.9	+0.5

Notes:

1. Values denote GC_p to be used with $q_{(h_D+f)}$ where $h_D + f$ is the height at the top of the dome.
2. Plus and minus signs signify pressures acting toward and away from the surfaces, respectively.
3. Each component shall be designed for the maximum positive and negative pressures.
4. Values apply to $0 \le h_D/D \le 0.5$, $0.2 \le f/D \le 0.5$.
5. θ = 0 degrees on dome springline, θ = 90 degrees at dome center top point. f is measured from springline to top.

Step 4: Determine velocity pressure exposure coefficient, K_z or K_h, see Table 27.3-1

Main Wind Force Resisting System – Part 1 | **All Heights**

Velocity Pressure Exposure Coefficients, K_h and K_z

Table 27.3-1

Height above ground level, z		Exposure		
ft	(m)	B	C	D
0-15	(0-4.6)	0.57	0.85	1.03
20	(6.1)	0.62	0.90	1.08
25	(7.6)	0.66	0.94	1.12
30	(9.1)	0.70	0.98	1.16
40	(12.2)	0.76	1.04	1.22
50	(15.2)	0.81	1.09	1.27
60	(18)	0.85	1.13	1.31
70	(21.3)	0.89	1.17	1.34
80	(24.4)	0.93	1.21	1.38
90	(27.4)	0.96	1.24	1.40
100	(30.5)	0.99	1.26	1.43
120	(36.6)	1.04	1.31	1.48
140	(42.7)	1.09	1.36	1.52
160	(48.8)	1.13	1.39	1.55
180	(54.9)	1.17	1.43	1.58
200	(61.0)	1.20	1.46	1.61
250	(76.2)	1.28	1.53	1.68
300	(91.4)	1.35	1.59	1.73
350	(106.7)	1.41	1.64	1.78
400	(121.9)	1.47	1.69	1.82
450	(137.2)	1.52	1.73	1.86
500	(152.4)	1.56	1.77	1.89

Notes:

1. The velocity pressure exposure coefficient K_z may be determined from the following formula:

   For $15 \text{ ft.} \le z \le z_g$: $K_z = 2.01\,(z/z_g)^{2/\alpha}$

   For $z < 15$ ft.: $K_z = 2.01\,(15/z_g)^{2/\alpha}$

2. α and z_g are tabulated in Table 26.9.1.
3. Linear interpolation for intermediate values of height z is acceptable.
4. Exposure categories are defined in Section 26.7.

Step 5: Determine velocity pressure q_z or q_h Eq. 27.3-1 **(P.g 204)**

$qz = 0.00256 \times K_z \times K_{zt} \times K_d \times V_s^2$ psf

Where:

q_z = velocity pressure calculated at height z

q_h = velocity pressure calculated at mean roof height h

K_d =wind directionality factor

k_z= velocity pressure exposure coefficient

Kzt= topographic factor

V_s =basic wind speed

Step 6: Determine external pressure coefficient, C_p or C_N **(P.g 206)**

Main Wind Force Resisting System – Part 1		All Heights
Figure 27.4-1	External Pressure Coefficients, C_p	Walls & Roofs
Enclosed, Partially Enclosed Buildings		

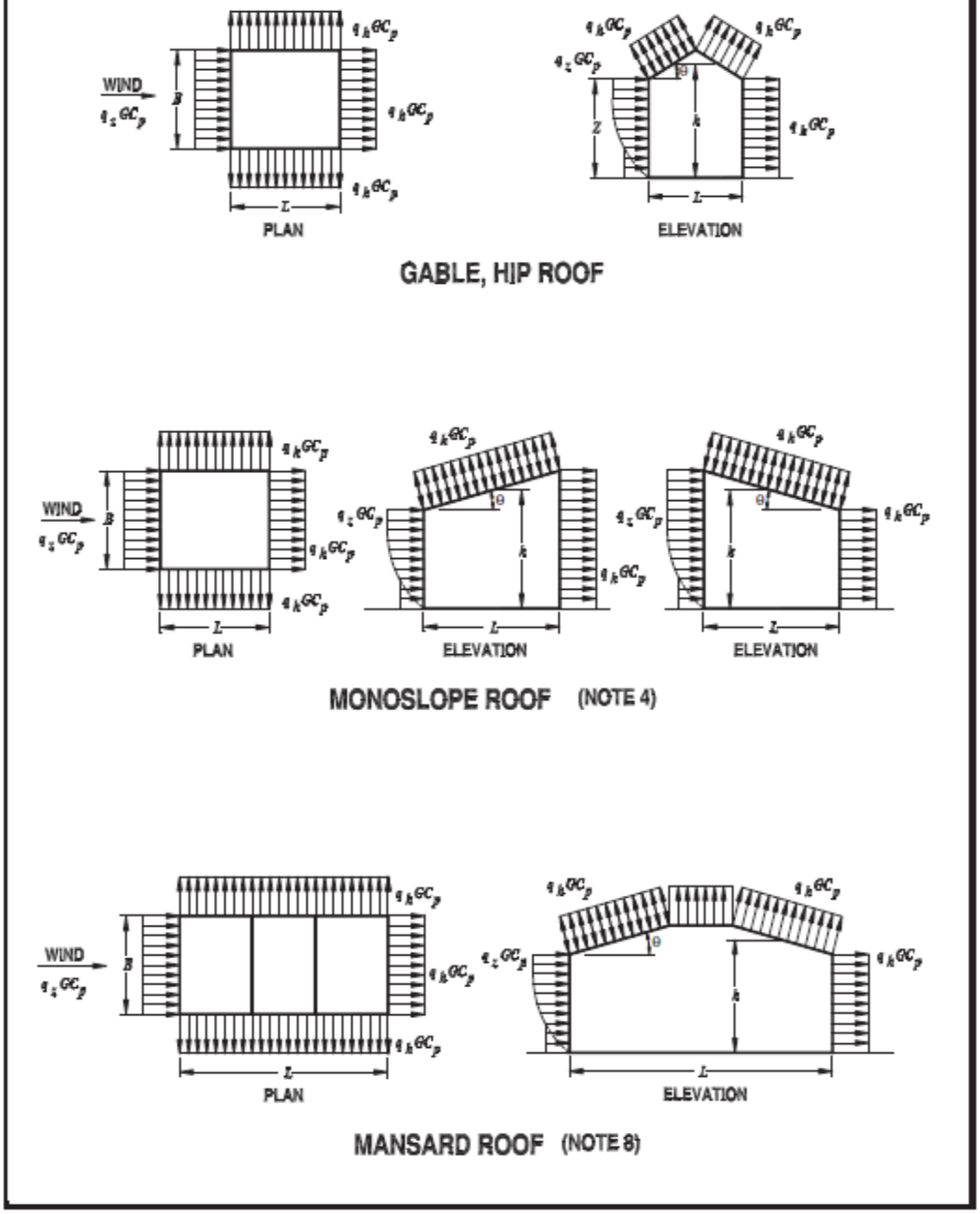

- Fig. 27.4-1 for walls and flat, gable, hip, monoslope or mansard roofs Values for other roof types **(P.g 207)**

Main Wind Force Resisting System – Part 1		All Heights
Figure 27.4-1 (cont.)	External Pressure Coefficients, C_p	Walls & Roofs
Enclosed, Partially Enclosed Buildings		

Wall Pressure Coefficients, C_p

Surface	L/B	C_p	Use With
Windward Wall	All values	0.8	q_z
Leeward Wall	0-1	-0.5	q_h
	2	-0.3	
	≥4	-0.2	
Side Wall	All values	-0.7	q_h

Roof Pressure Coefficients, C_p, for use with q_h

Wind Direction	Windward									Leeward		
	Angle, θ (degrees)									Angle, θ (degrees)		
	h/L	10	15	20	25	30	35	45	≥60#	10	15	≥20
Normal to ridge for θ ≥ 10°	≤0.25	-0.7 -0.18	-0.5 0.0*	-0.3 0.2	-0.2 0.3	-0.2 0.3	0.0* 0.4	0.4	0.01 θ	-0.3	-0.5	-0.6
	0.5	-0.9 -0.18	-0.7 -0.18	-0.4 0.0*	-0.3 0.2	-0.2 0.2	-0.2 0.3	0.0* 0.4	0.01 θ	-0.5	-0.5	-0.6
	≥1.0	-1.3** -0.18	-1.0 -0.18	-0.7 -0.18	-0.5 0.0*	-0.3 0.2	-0.2 0.2	0.0* 0.3	0.01 θ	-0.7	-0.6	-0.6

Normal to ridge for θ < 10 and Parallel to ridge for all θ		Horiz distance from windward edge	C_p
	≤ 0.5	0 to h/2	-0.9, -0.18
		h/2 to h	-0.9, -0.18
		h to 2 h	-0.5, -0.18
		> 2h	-0.3, -0.18
	≥ 1.0	0 to h/2	-1.3**, -0.18
		> h/2	-0.7, -0.18

*Value is provided for interpolation purposes.

**Value can be reduced linearly with area over which it is applicable as follows

Area (sq ft)	Reduction Factor
≤ 100 (9.3 sq m)	1.0
250 (23.2 sq m)	0.9
≥ 1000 (92.9 sq m)	0.8

Notes:

1. Plus and minus signs signify pressures acting toward and away from the surfaces, respectively.
2. Linear interpolation is permitted for values of *L/B*, *h/L* and θ other than shown. Interpolation shall only be carried out between values of the same sign. Where no value of the same sign is given, assume 0.0 for interpolation purposes.
3. Where two values of C_p are listed, this indicates that the windward roof slope is subjected to either positive or negative pressures and the roof structure shall be designed for both conditions. Interpolation for intermediate ratios of h/L in this case shall only be carried out between C_p values of like sign.
4. For monoslope roofs, entire roof surface is either a windward or leeward surface.
5. For flexible buildings use appropriate G_f as determined by Section 26.9.4.
6. Refer to Figure 27.4-2 for domes and Figure 27.4-3 for arched roofs.
7. Notation:
   B: Horizontal dimension of building, in feet (meter), measured normal to wind direction.
   L: Horizontal dimension of building, in feet (meter), measured parallel to wind direction.
   h: Mean roof height in feet (meters), except that eave height shall be used for θ ≤ 10 degrees.
   z: Height above ground, in feet (meters).
   G: Gust effect factor.
   q_z,q_h: Velocity pressure, in pounds per square foot (N/m^2), evaluated at respective height.
   θ: Angle of plane of roof from horizontal, in degrees.
8. For mansard roofs, the top horizontal surface and leeward inclined surface shall be treated as leeward surfaces from the table.
9. Except for MWFRS's at the roof consisting of moment resisting frames, the total horizontal shear shall not be less than that determined by neglecting wind forces on roof surfaces.

#For roof slopes greater than 80°, use C_p = 0.8

➢ Fig. 27.4-2 for domed roofs **(P.g 28)**

Main Wind Force Resisting System – Part 1		All Heights
Figure 27.4-2	External Pressure Coefficients, C_p	Domed Roofs
Enclosed, Partially Enclosed Buildings and Structures		

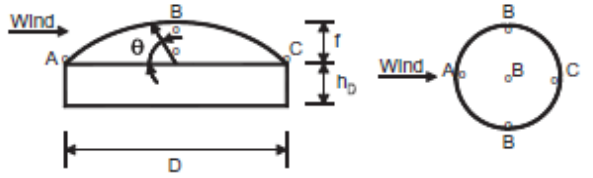

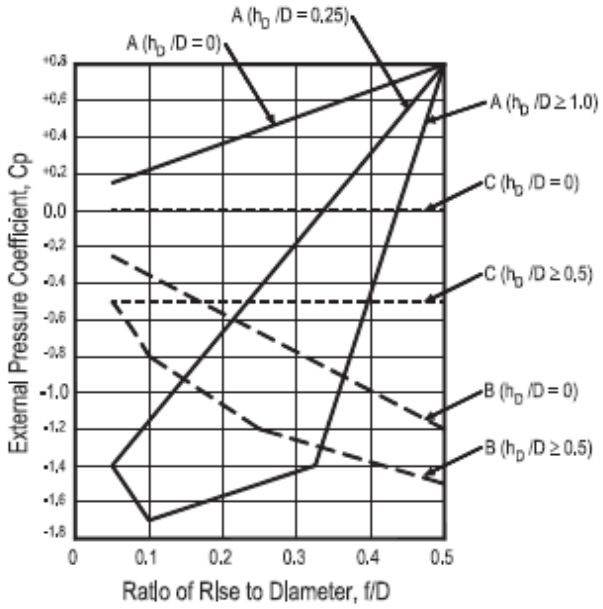

External Pressure Coefficients for Domes with a Circular Base.

(Adapted from Eurocode, 1995)

Notes:

1. Two load cases shall be considered:
   - Case A. C_p values between A and B and between B and C shall be determined by linear interpolation along arcs on the dome parallel to the wind direction;
   - Case B. C_p shall be the constant value of A for $\theta \leq 25$ degrees, and shall be determined by linear interpolation from 25 degrees to B and from B to C.
2. Values denote C_p to be used with $q_{(h_D+f)}$ where $h_D + f$ is the height at the top of the dome.
3. Plus and minus signs signify pressures acting toward and away from the surfaces, respectively.
4. C_p is constant on the dome surface for arcs of circles perpendicular to the wind direction; for example, the arc passing through B-B-B and all arcs parallel to B-B-B.
5. For values of h_D/D between those listed on the graph curves, linear interpolation shall be permitted.
6. $\theta = 0$ degrees on dome springline, $\theta = 90$ degrees at dome center top point. f is measured from springline to top.
7. The total horizontal shear shall not be less than that determined by neglecting wind forces on roof surfaces.
8. For f/D values less than 0.05, use Figure 27.4-1.

Step 7: Calculate wind pressure, *p*, on each building surface

- Eq. 27.4-1 for ridge buildings **(P.g 204)**
- Eq. 27.4-2 for flexible buildings **(P.g 204)**
- Eq. 27.4-3 for open buildings **(P.g 204)**

APPENDIX B: USE OF 3D CFD CODE

B.1 Introduction

The present study utilizes the 3D code developed by Dr. R. Panneer Selvam to directly simulate impact of a tornado with a dome and prism building. The flow equations are approximated by either Finite Element Method (FEM) or Finite Difference Method (FDM). The FEM code (ctt4.out) based on body fitted was developed to study flow around a dome building. The FDM code (thill.out) has been used to study flow over prism building.

B.2 Steps of using the 3D simulations

Step 1: Prepare the input file with grid + vortex parameters + building geometry

Step 2: Import input file to Linux account

Step 3: Run program (thill.out or ctt4.out)

Step 4: Export output files to Windows

Step 5: Change output files from ASCII to binary

Step 6: Analyze results in Tecplot

B.2.1 Input Data User Manual for ctt4.out code

Input file: ctt-i.txt

Output files: ctt-o.plt-gives time, Fx, Fy, Fz

Prc1.plt-maximum& minimum pressure in the whole domain

READ (5,*) IM, JM, KM, DTT, TTIME, TMIN, TMAX

IM Total number of the grid points in the x-axis

JM Total number of the grid points in the y-axis

KM Total number of the grid points in the z-axis

DTT Time step

TTIME Total time the computer run needs to be performed

TMIN Starting time to calculate the minimum pressure on the building

TMAX Ending time to calculate the maximum pressure on the building

READ (5,*) C11, C2, RAMAX, VTRAN, TLAG, ROTC, ANG, IFL2

C11 Calculated as u=C11= u*/k ln((z+z0)/z0

C2 The roughness length of the ground (usually z0=0.00375 for building)

RAMAX maximum radius of the inner core of the tornados

VTRAN Translating velocity

TLAG Time lag

ROTC Alpha which set to be constant = 1.5 unit (maximum flow intensity)

ANG Rotating Angle

IFL2 time step interval to write movie file- Max.movie 999

The following date comes from **domeg.f** out put

READ (5,*)(X(I),I=1,IM)

READ (5,*)(Y(J),J=1,JM)

READ (5,*)(Z(K),K=1,KM)

DO J=1, JM

READ (5,*) (HI (I, J), I=1, IM)

END DO

Comments

z is the height from the ground which sets to be equal to building height (h_{build})

u* is the frictional velocity

B.2.1.1 FORTRAN code for dome grid generation

```
c      PROG. DOMEG.F, OCT. 5, 2013
C      PROG. BU-GRID.F, MAR. 18, 2010
       PARAMETER(NX=500,NY=500,NZ=200)
       IMPLICIT REAL *8 (A-H, O-Z)
       DIMENSION R(NX),X(NX),Y(NY),Z(NZ),HI(NX,NY)
       OPEN(2,FILE='domeg.txt')
       OPEN(3,FILE='domep.plt')
C.....COMPUTE RADIAL POINTS WITH MINIMUM SPACING
       ZMIN=0.005
       HX=0.1
       DIAC=3.0
       NXB=DIAC/HX
       H=HX
       R(1)=0.0
       R(2)=H
       I1=2
       FAC=1.1
       DO I=1,300
       I1=I1+1
       IF(I.GT.5)FAC=1.2
       IF(I.GT.20)FAC=1.3
       H=H*FAC
       IF(H.GT.0.5)H=0.5
       R(I1)=R(I1-1)+H
       IF(R(I1).GT.10)GO TO 100
       END DO
100    NP=I1
C.....GENERATE X- POINTS BEFORE DOME
       DO I=1,NP
       X(I)=-R(NP-I+1)
       END DO
C.....GENERATE POINTS FOR DOME
       DO I=1,NXB
       X(NP+I)=X(NP)+I*HX
       END DO
C.....GENERATE POINTS BEYOND BUILDING
       DO I=2,NP
       X(NP+NXB+I-1)=X(NP+NXB)+R(I)
       END DO
       IM=NP+NXB+NP-1
       JM=IM
       print *,im
c.....MAKE THE CENTER OF THE DOME ZERO
       DO I=1,IM
       X(I)=X(I)-DIAC/2.
```

```
      END DO
C.....GNERATE POINTS FOR THE BUILDING IN Z
      Z(1)=0.0
      Z(2)=ZMIN
      H=ZMIN
      I1=2
      FAC=1.1
      DO I=1,200
      I1=I1+1
      IF(I.GT.5)FAC=1.2
      H=H*FAC
      IF(H.GT.0.5)H=0.5
      Z(I1)=Z(I1-1)+H
      IF(Z(I1).GT.7)GO TO 110
      END DO
110   KM=I1
C
      IMC=IM/2+1
      JMC=JM/2+1
      XLM=DIAC/2.
      XLM2=XLM*XLM
      HMAX=1.0
      HMAX2=HMAX
      RADM=(XLM2+HMAX2)/(2.*HMAX)
      YMAX=RADM-HMAX
      RADM2=RADM*RADM
      YMAX2=YMAX*YMAX
      DO J=1,JM
      DO I=1,IM
      HI(I,J)=0.0
      X11=X(I)-X(IMC)
      Y11=X(J)-X(JMC)
      XL2=X11*X11+Y11*Y11
      IF(XL2.LE.XLM2)THEN
      H12=RADM2-XL2
      HI(I,J)=SQRT(H12)-YMAX
      END IF
      END DO
      END DO
C
      WRITE(2,*)IM,IM,KM
      WRITE(2,20)(X(I),I=1,IM)
      WRITE(2,20)(X(I),I=1,IM)
      WRITE(2,20)(Z(K),K=1,KM)
      DO J=1,JM
      WRITE(2,20)(HI(I,J),I=1,IM)
      END DO
```

```
20     FORMAT(5(E14.7,1X))
       IFILE1=3
       write(IFILE1,*)'VARIABLES = "X","Y","Z"'
       write(IFILE1,*)'ZONE I=',IM, ',J=',JM,',K=',KM, ',F=POINT'
       do k=1,km
       do j=1,jm
       do i=1,im
       Z1=HI(I,J)+Z(K)
       write(IFILE1,*)x(i),X(j),Z1
       end do
       end do
       end do
       STOP
       END
```

B.2.1.2 Input file example for ctt4.out code

- This data is just presented for explanation purposes. This grid is 10x10x7.

84, 84, 38, 0.01, 11.0, 1.0, 9.0

0.179, 0.00375, 3.0, 1.0, 0.0, 0.0015, 0.0,20

-0.1169063E+02 -0.1119063E+02 -0.1069063E+02 -0.1019063E+02 -0.9690630E+01

-0.9190630E+01 -0.8690630E+01 -0.8190630E+01 -0.7690630E+01 -0.7190630E+01

-0.6690630E+01 -0.6190630E+01 -0.5690630E+01 -0.5190630E+01 -0.4690630E+01

-0.4190630E+01 -0.3709734E+01 -0.3308987E+01 -0.2975032E+01 -0.2696736E+01

-0.2464822E+01 -0.2271561E+01 -0.2110510E+01 -0.1964100E+01 -0.1831000E+01

-0.1710000E+01 -0.1600000E+01 -0.1500000E+01 -0.1400000E+01 -0.1300000E+01

-0.1200000E+01 -0.1100000E+01 -0.1000000E+01 -0.9000000E+00 -0.8000000E+00

-0.7000000E+00 -0.6000000E+00 -0.5000000E+00 -0.4000000E+00 -0.3000000E+00

-0.2000000E+00 -0.9999998E-01 0.2235174E-07 0.1000000E+00 0.2000000E+00

0.3000000E+00 0.4000000E+00 0.5000000E+00 0.6000000E+00 0.7000000E+00

0.8000000E+00 0.9000000E+00 0.1000000E+01 0.1100000E+01 0.1200000E+01

0.1300000E+01 0.1400000E+01 0.1500000E+01 0.1610000E+01 0.1731000E+01

0.1864100E+01 0.2010510E+01 0.2171561E+01 0.2364822E+01 0.2596736E+01

0.2875032E+01 0.3208987E+01 0.3609734E+01 0.4090630E+01 0.4590630E+01

0.5090630E+01 0.5590630E+01 0.6090630E+01 0.6590630E+01 0.7090630E+01

0.7590630E+01 0.8090630E+01 0.8590630E+01 0.9090630E+01 0.9590630E+01

0.1009063E+02 0.1059063E+02 0.1109063E+02 0.1159063E+02

-0.1169063E+02 -0.1119063E+02 -0.1069063E+02 -0.1019063E+02 -0.9690630E+01

-0.9190630E+01 -0.8690630E+01 -0.8190630E+01 -0.7690630E+01 -0.7190630E+01

-0.6690630E+01 -0.6190630E+01 -0.5690630E+01 -0.5190630E+01 -0.4690630E+01

-0.4190630E+01 -0.3709734E+01 -0.3308987E+01 -0.2975032E+01 -0.2696736E+01

-0.2464822E+01 -0.2271561E+01 -0.2110510E+01 -0.1964100E+01 -0.1831000E+01

-0.1710000E+01 -0.1600000E+01 -0.1500000E+01 -0.1400000E+01 -0.1300000E+01

-0.1200000E+01 -0.1100000E+01 -0.1000000E+01 -0.9000000E+00 -0.8000000E+00

-0.7000000E+00 -0.6000000E+00 -0.5000000E+00 -0.4000000E+00 -0.3000000E+00

-0.2000000E+00 -0.9999998E-01 0.2235174E-07 0.1000000E+00 0.2000000E+00

0.3000000E+00 0.4000000E+00 0.5000000E+00 0.6000000E+00 0.7000000E+00

0.8000000E+00 0.9000000E+00 0.1000000E+01 0.1100000E+01 0.1200000E+01

0.1300000E+01 0.1400000E+01 0.1500000E+01 0.1610000E+01 0.1731000E+01

0.1864100E+01 0.2010510E+01 0.2171561E+01 0.2364822E+01 0.2596736E+01

0.2875032E+01 0.3208987E+01 0.3609734E+01 0.4090630E+01 0.4590630E+01

0.5090630E+01 0.5590630E+01 0.6090630E+01 0.6590630E+01 0.7090630E+01

0.7590630E+01 0.8090630E+01 0.8590630E+01 0.9090630E+01 0.9590630E+01

0.1009063E+02 0.1059063E+02 0.1109063E+02 0.1159063E+02

0.0000000E+00 0.5000000E-02 0.1050000E-01 0.1655000E-01 0.2320500E-01

0.3052550E-01	0.3857805E-01	0.4824111E-01	0.5983679E-01	0.7375160E-01
0.9044937E-01	0.1104867E+00	0.1345315E+00	0.1633852E+00	0.1980097E+00
0.2395592E+00	0.2894184E+00	0.3492496E+00	0.4210470E+00	0.5072038E+00
0.6105921E+00	0.7346580E+00	0.8835371E+00	0.1062192E+01	0.1276578E+01
0.1533841E+01	0.1842557E+01	0.2213016E+01	0.2657566E+01	0.3157566E+01
0.3657566E+01	0.4157566E+01	0.4657566E+01	0.5157566E+01	0.5657566E+01
0.6157566E+01	0.6657566E+01	0.7157566E+01		

B.2.1.3 Import input file to HPC computers account for ctt4.out code

- Create a new account

All students, faculty and staff of the University of Arkansas, Fayetteville are eligible to create an account on the AHPCC clusters. A new account request must be sponsored by a member of faculty or staff (usually a major professor or adviser) if a student wants to apply for an account.

The link below can be followed to log in with a UofA credentials and complete the online request form.

- Internal User Account Request
- https://hpc.uark.edu/account-request/

Accounts are usually activated within 24 hours of the sponsor approval

- Log in to your account
  - Use SSH software
  - Host name (razor.uark.edu) or (stargate.uark.edu)
  - User name (your UARK email ID)
  - Password is your UARK email Password
- Rules

- *ALL* jobs must be submitted through the job scheduler. Execution of jobs from the command line is not allowed.
- Jobs should be run in your scratch directory
- The others queues can find in http://hpc.uark.edu/hpc/support/queues.html page
- All commands for HPC computers can be found Ahmed (2016).

B.2.2 Input File (thill.txt) for thill-out code

Input file: thill.txt

Output: tor3d-o.plt gives x, y, z, p, vx, vy, vz

Force coefficients with Vref = Vtrans (1.0)

Pressures

READ (5,*) IM, JM, KM, IMK1, IMK2, JMK1, JMK2, KH, DTT

IM	Total number of the grid points in the x-axis
JM	Total number of the grid points in the y-axis
KM	Total number of the grid points in the z-axis
IMK1	Starting point of the building in the x-axis
IMK2	Ending point of the building in the x-axis
JMK1	Starting point of the building in the y-axis
JMK2	Ending point of the building in the y-axis
KH	Total number of the grid points of the building in the z-axis
DTT	Time step (program calculates the required time step)

READ (5,*) TT1, TT2, TT3, TT4, TMIN, TMAX, Xref, Yref (don't care, we are not using it)

TT1	Time at which data written in a separate file at TT1
TT2	Time at which data written in a separate file at TT2
TT3	Time at which data written in a separate file at TT3

TT4 Time at which data written in a separate file at TT4

TMIN Starting time to calculate the minimum pressure on the building

TMAX Ending time to calculate the maximum pressure on the building

Xref The perpendicular distance to calculate the moment arm on the building

Yref The perpendicular distance to calculate the moment arm on the building

READ (5,*) C11, C2, RAMAX, VTRAN, TLAG, ROTC, ANG, IFL2

C11 Calculated as u=C11= 1/ln((z+z0)/z0) atmospheric boundary layer (if h=1 then C11=0.179) k=0.4, z=height of the building

C2 The roughness length of the ground (usually z0=0.00375 for building)

RAMAX maximum radius of the inner core of the tornados

VTRAN Translating velocity

TLAG Time lag

ROTC Alpha which set to be constant = 1.5 unit (maximum flow intensity)

ANG Angle of attack

IFL2 time step interval to write movie file- Max.movie 999

READ (5,*) X (I), I=1, IM)

READ (5,*) (Y (J), J=1, JM)

READ (5,*) (Z K), K=1, KM)

Comments

z is the height from the ground which sets to be equal to building height (hbuild)

*u** is the frictional velocity

TECPLOT- converting ASC to Binary

Preplot file1.dat file1.plt

B.2.2.1 FORTRAN code for prism grid generation

```
C      PROG. BU-GRID.F, MAR. 18, 2010
       PARAMETER(NX=290)
       DIMENSION RA(NX),X(NX),Z(NX),RB(NX),RZ(NX)
       OPEN(2,FILE='bu2d-3D.txt')
C.....COMPUTE RADIAL POINTS WITH MINIMUM SPACING
       RMIN=0.005
       HX=0.1
       NXB=1.0/0.1
       H=RMIN
       RB(1)=0.0
       RB(2)=H
       I1=2
       FAC=1.0
       DO I=1,300
       I1=I1+1
       IF(I.GT.10)FAC=1.005
       IF(I.GT.40)FAC=1.05
       H=H*FAC
       IF(H.GT.1)H=1.0
       RB(I1)=RB(I1-1)+H
       IF(RB(I1).GT.12)GO TO 100
       END DO
100    NP=I1
C.....COMPUTE RADIAL POINTS WITH MINIMUM SPACING
       RMIN=0.005
       H=RMIN
       RA(1)=0.0
       RA(2)=H
       I1=2
       FAC=1.0
       DO I=1,300
       I1=I1+1
       IF(I.GT.10)FAC=1.005
       IF(I.GT.40)FAC=1.05
       H=H*FAC
       IF(H.GT.1)H=1.
       RA(I1)=RA(I1-1)+H
       IF(RA(I1).GT.12)GO TO 200
       END DO
200    NP1=I1
C.....GENERATE X- POINTS BEFORE BUILDING
       DO I=1,NP
       X(I)=-RB(NP-I+1)-(NXB*HX*0.5)
       END DO
C.....GENERATE POINTS FOR BUILDING
```

```
      DO I=1,NXB
      X(NP+I)=X(NP)+I*HX
      END DO
C.....GENERATE POINTS BEYOND BUILDING
      DO I=2,NP1
      X(NP+NXB+I-1)=X(NP+NXB)+RA(I)
      END DO
      IM=NP+NXB+NP1-1
C.....GNERATE POINTS FOR THE BUILDING IN Z
C.....COMPUTE vertical POINTS WITH MINIMUM SPACING
      ZMIN=0.005
      ZX=0.1
      NZB=1.0/0.1
      HZ=ZMIN
      RZ(1)=0.0
      RZ(2)=HZ
      I1=2
      FAC=1.01
      DO I=1,300
      print*,I
      I1=I1+1
      IF(I.GT.40)FAC=1.05
      IF(I.GT.65)FAC=1.1
      HZ=HZ*FAC
      IF(HZ.GT.1)HZ=1.0
      RZ(I1)=RZ(I1-1)+HZ
      IF(RZ(I1).GT.28)GO TO 300
      END DO
300   NPZ=I1
      print*,NPZ
      DO I=1,NZB+1
      Z(I)=(I-1)*ZX
      END DO
      DO I=2,NPZ
      Z(NZB+I)=Z(NZB+1)+RZ(I)
      END DO
      KM=NZB+NPZ
      IMK1=NP
      IMK2=NP+NXB
      KH=NZB+1
      WRITE(2,*)IM,KM,IMK1,IMK2,KH
      WRITE(2,20)(X(I),I=1,IM)
      WRITE(2,20)(Z(K),K=1,KM)
20    FORMAT(5(F10.4,2X))
      STOP
      END
```

B.2.2.2 Input file example for thill-out code

This data is just presented for explanation purposes. This grid is 10x10x7

52,52,42,12,42,12,42,11,0.02

15.0, 30.0, 45.0, 60.0, 15.0, 15.0, 3.75, 5.25

0.179, 0.00375, 3.0, 1.0, 30.0, 1.5, 0.0,600

-11.5529 +00	-11.0378+00	-10.5251+00	-10.0150+00	-9.5075+00
-9.0025+00	-8.5000+00	-8.0000+00	-7.5000+00	-7.0000+00
-6.5000 +00	-6.0000 +00	-5.5000+00	-5.0000+00	-4.5000 +00
-4.0000+00	-3.5000+00	-3.0000+00	-2.9000 +00	-2.8000 +00
-2.7000+00	-2.6000+00	-2.5000+00	-2.4000+00	-2.3000+00
-2.2000+00	-2.1000+00	-2.0000+00	-1.9000 +00	-1.8000+00
-1.7000+00	-1.6000+00	-1.5000+00	-1.4000 +00	-1.3000 +00
-1.2000+00	-1.1000+00	-1.0000+00	-0.9000+00	-0.8000 +00
-0.7000 +00	-0.6000+00	-0.5000+00	-0.4000+00	-0.3000 +00
-0.2000+00	-0.1000+00	0.0000+00	0.1000+00	0.2000+00
0.3000+00	0.4000+00	0.5000+00	0.6000+00	0.7000+00
0.8000+00	0.9000 +00	1.0000+00	1.1000+00	1.2000+00
1.3000+00	1.4000+00	1.5000+00	1.6000+00	1.7000+00
1.8000+00	1.9000+00	2.0000+00	2.1000+00	2.2000 +00
2.3000+00	2.4000+00	2.5000+00	2.6000 +00	2.7000+00
2.8000+00	2.9000 +00	3.0000+00	3.5000+00	4.0000+00
4.5000+00	5.0000+00	5.5000+00	6.0000+00	6.5000+00

7.0000 +00	7.5000+00	8.0000+00	8.5000+00	9.0025+00
9.5075+00	10.0150+00	10.5251+00	11.0378+00	11.5529+00
-11.5529+00	-11.0378+00	-10.5251+00	-10.0150+00	-9.5075+00
-9.0025+00	-8.5000+00	-8.0000+00	-7.5000+00	-7.0000+00
-6.5000 +00	-6.0000 +00	-5.5000+00	-5.0000+00	-4.5000+00
-4.0000+00	-3.5000+00	-3.0000+00	-2.9000+00	-2.8000+00
-2.7000+00	-2.6000 +00	-2.5000+00	-2.4000+00	-2.3000+00
-2.2000+00	-2.1000+00	-2.0000+00	-1.9000+00	-1.8000+00
-1.7000+00	-1.6000+00	-1.5000+00	-1.4000+00	-1.3000+00
-1.2000+00	-1.1000+00	-1.0000+00	-0.9000+00	-0.8000+00
-0.7000+00	-0.6000+00	-0.5000+00	-0.4000+00	-0.3000+00
-0.2000+00	-0.1000+00	0.0000+00	0.1000+00	0.2000+00
0.3000+00	0.4000+00	0.5000+00	0.6000+00	0.7000+00
0.8000+00	0.9000+00	1.0000+00	1.1000+00	1.2000+00
1.3000+00	1.4000+00	1.5000+00	1.6000+00	1.7000+00
1.8000+00	1.9000+00	2.0000+00	2.1000+00	2.2000+00
2.3000+00	2.4000+00	2.5000+00	2.6000+00	2.7000+00
2.8000+00	2.9000+00	3.0000+00	3.5000+00	4.0000+00
4.5000+00	5.0000+00	5.5000+00	6.0000+00	6.5000+00
7.0000+00	7.5000+00	8.0000+00	8.5000+00	9.0025+00
9.5075+00	10.0150+00	10.5251+00	11.0378+00	11.5529+00

0.0000+00	0.1000+00	0.2000+00	0.3000+00	0.4000+00
0.5000+00	0.6000+00	0.7000+00	0.8000+00	0.9000+00
1.0000+00	1.1000+00	1.2000+00	1.3000+00	1.4000+00
1.5000+00	1.6000+00	1.7000 +00	1.8000+00	1.9000+00
2.0000+00	2.2500+00	2.5025+00	2.7575+00	3.0151+00
3.2753+00	3.5380+00	3.8034+00	4.0714+00	4.3421+00
4.6156+00	4.8917+00	5.1706+00	5.4523+00	5.7369+00
6.0242+00	6.3145+00	6.6076+00	6.9037+00	7.2027+00
7.5048+00	7.8098+00			

B.2.2.3Import input file to Linux account for thill-out code

- Log in to your account
  - Open Secure Shell Client program
  - desktop >CVEG Programs> Secure Shell Client
  - Click: “Quick connect”
  - Host name: cmln1.ddns.uark.edu
  - User Name: (your user name)
  - Hit enter and write your password
  - Now you are in your main directory /home/your name/
- Rules
  - All jobs should be run on scratch disk /scr
  - Create folders as you wish in your directory
  - Click button  on general interface of Secure Shell Client program
  - By doing that you can transfer filed from computer to your Linux account

- The files you transfer goes to /home/your name/ directory
- All commands for Linux can find in 'linux-commands.doc' file

B.2.3 TECPLOT- Converting ASCII to Binary

The following code is a Windows batch file (pre.dat). The first line is just a default command for the batch file. The second line specifies the loop start (1), the loop increment (1) and the loop end (100). The third line start the program preplot.exe to convert the files which start with (mv**.plt) from ascii to binary as (m**.plt). The fourth line sets the time increment for the loop in millisecond (W 5000).

```
@echo off
FOR /L %%G IN (1,1,100) DO (
start preplot.exe mv%%G.plt m%%G.plt
ping 192.0.2.2 -n 1 -w 5000 > nul
)
```

Where:
%%G –loop integer (like i in fortran)
(1,1,20)- starting number, increment, final number
start preplot.exemv%%G.plt m%%G.plt - open preplot program first is ascii mv file, second is result binary
ping 192.0.2.2 -n 1 -w 25000 >nul - time delay for next step of the loop 25000=25sec
) - end of the loop

B.2.4 TECPLOT-The Contour on the structure

B.2.4.1 Open the file named: prc1.plt that gives x, y, z, p, vx, vy, vz

- On the insert tab, click data, pick extract then subzone (Figure B.1)

B.2.4.1 Generate prism building

- Fill the needed information in the table shown in Figure B.2
- I-index: start(IMK2), End (IMK2)
- J-index: start(JMK1), End (JMK2)
- K-index: start(1), End (KH)

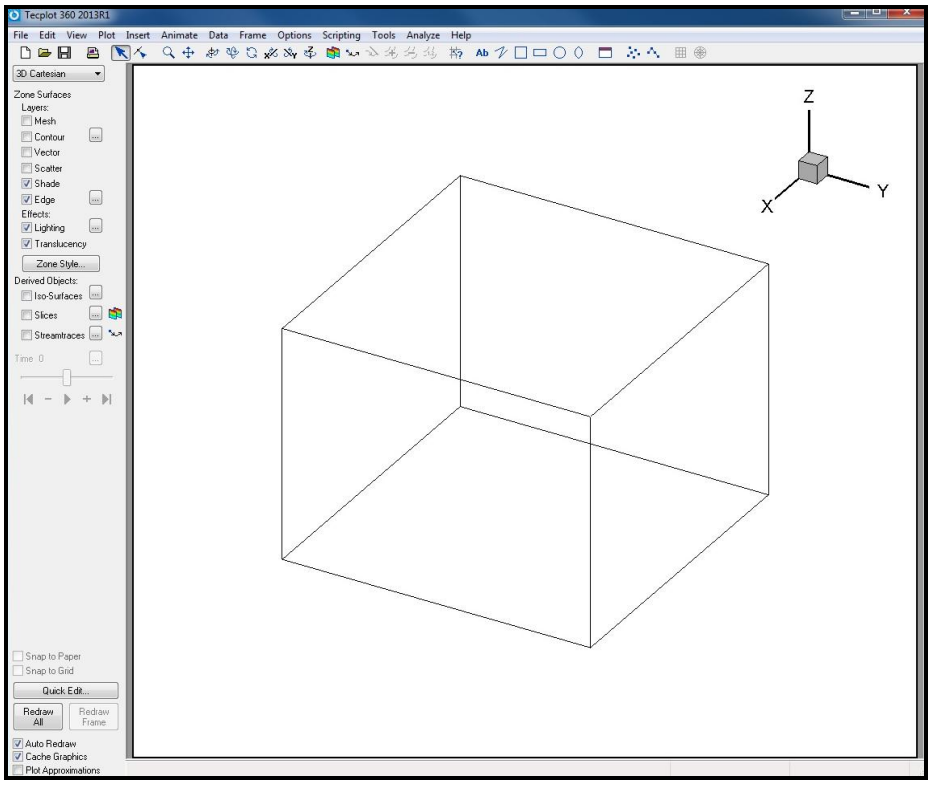

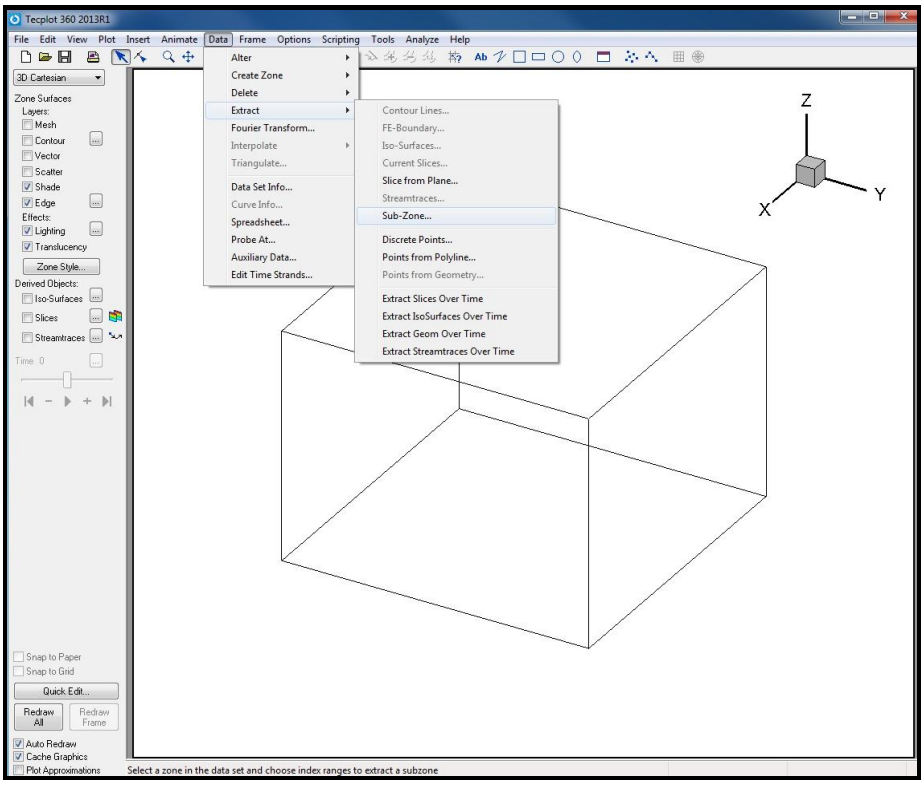

Figure B.1: Domain

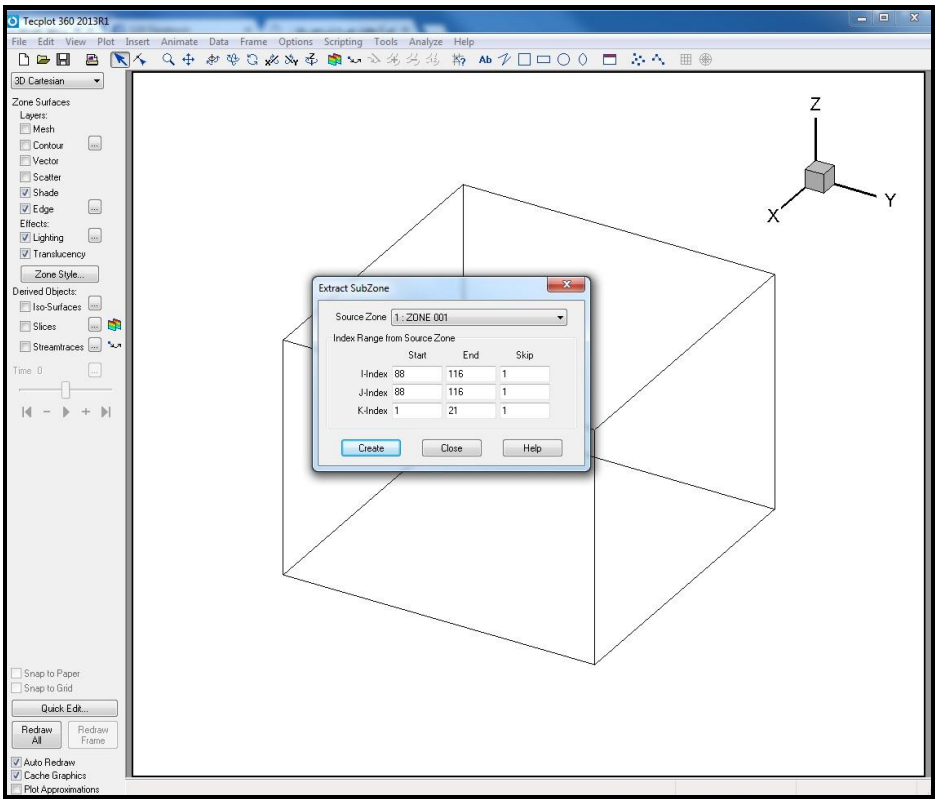
Tecplot 360 2013R1
File Edit View Plot Insert Animate Data Frame Options Scripting Tools Analyze Help
3D Cartesian
Zone Surfaces
Layers:
Mesh
Contour
Vector
Scatter
Shade
Edge
Effects:
Lighting
Translucency
Zone Style...
Derived Objects:
Iso-Surfaces
Slices
Streamtraces
Time 0
Snap to Paper
Snap to Grid
Quick Edit...
Redraw All
Redraw Frame
Auto Redraw
Cache Graphics
Plot Approximations
Extract SubZone
Source Zone 1 : ZONE 001
Index Range from Source Zone
Start End Skip
I-Index 88 116 1
J-Index 88 116 1
K-Index 1 21 1
Create
Close
Help
Z
X
Y

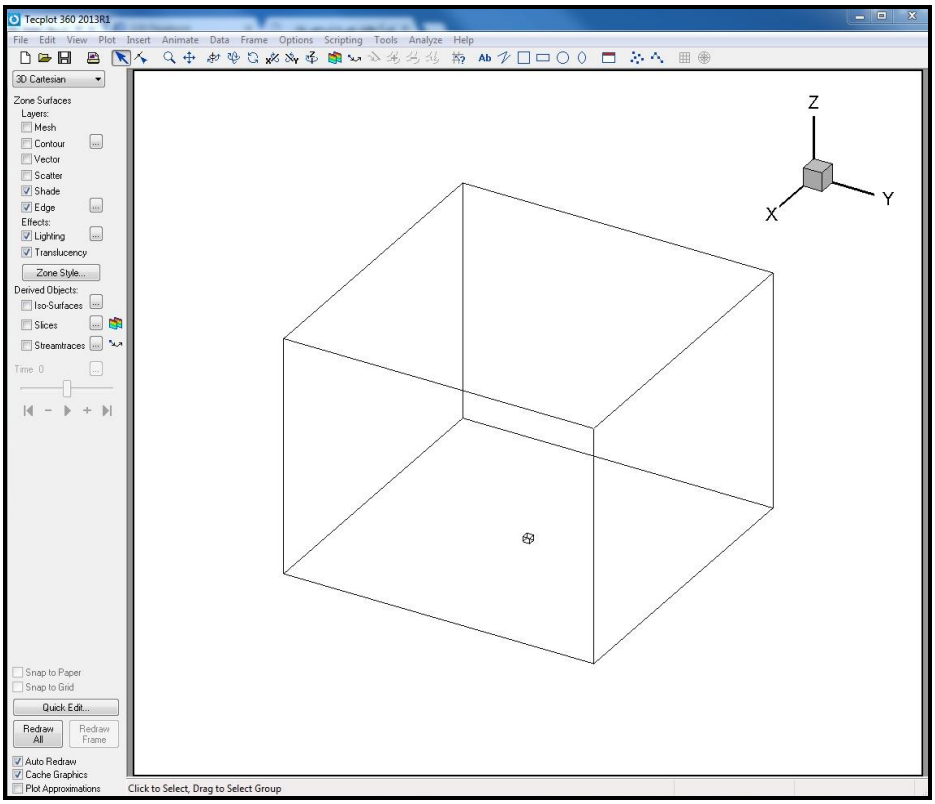
Tecplot 360 2013R1
File Edit View Plot Insert Animate Data Frame Options Scripting Tools Analyze Help
3D Cartesian
Zone Surfaces
Layers:
Mesh
Contour
Vector
Scatter
Shade
Edge
Effects:
Lighting
Translucency
Zone Style...
Derived Objects:
Iso-Surfaces
Slices
Streamtraces
Time 0
Snap to Paper
Snap to Grid
Quick Edit...
Redraw All
Redraw Frame
Auto Redraw
Cache Graphics
Plot Approximations
Click to Select, Drag to Select Group
Z
X
Y

Figure B.2

B.2.4.2 Showing the pressure on building

- On the insert tab, zone style, pick show zone and show contour **(Figure B.5)**

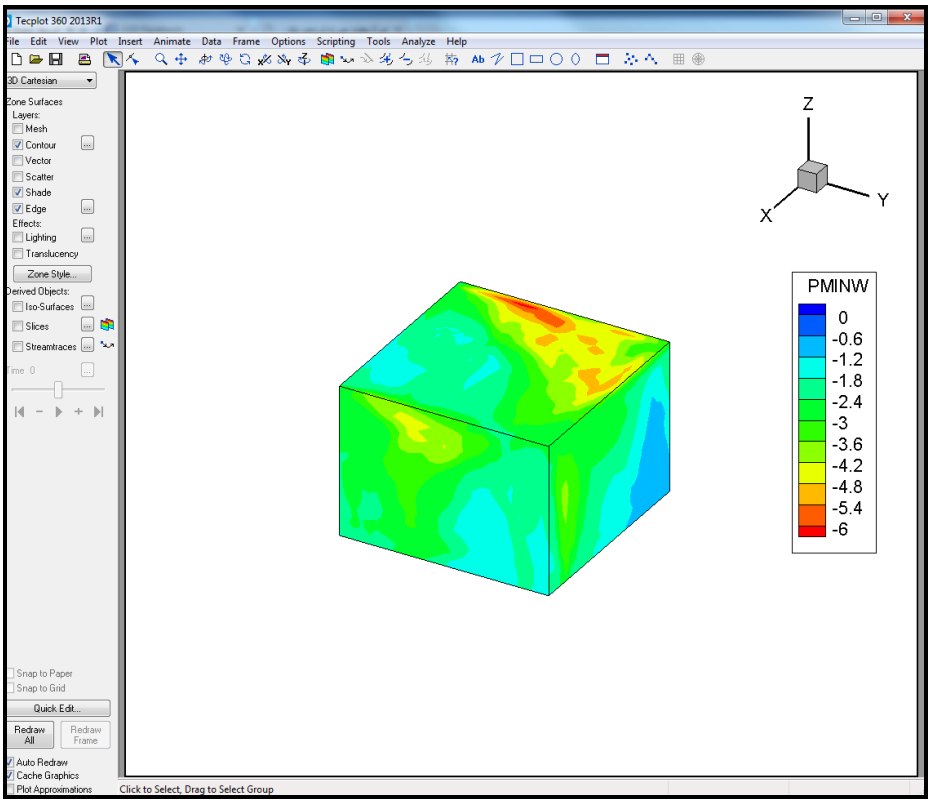

Figure B.3

B.2.4.2 The Contour on the Side Wall and Roof Together

- On the insert tab, view, pick rotate
- Fill the needed information in the table shown in Figure B.6
- For x-y plan view (Figure B.6)
  - Phi = zero
  - Theta = zero
  - Alpha = zero
- For x-z plan view (Figure B.7)
  - Phi = 90, 90
  - Theta = zero, -180
  - Alpha = zero, zero

- For y-z plan view (Figure B.8)

  - Phi = 90, 90
  - Theta = -90, 90
  - Alpha = zero, zero

- Paint was used to bring the faces together as shown in Figure

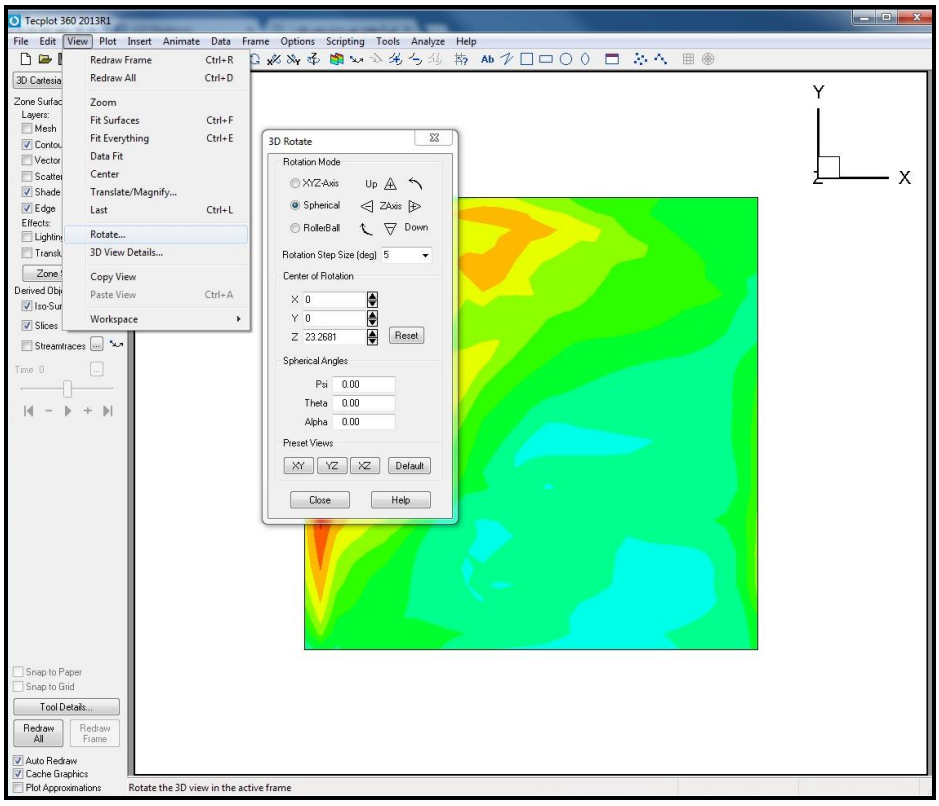

Figure B.4

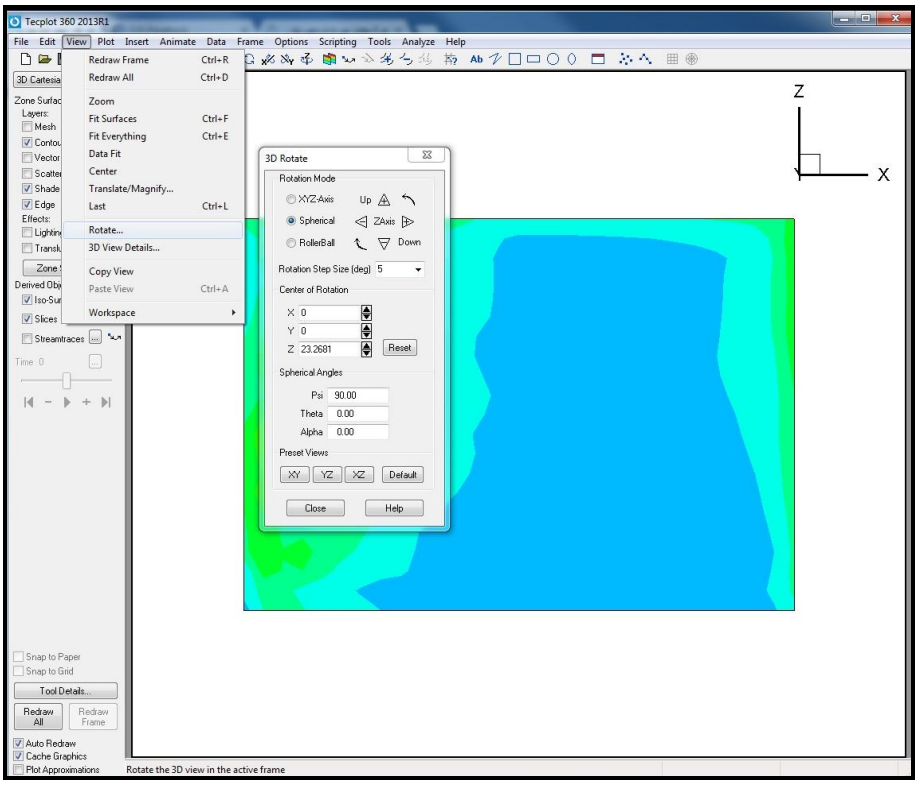
Tecplot 360 2013R1
File Edit View Plot Insert Animate Data Frame Options Scripting Tools Analyze Help
Redraw Frame Ctrl+R
Redraw All Ctrl+D
Zoom
Fit Surfaces Ctrl+F
Fit Everything Ctrl+E
Data Fit
Center
Translate/Magnify...
Last Ctrl+L
Rotate...
3D View Details...
Copy View
Paste View Ctrl+A
Workspace
3D Rotate
Rotation Mode
XYZ-Axis
Spherical
RollerBall
Up
ZAxis
Down
Rotation Step Size (deg) 5
Center of Rotation
X 0
Y 0
Z 23.2681
Reset
Spherical Angles
Psi 90.00
Theta 0.00
Alpha 0.00
Preset Views
XY YZ XZ Default
Close Help
Z
X
Snap to Paper
Snap to Grid
Tool Details...
Redraw All
Redraw Frame
Auto Redraw
Cache Graphics
Plot Approximations
Rotate the 3D view in the active frame

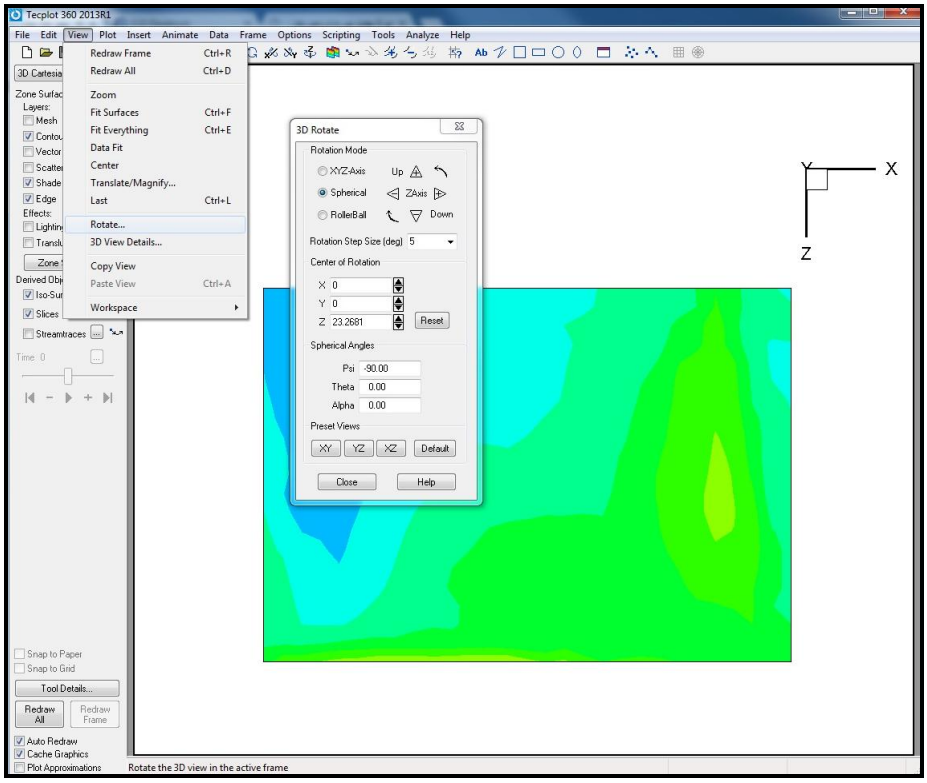
Tecplot 360 2013R1
File Edit View Plot Insert Animate Data Frame Options Scripting Tools Analyze Help
Redraw Frame Ctrl+R
Redraw All Ctrl+D
Zoom
Fit Surfaces Ctrl+F
Fit Everything Ctrl+E
Data Fit
Center
Translate/Magnify...
Last Ctrl+L
Rotate...
3D View Details...
Copy View
Paste View Ctrl+A
Workspace
3D Rotate
Rotation Mode
XYZ-Axis
Spherical
RollerBall
Up
ZAxis
Down
Rotation Step Size (deg) 5
Center of Rotation
X 0
Y 0
Z 23.2681
Reset
Spherical Angles
Psi -90.00
Theta 0.00
Alpha 0.00
Preset Views
XY YZ XZ Default
Close Help
Y
X
Z
Snap to Paper
Snap to Grid
Tool Details...
Redraw All
Redraw Frame
Auto Redraw
Cache Graphics
Plot Approximations
Rotate the 3D view in the active frame

Figure B.5

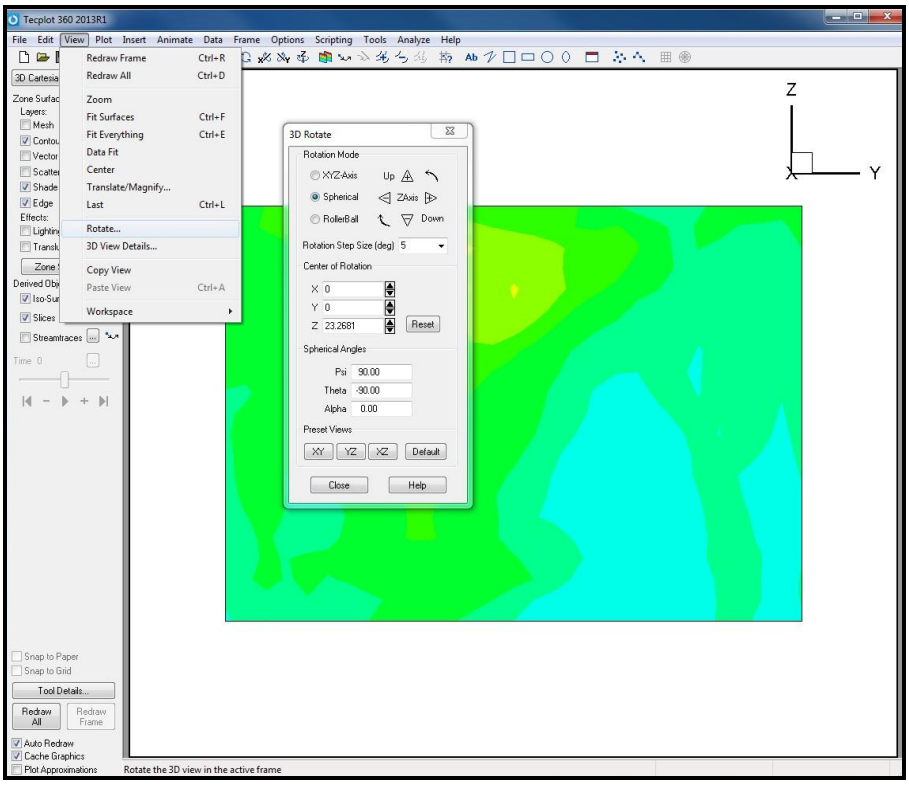
Tecplot 360 2013R1
File Edit View Plot Insert Animate Data Frame Options Scripting Tools Analyze Help
Redraw Frame Ctrl+R
Redraw All Ctrl+D
Zoom
Fit Surfaces Ctrl+F
Fit Everything Ctrl+E
Data Fit
Center
Translate/Magnify...
Last Ctrl+L
Rotate...
3D View Details...
Copy View
Paste View Ctrl+A
Workspace
3D Rotate
Rotation Mode
XYZ-Axis
Spherical
RollerBall
Up
ZAxis
Down
Rotation Step Size (deg) 5
Center of Rotation
X 0
Y 0
Z 23.2681
Reset
Spherical Angles
Psi 90.00
Theta -90.00
Alpha 0.00
Preset Views
XY YZ XZ Default
Close Help
Z
Y
X
Snap to Paper
Snap to Grid
Tool Details...
Redraw All
Redraw Frame
Auto Redraw
Cache Graphics
Plot Approximations
Rotate the 3D view in the active frame

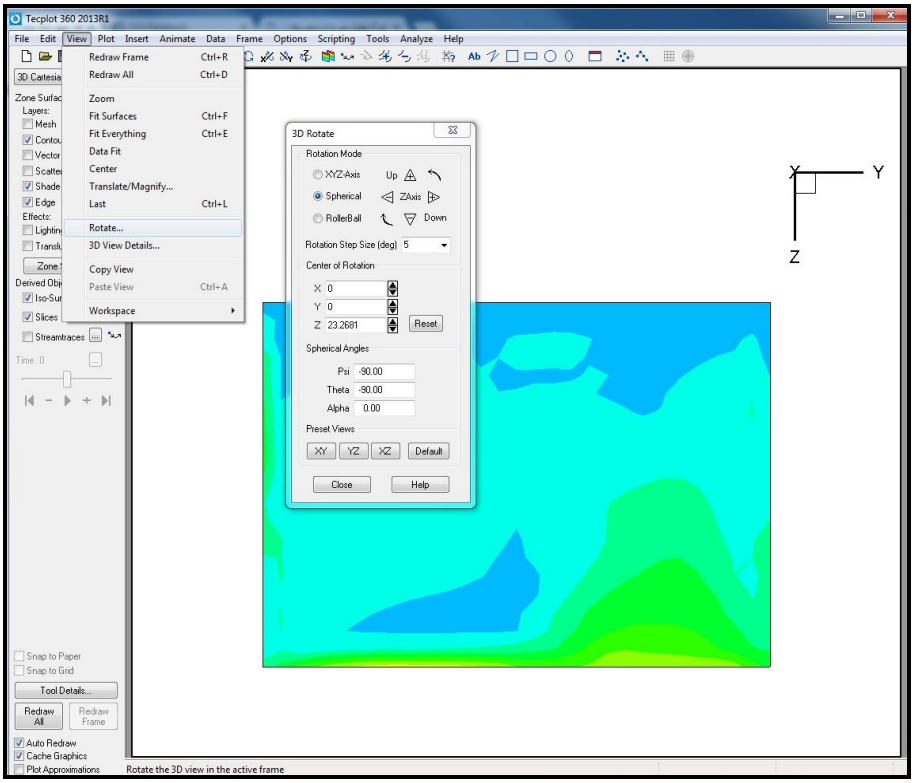
Tecplot 360 2013R1
File Edit View Plot Insert Animate Data Frame Options Scripting Tools Analyze Help
Redraw Frame Ctrl+R
Redraw All Ctrl+D
Zoom
Fit Surfaces Ctrl+F
Fit Everything Ctrl+E
Data Fit
Center
Translate/Magnify...
Last Ctrl+L
Rotate...
3D View Details...
Copy View
Paste View Ctrl+A
Workspace
3D Rotate
Rotation Mode
XYZ-Axis
Spherical
RollerBall
Up
ZAxis
Down
Rotation Step Size (deg) 5
Center of Rotation
X 0
Y 0
Z 23.2681
Reset
Spherical Angles
Psi -90.00
Theta -90.00
Alpha 0.00
Preset Views
XY YZ XZ Default
Close Help
X
Y
Z
Snap to Paper
Snap to Grid
Tool Details...
Redraw All
Redraw Frame
Auto Redraw
Cache Graphics
Plot Approximations
Rotate the 3D view in the active frame

Figure B.6

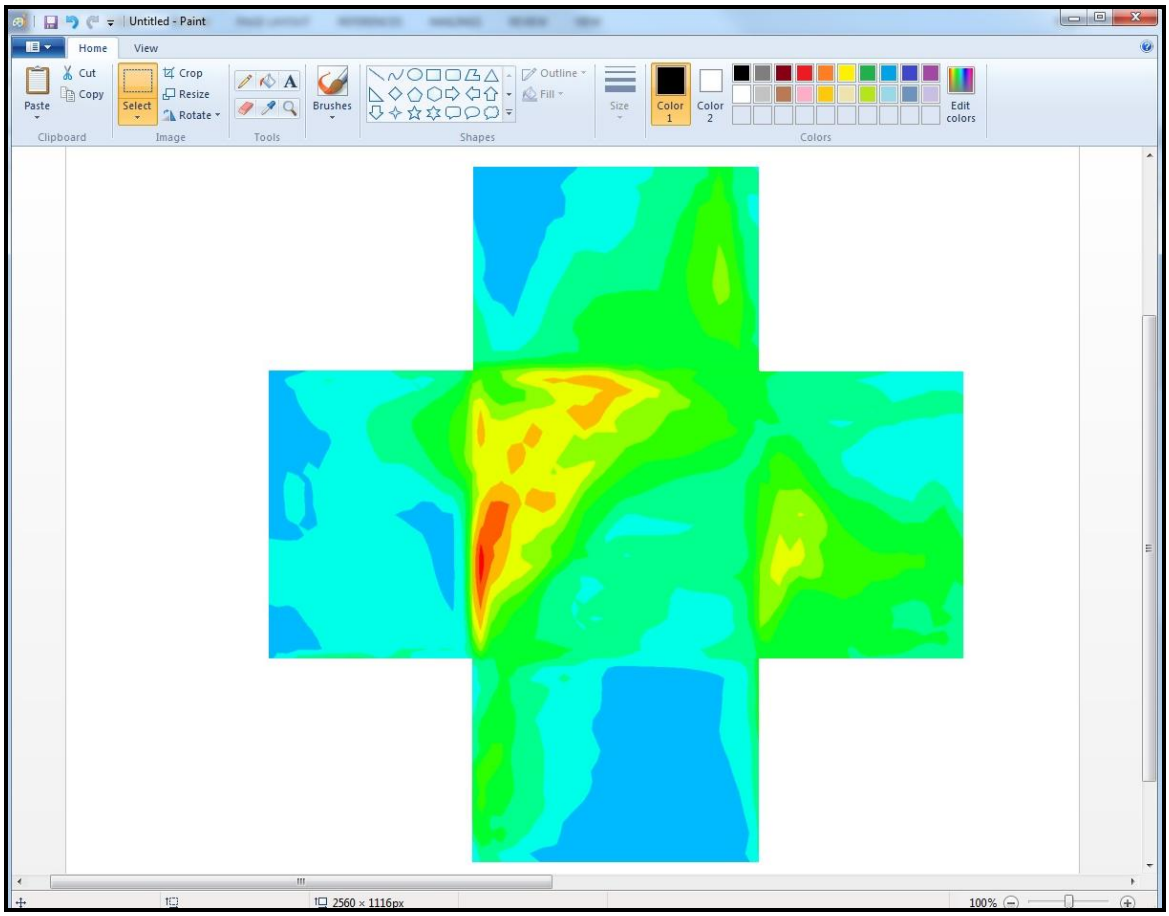
Untitled - Paint
Home
View
Cut
Copy
Paste
Clipboard
Select
Crop
Resize
Rotate
Image
Tools
Brushes
Outline
Fill
Shapes
Size
Color 1
Color 2
Edit colors
Colors
2560 × 1116px
100%

Figure B.7

CURRICULUM VITAR

EDUCATION

Doctor of Philosophy, Civil Engineering (Structural) May 2017

University of Arkansas, USA

GPA: 3.73/4.00

Dissertation: Investigate the effect of straight line and tornado wind on dome and prism buildings using 3D computational fluid dynamics simulations

Committee: R. Panneer Selvam, Micah Hale, Ernest Heymsfield, and Rick Couvillion

Master of Science, Civil Engineering (Structural) Dec. 2005

University Putra Malaysia, Malaysia

Thesis: Developed and analyzed model of existing concrete water tank using the code and the finite element method (STAAD PRO)

GPA: 3.27/4.00

Committee: Dr. Waleed Thanoon, Dr. Mohd Saleh Jaafar, and Dr. Jamaloddin Noorzaei

Bachelor of Science, Civil Engineering July 2000

University of Omar Al-Mukhtar, Libya

GPA: 2.5/4.00

Bachelor's project: Analysis and design of concrete multi-story building

English Diploma March 2012

Spring International Language Center, USA

TEACHING EXPERIENCE

Teaching Assistant (Aug. 2016 – May 2017)

University of Arkansas, Fayetteville, AR

Teach Statics / Mechanics class

Research Assistant (June 2013 – May 2017)

University of Arkansas, Fayetteville, AR

- Study the effect of straight line and tornado wind on dome and prism building using 3D computational fluid dynamics simulations.
- Investigate the tornado dynamic effects on cylinder building using 2D computational fluid dynamics simulations.

University Instructor (Jan. 2008 – Nov. 2010)

University of Omar Al-Mukhtar, Libya

- Served as coordinator of the College of Engineering and Civil Engineering Department Head
- Taught concrete design II, construction building, steel design, surveying, static & dynamic, and civil drawing courses
- Sponsored by university to earn my PhD from Dec. 2010 to Dec. 2016.

University Instructor **(**Mar. 2005 – Nov. 2010)

University of Benghazi, Libya

- Taught structural analysis I &II, construction building, steel design, surveying, statics & dynamics, and civil drawing

ENGINEERING EXPERIENCE

Civil Structural Engineer (Oct. 2000 – Jan. 2008)

Great Manmade River, Libya

- The Great Man-Made River is a network of pipes that supplies water to the Sahara in Libya, from the Nubian Sandstone Aquifer System fossil aquifer. It is the world's largest irrigation project. It is the largest underground network of pipes (2,820 kilometers (1,750 mi) and aqueducts in the world. It consists of more than 1,300 wells, more than 500 m deep, and supplies

6,500,000 m3 of fresh water per day to the cities of Tripoli, Benghazi, Sirte and elsewhere. The late Libyan calls it as the "Eighth Wonder of the World.

- Supervised construction projects, verified contractor invoices and ensured works were performed to specifications. Projects included: conveyance pumping station, roads, concrete water tanks, silos and concrete houses
- Performed quality control checks on engineering materials
- Verified quantities and payment certificates
- Drafted and verified design calculations for steel and concrete structures such as water tanks, storage buildings, silos and houses.
- On behalf of company, prepared and presented bids to various engineering and consulting organizations
- Sponsored by company to study English and completion of my master degree from Jan. 2003 to Dec. 2004.

SKILLS AND SOFTWARE

Development of Technical Documents and Structural Designs, AutoCAD, STAAD PRO, SAP2000, MATLAB, FORTRAN, Tecplot and MS Office

PUBLICATIONS

Paper Published in Journal

Yousef, M.A. and Selvam, R.P. (2016), "A comparison of the forces on dome and prism for straight and tornadic wind using CFD model", Wind and Structures, An International Journal. Status: Submitted.

Strasser, M.N., Yousef, M.A. and Selvam, R.P. (2015), "Defining the vortex loading period and application to assess dynamic amplification of tornado-like wind loading", Journal of Fluids and Structures. Status: Published.

Yousef, M.A. and Selvam, R.P. (2016), "Three Dimensional Computational Fluid Dynamics Model, the influence of equivalent surface area, volume, width of dome to prism on tornado

coefficients with tangential to translational velocity ratio", Wind and Structures, An International Journal. Status: Submit April 2017.

Paper Published in Conferences

Yousef, M.A. and Selvam, R.P. (2016), "Compare the tornado force coefficients on dome and prism building using three dimensional computational fluid dynamics model, International Conference on Applications of Fluid Dynamics, 2016, Jharkhand, India, December19-21.

Yousef, M.A. and Selvam, R.P. (2016), "Effect of equivalent height, surface area and volume of dome to prism on tornado forces using CFD", 8th International Colloquium on Bluff Body Aerodynamics and Applications Northeastern University, Boston, Massachusetts, USA June 7-11.

Yousef, M.A. and Selvam, R.P. (2016), "The influence of tornado's size on forces on dome and regular cubic Building using CFD", 4th American Association for Wind Engineering Workshop, Miami, Florida, USA, August 14-16.

Yousef, M.A. and Selvam, R.P. (2017), "The influence of tangential to translational velocity ratio on tornado force coefficients on building using CFD", 13th Americas Conference on Wind Engineering Gainesville, Florida, USA May 21-24, 2017.

Selvam, R.P., N. Ahmed, M.N, Strasser, M. Yousef and Q.S. Ragan (2015b), Observations of the Influence of Hilly Terrain on Tornado Path and Intensity from Damage Investigation of the 2014 Tornado in Mayflower Arkansas, Structures Congress, 2015,Portland, Oregon, USA April 23-25.

Abstract Published in Conferences

Yousef, M.A. and Selvam, R.P. (2014), "Dynamic effect of tornado forces on cylindrical structures", 98th Annual meeting of the Arkansas Academy of Science, 2014 Searcy, Arkansas, April 4-5.

Yousef, M.A. and Selvam, R.P. (2015), "Comparing the effect of hemispherical dome and rectangular prism building on tornado force coefficients using CFD Simulation", 99th Annual meeting of the Arkansas Academy of Science, 2015, Arkadelphia, Arkansas, April 10-11.

Yousef, M.A. and Selvam, R.P. (2016), "Effect of equivalent height, surface area and volume of dome to prism on tornado forces using CFD", 100th Annual meeting of the Arkansas Academy of Science, 2016, Fayetteville, Arkansas, April 1-2.